SANDIA REPORT SAND85-8250 • Unlimited Release • UC-62a
Printed January 1986

Convective Loss Measurements at the 10 MWe Solar Thermal Central Receiver Pilot Plant

M. C. Stoddard

Prepared by
Sandia National Laboratories
Albuquerque, New Mexico 87185 and Livermore, California 94550
for the United States Department of Energy
under Contract DE-AC04-76DP00789

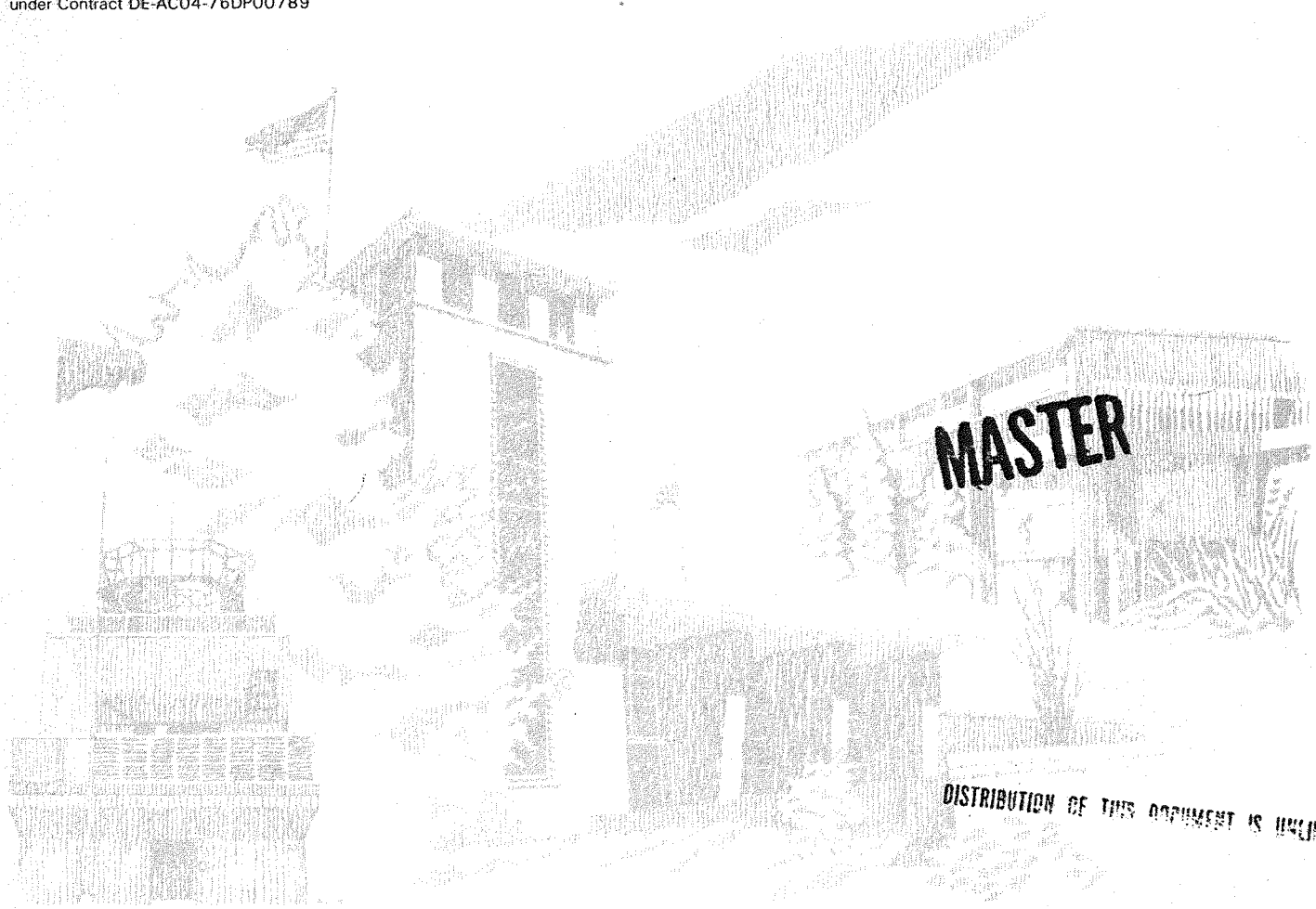

SAND 85-8250
Unlimited Release
Printed January 1986

UC-62a

DISCLAIMER

CONVECTIVE LOSS MEASUREMENTS AT THE 10 MW_e SOLAR THERMAL CENTRAL RECEIVER PILOT PLANT

SAND--85-8250

DE86 006651

Mary Clare Stoddard
Solar Central Receiver Systems Division
Sandia National Laboratories, Livermore

ABSTRACT

Experiments were performed at the 10 MW_e Solar Thermal Central Receiver Pilot Plant to measure the convective heat transfer from the receiver. Determining the convective loss will help reduce the uncertainty in the calculation of thermal efficiency for solar central receivers. Two types of results are presented from the data: (*i*) the overall receiver convective coefficient, and (*ii*) detailed information on the local (panel) losses as a function of wind direction. The overall measured convective coefficient is also compared with predictions from correlations developed to calculate the convective coefficient. The comparison between the measured and predicted convective coefficients is good, although the correlations tend to overpredict the measured data by about 10% .

SOLAR THERMAL TECHNOLOGY
FOREWORD

The research and development described in this document was conducted within the U.S. Department of Energy's (DOE) Solar Thermal Technology Program. The goal of the Solar Thermal Technology Program is to advance the engineering and scientific understanding of solar thermal technology, and to establish the technology base from which private industry can develop solar thermal power production options for introduction into the competitive energy market.

Solar thermal technology concentrates solar radiation by means of tracking mirrors or lenses onto a receiver where the solar energy is absorbed as heat and converted into electricity or incorporated into products as process heat. The two primary solar thermal technologies, central receivers and distributed receivers, employ various point and line-focus optics to concentrate sunlight. Current central receiver systems use fields of heliostats (two-axis tracking mirrors) to focus the sun's radiant energy onto a single tower-mounted receiver. Parabolic dishes up to 17 meters in diameter track the sun in two axes and use mirrors or Fresnel lenses to focus radiant energy onto a receiver. Troughs and bowls are line-focus tracking reflectors that concentrate sunlight onto receiver tubes along their focal lines. Concentrating collector modules can be used alone or in a multi-module system. The concentrated radiant energy absorbed by the solar thermal receiver is transported to the conversion process by a circulating working fluid. Receiver temperatures range from 100°C in low-temperature troughs to over 1500°C in dish and central receiver systems.

The Solar Thermal Technology Program is directing efforts to advance and improve promising system concepts through the research and development of solar thermal materials, components, and subsystems, and the testing and performance evaluation of subsystems and systems. These efforts are carried out through the technical direction of DOE and its network of national laboratories who work with private industry. Together they have established a comprehensive, goal directed program to improve performance and provide technically proven options for eventual incorporation into the Nation's energy supply.

To be successful in contributing to an adequate national energy supply at reasonable cost, solar thermal energy must eventually be economically competitive with a variety of other energy sources. Components and system-level performance targets have been developed as quantitative program goals. The performance targets are used in planning research and development activities, measuring progress, assessing alternative technology options, and making optimal component developments. These targets will be pursued vigorously to insure a successful program.

ACKNOWLEDGEMENT

I would like to express my sincere appreciation to John Raetz, of McDonnell Douglas Astronautics Company, who developed the test plan and oversaw its implementation for this experiment, thus translating it from a concept to a reality at the Solar One Pilot Plant.

CONTENTS

ILLUSTRATIONS

TABLES

Nomenclature

a	Exponent in Equation (9)
A	Area, m^2
C_p	Specific heat, Ws/kg°C
d	Receiver diameter, m
G_r	Grashof number, $g\beta(T_{wall} - T_\infty)L^3/\nu^2$
h	Convective heat transfer coefficient, $W/m^2°C$
k	Conductive heat transfer coefficient, W/m^2 °C
k_s	Tube radius (m), used to calculate roughness parameter k_s/d
L	Length, m
$\dot{m}$	Mass flow rate, kg/s
Nu	Nusselt number, hL/k or hd/k
Q	Rate of heat transfer, W
Re	Reynolds number, $u_\infty d/\nu$
T	Temperature, °C
u	Wind velocity, m/s

Greek

β	Coefficient of volumetric expansion, K^{-1}
δ	Uncertainty in accompanying quantity
ϵ	Emissivity
η	Efficiency
ν	Kinematic viscosity, m^2/s
σ	Stefan-Boltzmann constant, 5.669×10^{-8} W/m^2K^4
ϕ	Angular distance around a cylinder, degrees

Subscripts

abs	Absorbed
$cond$	Conduction
$conv$	Convection
d	Diameter
$dewpt$	Dewpoint temperature
f	Film temperature
$forc$	Forced convection
in	Inlet
inc	Incident

L	Length
meas	Measured convective coefficient
pred	Predicted mixed convective coefficient
nat	Natural convective coefficient
out	Outlet
panel	Solar One boiler panel
rad	Radiation
refl	Reflection
∞	Ambient

EXECUTIVE SUMMARY

Introduction

The 10 MW_e Solar Thermal Central Receiver Pilot Plant, also known as Solar One, near Barstow, California, is the world's largest operational solar central receiver power plant. A two year Test and Evaluation Phase, which was concluded in August 1984, characterized the various plant subsystems (receiver, collector, turbine generator, and thermal storage). As part of the receiver evaluation, experiments were performed to measure the convective heat transfer from the receiver.

Determining the convective loss will help reduce the uncertainty in the calculation of thermal efficiency for solar central receivers [1,2]. Early predictions indicated that under certain conditions as much as 30% of the collected energy could be lost due to convection from the receiver. Therefore, it is important that receiver designers have an accurate method to predict convective losses.

The goal of the experiments reported here was to provide convective loss measurements in order to determine the convective coefficient for the receiver. The measured convective coefficient is compared to the convective coefficient predicted from correlations developed for predicting convective heat transfer coefficients for solar central receivers by Siebers and Kraabel [3] . The agreement between the measured and predicted convective coefficients is assessed.

The convective heat transfer process at Solar One is characterized by mixed convection, a combination of both natural and forced convection. Two important dimensionless numbers in correlations for mixed convection are the Grashof number and the Reynolds number. The Grashof number (for natural convection), Gr, is a measure of the ratio of bouyant to viscous forces, and the Reynolds number (for forced convection), Re, is a measure of the ratio of inertial to viscous forces. For the case of an external central receiver, these forces interact to produce a fully three-dimensional flow field. Little experimental data exist for a cylinder in three-dimensional mixed convection, especially in the Grashof and Reynolds number range that characterizes the Solar One receiver.

The experiments were performed with no flux on the receiver to eliminate uncertainties associated with determining incident solar flux. The wall to ambient temperature difference was a factor of three below that of a normal operating receiver. The reduced wall temperature, however, does not greatly alter the results. The correlations [3] indicate that as the wall temperature is increased toward the normal operating temperature, the convective heat transfer coefficient decreases

slightly. As wall temperature increases, natural convection increases (due to enhanced buoyancy), but forced convection decreases (due to changing air properties). Since forced convection effects usually dominate the mixed convection heat transfer coefficient in this experiment, the net effect is a decrease in convection.

This report provides both qualitative and quantitative information on convective losses from the Solar One central receiver. Two types of results are presented from this data: (*i*) the overall receiver convective coefficient, and (*ii*) detailed information on the local (panel) losses as a function of wind direction.

Receiver and Experiment Description

Description of Receiver

The Solar One central receiver is composed of twenty-four panels, six of which are preheat and the remaining eighteen being "once-through to superheat" boiler panels. Each panel is made up of seventy 1.27 cm (1/2-inch) diameter tubes, welded together, and is 0.9 meters (35 in) wide by 13.7 meters (45 ft) long. The receiver, shown in Figure 1, is a cylinder 7.0 meters (23 ft) in diameter and 13.7 meters in length. Water flows up the tower through a single pipe. The pipe splits and water flows up through the first three preheat panels and then up through the next three preheat panels. The flows are then recombined in a ring manifold which simultaneously feeds all eighteen boiler panels. All panel flows are from the bottom to the top of the panel. Boiler panel flows are individually controlled and monitored to provide the desired output: steam at 455 °C (850 °F) and 10.0×10^6 N/m^2 (1450 psi).

Description of Experiment

Heated receiver feedwater is circulated through the receiver exactly as it is during normal receiver operations; however, there is no solar flux on the receiver. The total energy loss to the environment is measured as the energy loss in the feedwater as it passes through the receiver. The energy lost by conduction and thermal radiation is then calculated, and the balance of the loss is attributed to convection. A root-sum-square error analysis is performed on the data analysis equations to quantify the uncertainty in the resultant convective coefficient.

The flow diagram of this experiment is shown in Figure 2. The major experimental requirement was to find a way to heat the receiver feedwater. The thermal storage subsystem answered this requirement. Prior to running the test, the thermal storage tank was fully "charged"; that is, the thermal storage medium (oil) was heated during solar operations. Steam was then generated by operating an extraction heat exchanger, which transfers heat stored in the oil to generate steam. This steam is used in the feedwater heater to heat the water which flows through the receiver. The Solar One Pilot Plant Data Acquisition System was used to record the

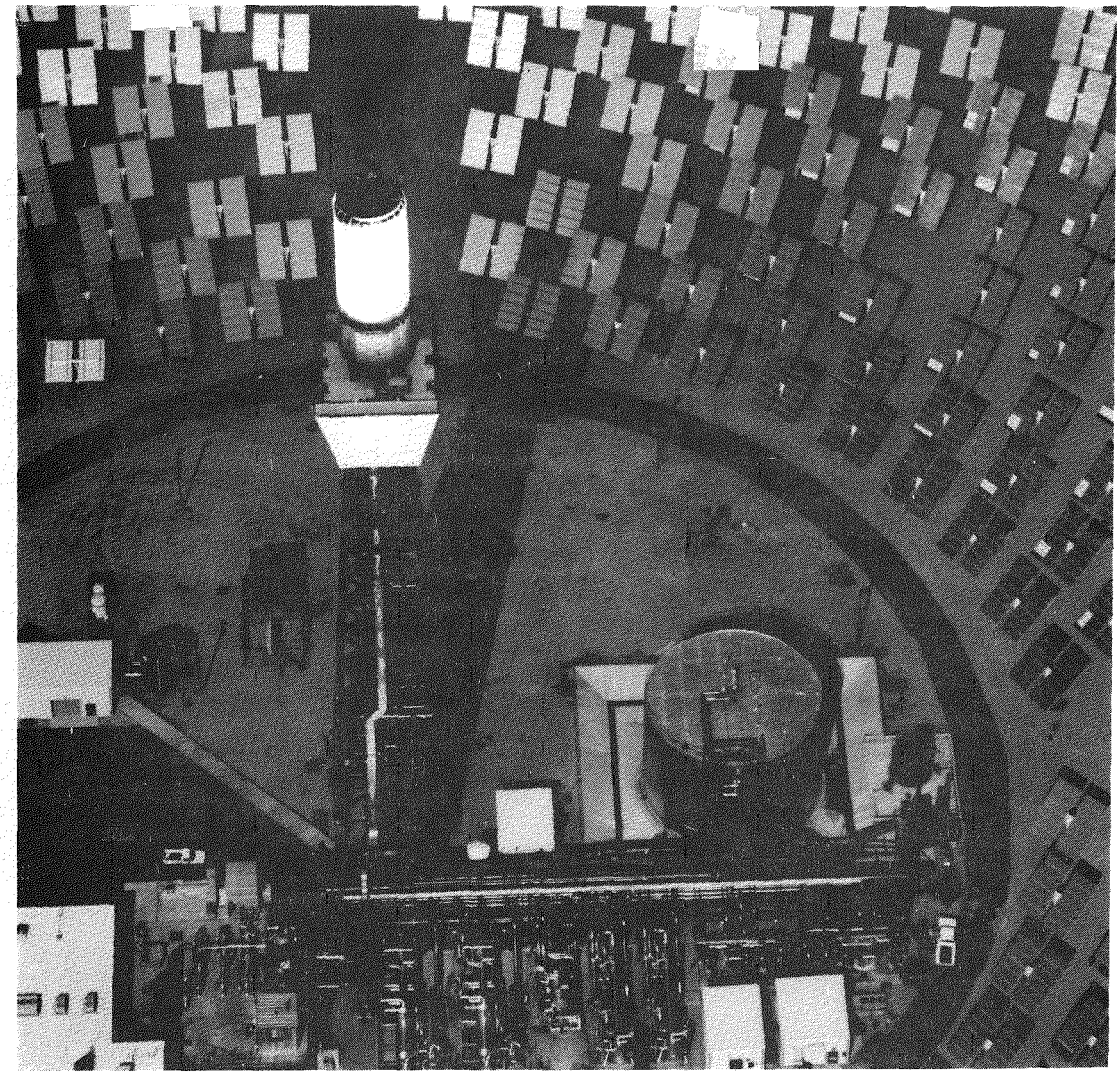

Figure 1. Solar One central receiver with associated piping

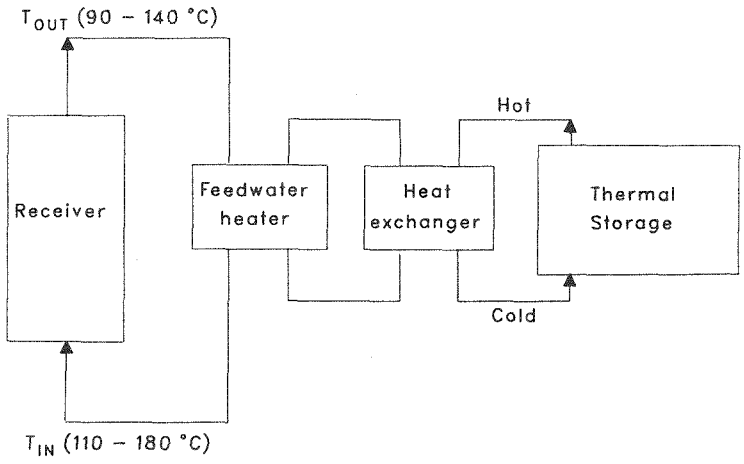

Figure 2. Convective loss experiment flow diagram

test data. Plant instrumentation which provided the data included thermocouples, flowmeters, and meteorological instruments.

The primary sources of error were identified prior to the experiments as solar flux calculation, receiver mass flow rate measurement, and receiver fluid temperature measurement. These potential problem areas were addressed in the experimental design in the following ways.

1. All tests were conducted with no solar flux on the receiver to eliminate the uncertainty associated with flux calculations (there are no solar flux measurements at Solar One). Except for one test set which was conducted on an overcast day, all tests were conducted at night, which eliminated the need to account for any solar input.

2. Individual boiler panel flow rates were limited to a minimum of 0.13 kg/s (1000 lb/hr). Flow rates less than this are subject to unacceptably large measurement uncertainties.

3. All receiver fluid thermocouples to be used in the data analysis were calibrated. Those which could not be adjusted to read correctly were eliminated from the analysis.

Data Analysis Approach

The data analysis was divided into two categories: total receiver and panel data analyses. Both analyses refer to the measurement of energy loss in the receiver water: $\dot{m}C_p(T_{in} - T_{out})$.

In the receiver analysis, the receiver is considered a cylinder, with only one inlet, one outlet, and one mass flow rate. One convective coefficient is calculated for the entire cylinder. This convective coefficient is then compared with that predicted using the correlations from Siebers and Kraabel [3]. A goal of this experiment is to validate these correlations for an operating receiver.

Local mixed convection heat transfer data has been obtained from individual panel measurements. An energy balance is formed for each panel in the same manner as for the entire cylinder. Thus, a convective coefficient is calculated for each panel. No comparison with correlation can be made since there are no available correlations to predict convective coefficients on roughened flat plates as a function of wind speed and direction. However, the results of this analysis are presented and the trends in heat transfer versus wind direction are compared with published data on flow over a roughened cylinder. An area-averaged convective coefficient is also calculated for the cylinder from the panel data and compared with the total cylinder calculation of the same quantity.

Measured Convective Coefficient

Total Heat Loss–The total heat transfer, Q_{total}, is the primary measurement in the experiments. It is calculated as:

$$Q_{total} = \dot{m}\, C_p\, \Delta T \tag{1}$$

After the total heat loss from the receiver or the panel is measured, the convection heat loss is obtained by subtracting the calculated radiation and conduction losses.

The mass flow rate, $\dot{m}$, for the entire receiver is the sum of the eighteen measured boiler panel flows. The specific heat is calculated at the average water temperature. The temperature difference, ΔT, for the entire receiver is measured directly using a differential thermocouple installed between the inlet and outlet of the receiver. The differential thermocouple is used for improving the accuracy of the measurement. The temperature difference between the inlet and outlet of a boiler panel is the difference between the mixed fluid temperature in the ring manifold and the average of the two outlet thermocouples located at the outlet of each panel.

Thermal Radiation Loss–The receiver loses thermal energy by radiating to its surroundings—the sky and the ground.

$$Q_{rad} = \epsilon\, A\, \sigma(0.5\,(T_{wall}^4 - T_{sky}^4) + 0.5\,(T_{wall}^4 - T_{\infty}^4)) \tag{2}$$

The radiation, Q_{rad}, is split between the ground and the sky. The ground is assumed to be at the ambient air temperature, T_{∞} and the sky temperature, T_{sky}, is estimated using a method described by Berdahl and Fromberg [4], where a relationship between sky temperature and ambient temperature is defined in terms of sky emissivity.

Conduction Loss–The conduction heat loss is a small percentage of the total heat loss from the cylinder, usually ranging from 3 to 6 percent. Nevertheless, a conduction calculation is used in the data analysis. The conduction heat transfer, Q_{cond}, is calculated by:

$$Q_{cond} = kA(T_{wall} - T_{core}). \tag{3}$$

The back of the receiver is insulated with Kaowool insulation, with a conduction coefficient, k, of $1.136\,\mathrm{W/m^2\,^{\circ}C}$ [5]. The receiver front wall temperature is used as T_{wall} for this calculation and the ambient air temperature serves as T_{core}, the receiver core temperature.

Convective Heat Loss–The convective heat loss, Q_{conv}, is computed as the total heat loss minus the radiative and conduction losses.

$$Q_{conv} = \dot{m}\, C_p\, \Delta T - \epsilon\, A\, \sigma(0.5(T_{wall}^4 - T_{sky}^4) + 0.5(T_{wall}^4 - T_{\infty}^4)) - k\, A(T_{wall} - T_{\infty}) \tag{4}$$

$$Q_{conv} = h_{meas}\, A\, (T_{wall} - T_{\infty}). \tag{5}$$

Using equations (4) and (5), the measured convection coefficient, h_{meas}, is computed.

Predicted Mixed Convective Coefficient

The mixed convective coefficient, h_{pred}, is calculated using correlations proposed by Siebers and Kraabel for an external, cylindrical central receiver. The natural and forced convective coefficients are calculated separately and then combined using the relation:

$$h_{pred} = (h_{nat}^a + h_{forc}^a)^{1/a}. \tag{6}$$

A value of 3.2 is recommended for the exponent a [3].

Natural Convective Coefficient–The natural convection correlation was developed by Siebers [6] for heat transfer from a heated flat plate. The Solar One receiver is large enough that, in natural convection, it can be treated as a flat plate. Properties are calculated at the ambient temperature.

$$Nu_L = \frac{h_{nat}\,L}{k} = 0.098 Gr_L^{1/3} \left(\frac{T_{wall}}{T_\infty}\right)^{-0.14} \tag{7}$$

$$h_{nat}(rough) = \left(\frac{\pi}{2}\right) h_{nat}(smooth) \tag{8}$$

The factor $\pi/2$ accounts for the effects of surface roughness due to the tubes [3], which could enhance the heat transfer.

Forced Convective Coefficient–The forced convection correlation has been interpolated for Solar One tube-sized roughness elements from the correlations presented by Siebers and Kraabel. A roughness parameter, k_s/d, of 90×10^{-5} is computed by defining k_s as the tube radius and d as the receiver diameter. Thus the forced convection correlation becomes:

$$Nu_D = \frac{h_{forc}\,D}{k} = 0.93(2.57 \times 10^{-3}) Re_D^{0.98} + 0.07(0.0135 Re_D^{0.89}). \tag{9}$$

This correlation is valid for $3.7 \times 10^5 \leq Re_D < 1.0 \times 10^7$. Properties are calculated at the film temperature. Data required for the calculation of h_{pred} include: T_{wall}, T_∞, and u_∞. The wall and ambient temperatures are identical to those used in calculating h_{meas}.

Cylinder Data Analysis

Convective loss tests were conducted on nine test days from February through July 1984. During these test days, twenty-three data points were gathered. The data were analyzed to provide both measured and predicted convective coefficients for each data point.

Convective Coefficient Versus Wind Speed

The measured convective coefficient, calculated from Equations (1–5), is plotted versus the ambient wind speed in Figure 3. The plot shows a clear increase in the convection coefficient as wind speed increases.

Measured versus Predicted Convective Coefficient

The measured convective coefficient is plotted against the predicted convective coefficient in Figure 4. The solid line indicates where a perfect agreement between the measured and predicted quantities would lie. The agreement between h_{meas} and h_{pred} is quite good, considering the uncertainties associated with the data and the predictions. The agreement between h_{meas} and h_{pred} for low values of h was improved by removing the roughness factor $(\pi/2)$ from the natural convection calculation. The results shown in Figure 4 were calculated with the $(\pi/2)$ factor removed from the correlations.

The results of the data analysis show good agreement between the measured convective coefficient and that predicted using the correlations proposed by Siebers and Kraabel. The scatter in the data is primarily the result of the large experimental uncertainties inherent in field testing.

Interpretation of the Results

Test conditions were examined to determine if they created any biases in the data. Test characteristics that are considered include: wall temperature, mass flow rate, wind direction, wind direction fluctuations, and percent wind speed fluctuations.

The only factor which was found to influence the agreement between the measured and predicted convective coefficient was the receiver mass flow rate. For higher values of $\dot{m}$, the agreement is better than for lower values. This result is not totally unexpected, since it is known that the flowmeter errors increase with decreasing flow. Figure 5 shows a more dramatic representation of the influence of mass flow rate with a plot of only data which have a flow over 5 kg/s (40,000 lb/hr).

Uncertainty Analysis–A root-sum-square uncertainty analysis for determining the uncertainty in single-sample experiments was performed on the data analysis and correlation equations. The uncertainty in the predicted convective coefficient, h_{pred}, is from 40 to 60% and for the measured convective coefficient, h_{meas}, it is 30 to 50%. The uncertainty in h_{pred} is due to uncertainties in the correlations; the uncertainty in h_{meas} is due to instrument uncertainties.

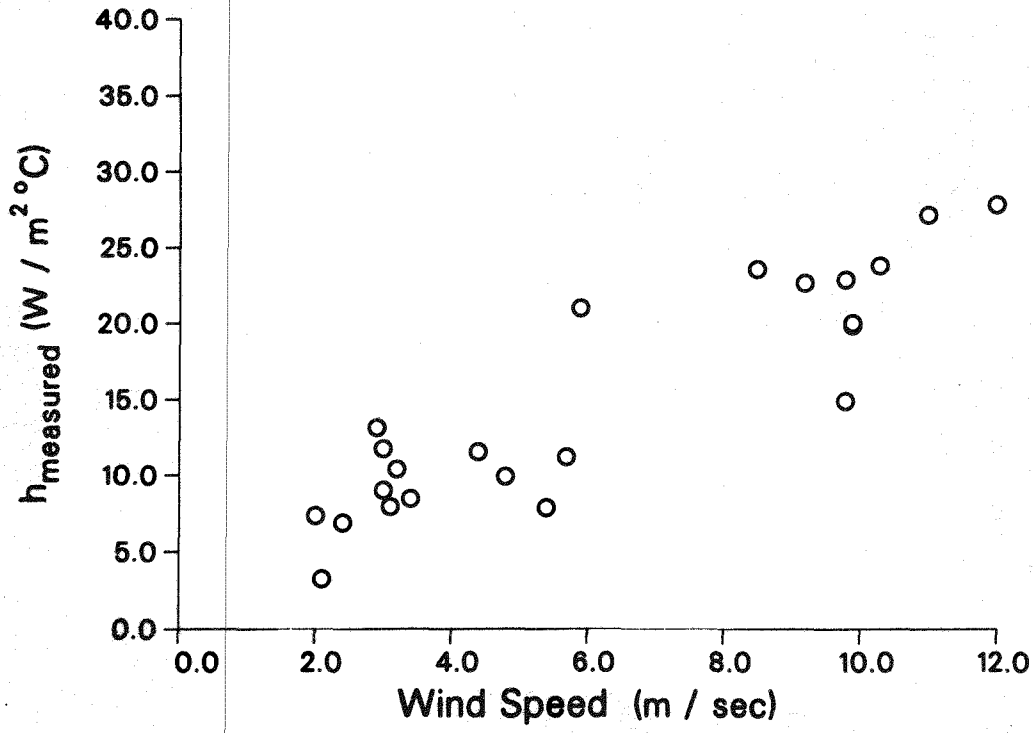

Figure 3. Measured convective coefficient versus wind speed

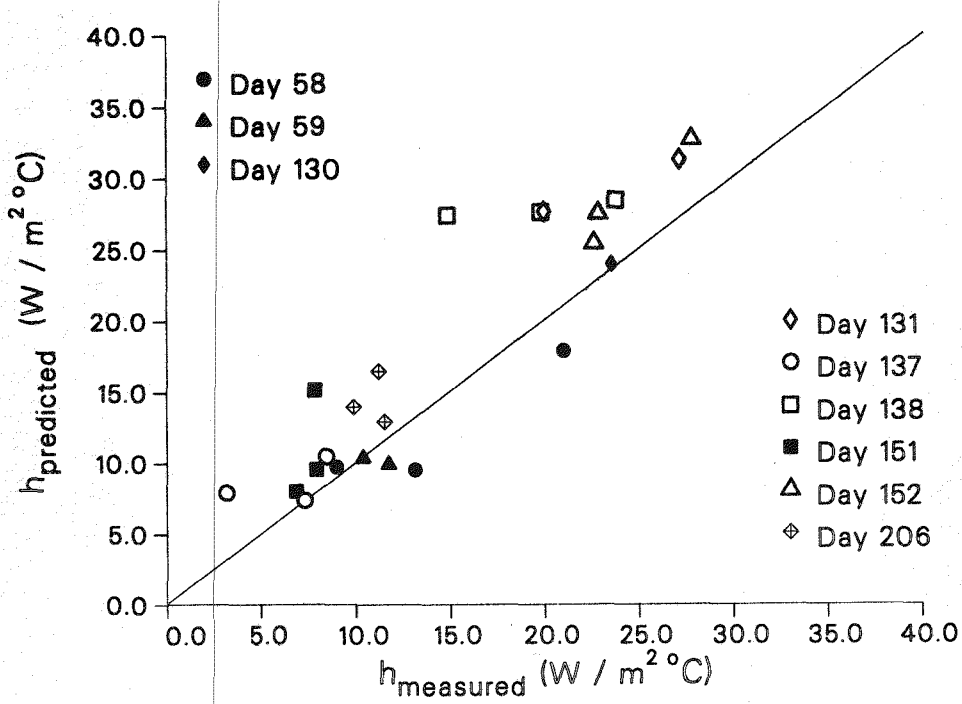

Figure 4. Measured versus predicted convective coefficient

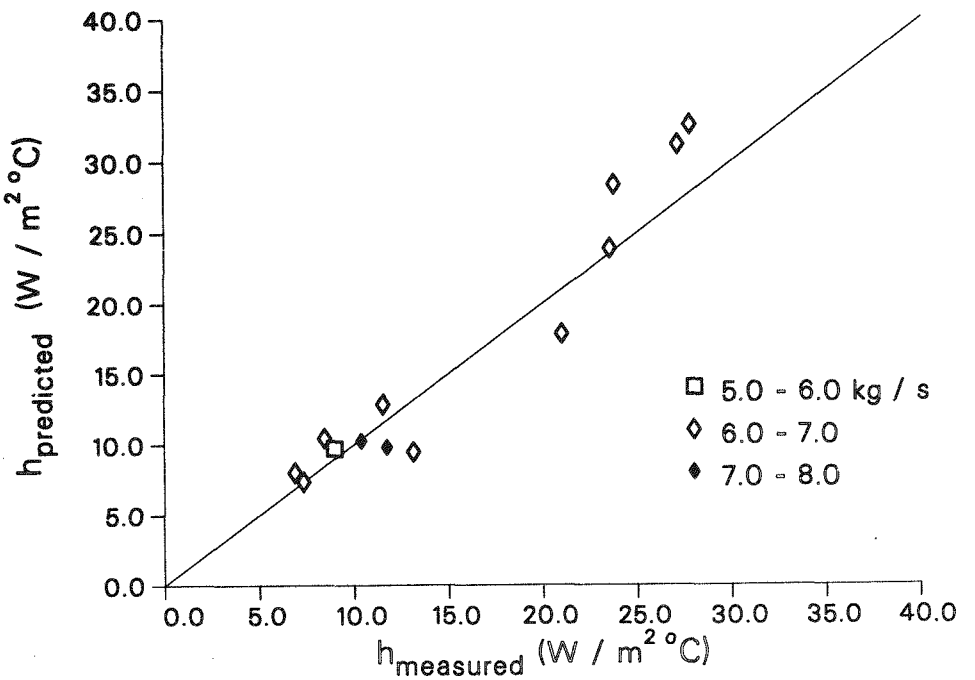

Figure 5. Measured versus predicted convective coefficient, high receiver mass flow rate only

Panel Data Analysis

The panel data analysis shows the variation of the convective coefficient around the receiver as a function of wind direction. The panel data analysis allows a more detailed examination of the data. The trends in the convective coefficient around the receiver are qualitatively compared to results in the literature for flow over roughened cylinders. Finally, an area-averaged convective coefficient is calculated for the cylinder from the panel data and compared with the total cylinder calculation and the correlation prediction of the same quantity.

Convective Coefficient versus Wind Direction

The convective coefficient, h, is calculated for each boiler panel, according to equations (1–5). The six preheat panels are treated as a large, single panel. Adjacent panels are fifteen degrees apart. The relative wind direction for a panel was estimated as the angle between the panel normal and the ambient wind direction.

In general, all of the plots show similar trends in the heat transfer as a function of wind angle. Figure 6 shows a typical "well-defined" profile. The wind was incident at Panel 18 and had a velocity of 9.9 m/s (22 mph). The heat transfer is fairly uniform up to 90 degrees from stagnation, where it increases to a maximum at about 115 degrees and then falls to minimum at about 180 degrees. These results are typical for all tests, although some of the profiles are not as uniform or as

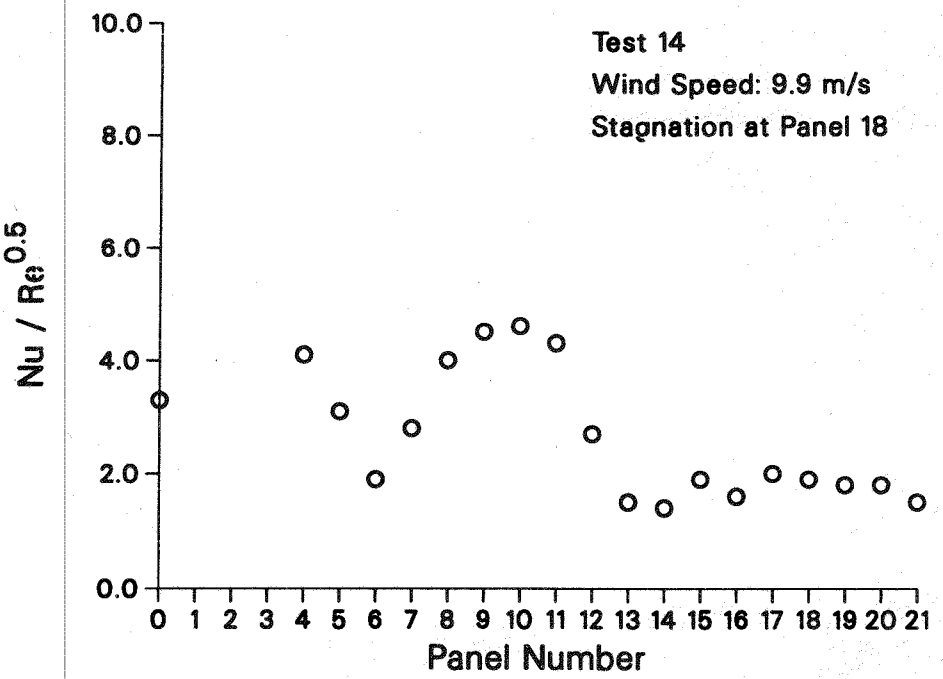

Figure 6. Convective heat transfer versus panel number—wind incident on Panel 18

clearly defined. One factor which contributes to the smoothness of the profile is receiver mass flow rate. The lower mass flow rate tests show more erratic profiles.

Total Receiver Convective Coefficient

The total convective coefficient was calculated from the individual boiler panel and preheat panel convective coefficients, according to the equation:

$$h_{total} = \frac{\sum_{i=4}^{21}(h_i\, A_{panel}) \;+\; 6\, h_{preheat}\, A_{panel}}{24\, A_{panel}} \tag{10}$$

The agreement between h_{total} and h_{meas} (calculated from equations (1–5)) is quite good.

The calculations of h_{total} and h_{meas} use the same flowmeter readings, but different temperature data to calculate h. So, although the calculations of h_{total} and h_{meas} are not completely independent, the excellent agreement between h_{total} and h_{meas} adds confidence to both sets of data.

Conclusions

Comparison of Receiver Convective Coefficient with Predictions

The data analysis yielded convective coefficients over a range of ambient wind speeds and wall temperatures. The measured convective coefficient, h_{meas}, calculated from the receiver energy balance is a function of wind speed. As wind speed increased from 2.0 to 12.0 m/s (4.5 to 27 mph), h_{meas} increased from 3.2 to 27.8 $W/m^2\,°C$.

Mixed convective coefficients for the test conditions were predicted from correlations developed by Siebers and Kraabel [3]. The comparison between the measured and predicted convective coefficients is good, although the correlations tend to overpredict the measured data by about 10% . Another important conclusion from this experiment is that atmospheric turbulence does not enhance the convective heat transfer from the receiver. Siebers and Kraabel estimated that turbulence effects could increase the convective heat transfer coefficient by as much as 70 % above the correlation results.

The predicted mixed convective coefficient, h_{pred}, is calculated from the natural and forced convective coefficients (h_{nat} and h_{forc}). The correlations for both h_{nat} and h_{forc} account for the surface roughness introduced by the receiver tubes. The predicted mixed convective coefficient fits the experimental results better if the roughness factor is removed from the natural convection correlation.

Local Measurements

The convective coefficient was calculated for individual receiver panels. The variation of convective energy loss ($Nu/Re^{0.5}$) as a function of wind direction was examined. These results were qualitatively compared with data presented in the literature [7] for forced convection heat transfer over a roughened cylinder. The comparison is not rigorous since (i) the Solar One measurement of wind direction is approximate, (ii) the wind speed and turbulence intensity are not well characterized, (iii) the local heat transfer measurement is averaged for each panel and (iv) it is not known how the bouyancy effects (natural convection) influence the results. However, a consistent trend is observed in the heat transfer around the receiver. The smoothness of the plot is related to the receiver mass flow rate; low flow rate tests have more irregularly shaped curves, reflecting the inaccuracy of the flow meters at low flows.

The panel data were also averaged to give an overall convective coefficient for the receiver. These results compared well with the convective coefficient as calculated from the single measurement of $\dot{m}\, C_p\, \Delta T$.

References

[1] Abrams, M., Sandia memorandum to A. C. Skinrood, "Plan for Determining the Thermal Performance of the Receiver at the Solar 10 MW_e Power Plant," February 10, 1982.

[2] Kraabel, J. S., "Receiver Efficiency, Fall Measurement Campaign, 1982," Sandia National Laboratories report in preparation.

[3] Siebers, D. L. and J. S. Kraabel, "Estimating Convective Energy Losses From Solar Central Receivers," Sandia National Laboratories report, SAND84-8717, April 1984.

[4] Berdahl, P. and R. Fromberg, "The Thermal Radiance of Clear Skies," *Solar Energy* **29**, 299 (1982).

[5] Kaowool data sheet, Babcock and Wilcox.

[6] Siebers, D. L., R. G. Schwind, and R. J. Moffat, "Experimental Mixed Convection Heat Transfer from a Large, Vertical Surface in a Horizontal Flow," Sandia National Laboratories report, SAND83-8225, July 1983.

[7] Achenbach, E. "The Effect of Surface Roughness on the Heat Transfer from a Circular Cylinder to the Cross Flow of Air," *Int. J. Heat Mass Transfer* **20** 359 (1977).

Introduction

The 10 MW_e Solar Thermal Central Receiver Pilot Plant, also known as Solar One, near Barstow, California, is the world's largest operational solar central receiver power plant (Figure 1). Solar One is jointly owned by the U. S. Department of Energy and Southern California Edison. A two year Test and Evaluation Phase, which was concluded in August 1984, characterized the various plant subsystems (receiver, collector, turbine generator, and thermal storage). During the three year Power Production Phase, which followed the Test and Evaluation Phase, the plant was operated as a power plant and supplied electricity to the Southern California Edison grid. These experiments were performed as part of the receiver evaluation, to measure the convective heat transfer from the receiver. The results of these convective loss experiments are described in this report. Preliminary results were presented in a status report [1] in June 1984.

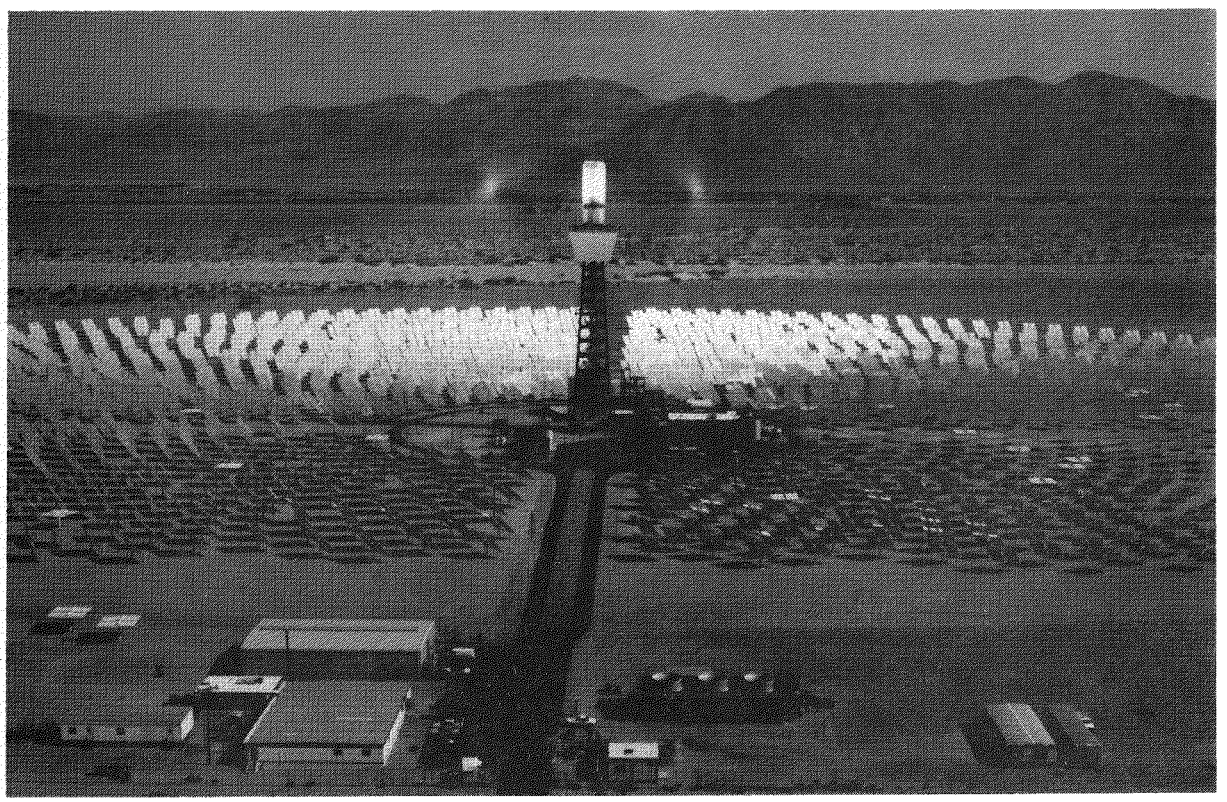

Figure 1. 10 MW_e Solar Thermal Central Receiver Pilot Plant near Barstow, California

Determining the convective loss will help reduce the uncertainty in the calculation of thermal efficiency for solar central receivers [2,3]. Receiver thermal efficiency calculation which makes use of thermal loss measurements and/or loss calculations has been shown to be more accurate in some cases than simply dividing absorbed power by incident power. Convective heat transfer represents a significant fraction of the energy lost from the front surface of the receiver. While energy transfer by radiation and conduction from an external receiver can be well characterized, the same cannot be said for convection.

The problem of quantifying convective losses from solar central receivers with reasonable accuracy was recognized in the late 1970's. Programs were then initiated to address the issue from several angles. An overview of these studies is presented in Reference 4.

University research programs were conducted to develop computer models of this complex, three-dimensional problem for both external and cavity receivers. Afshari and Ferziger [5,6] worked on modeling mixed convection around an external, cylindrical receiver. Evans and Plumb [7,8] successfully modeled both laminar and turbulent mixed convection from a vertical, heated surface. LeQuere et al. [9] worked on the cavity receiver modeling effort at the University of California at Berkeley.

Controlled laboratory experiments were performed to study the basic problem of turbulent, mixed convection from a heated surface. Kraabel [10] studied the convection heat transfer from a 2.15m x 2.15m x 2.15m, electrically heated cavity. Humphrey et al. [11] used detailed heat transfer measurements in addition to flow visualization to study the convection heat transfer from a cavity. These measurements were also used to verify portions of the cavity modeling effort. Clausing et al. [12] studied mixed convection heat transfer from a cylinder in a cryogenic wind tunnel, and Siebers et al. [13,14,15] studied mixed convection from a 3m x 3m electrically heated flat plate in a wind tunnel.

Field experiments were also undertaken to provide overall measurements of convective losses from central receivers. Kraabel [16] made convective loss measurements from a cavity receiver in Almeria, Spain. Jacobs et al. [17] made additional measurements of convective losses at the Almeria cavity receiver. McMordie [18] made convective loss measurements from a cavity receiver at the Central Receiver Test Facility in Albuquerque. Beninga and Buna [19] reported a single convective coefficient for the same cavity receiver as McMordie studied in addition to describing an alternative way to make field measurements of convective losses. All of these field tests have been conducted with cavity receivers. Solar One is the only cylindrical external receiver currently in the field and thus presents a unique opportunity to conduct field measurements of convective losses.

The goal of the Solar One experiments described in this report was to provide convective loss measurements to determine the convective coefficient for the receiver. The measured convective coefficient has been compared to the convective coefficient predicted from correlations developed by Siebers and Kraabel [20]; the

agreement between the two has been assessed. Experimentally verified correlations are necessary to predict convective losses from Solar One or from other external central receiver designs. The Solar One receiver presents a unique opportunity for performing convective heat transfer measurements on a large cylinder.

The convective heat transfer process at Solar One is characterized by mixed convection, a combination of both natural and forced convection. Two important dimensionless numbers in correlations for mixed convection are the Grashof number and the Reynolds number. The Grashof number (for natural convection), Gr, is a measure of the ratio of buoyant to viscous forces, and the Reynolds number (for forced convection), Re, is a measure of the ratio of inertial to viscous forces. For the case of an external central receiver, these forces interact to produce a fully three-dimensional flow field. Fundamental understanding of the mixed convection process for a cylindrical geometry is poor. Abrams [21] has recently summarized the available mixed convection literature, particularly that which applies to solar central receiver operation. Figure 2 shows the additions that have been made by recent convection research. Little experimental data exist for the case of a cylinder in three-dimensional mixed convection, especially in the Grashof number range (10^{14}) that characterizes the Solar One receiver. The range of wind speeds and wall temperatures in the experiments as well as under operating conditions includes both natural and forced convective effects.

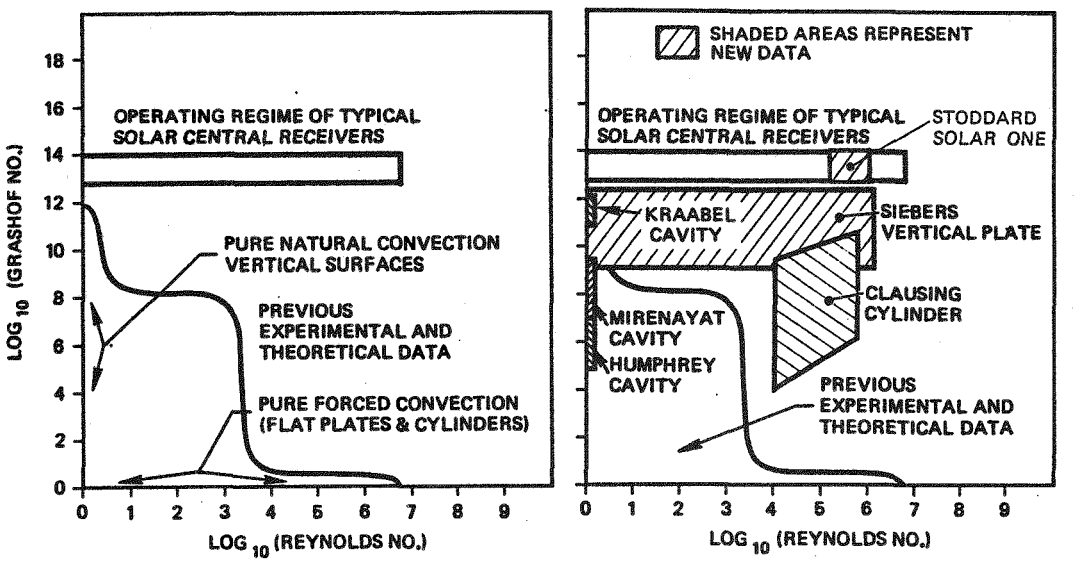

(a) 1979 (a) 1985

Figure 2. Progress in convective loss research from 1979-1985. Boundaries of the regions are approximate.

The experiments in this study were performed with no flux on the receiver to eliminate uncertainties associated with determining incident solar flux. The wall to ambient temperature difference was a factor of three below that of the normal operating receiver. The reduced wall temperature, however, does not greatly alter the results. Correlations [20] indicate that as the wall temperature is increased toward the normal operating temperature, the mixed convective coefficient decreases slightly. As wall temperature increases, natural convection increases (due to enhanced buoyancy), but forced convection decreases (due to changing air properties). Since forced convective effects usually dominate the mixed convective coefficient in this experiment, the net effect is a decrease in mixed convection. Calculations which illustrate this conclusion are presented in Appendix B.

This report provides both qualitative and quantitative information on total and local convective losses from the Solar One central receiver. In the first section, a physical description of the receiver and the test method is provided. This is followed by a development of the data analysis equations and a description of the test results. Two types of results are derived from this data: (*i*) the overall receiver convective coefficient, and (*ii*) detailed information on the local (panel) losses as a function of wind direction. The most important results from the experiments are summarized in the conclusion section. Four appendices describe (*i*) the root-sum-square uncertainty analysis, (*ii*) the effect of lower wall temperature testing, (*iii*) the complete panel data, in plotted form, and (*iv*) the effect of convective losses on receiver performance during normal plant operation, using the Siebers and Kraabel correlations.

Receiver and Experiment Description

Solar One Central Receiver

The Solar One central receiver is composed of twenty-four panels, six of which are preheat and the remaining eighteen being "once-through to superheat" boiler panels. Each panel is made up of seventy 1.27 cm (1/2-inch) diameter tubes, welded together, and is 0.9 meters (35 in) wide by 13.7 meters (45 ft) long. The receiver, shown in Figures 3 and 4, is a cylinder 7.0 meters (23 ft) in diameter and 13.7 meters in length. Water flows up the tower through a single pipe. The pipe splits and water flows up through the first three preheat panels and then up through the next three preheat panels. The flows are then recombined in a ring manifold which simultaneously feeds all eighteen boiler panels. All panel flows are from the bottom to the top of the panel. Boiler panel flows are individually controlled and monitored to provide the desired output: steam at 455 °C (850 °F) and 10.0×10^6 N/m^2 (1450 psi).

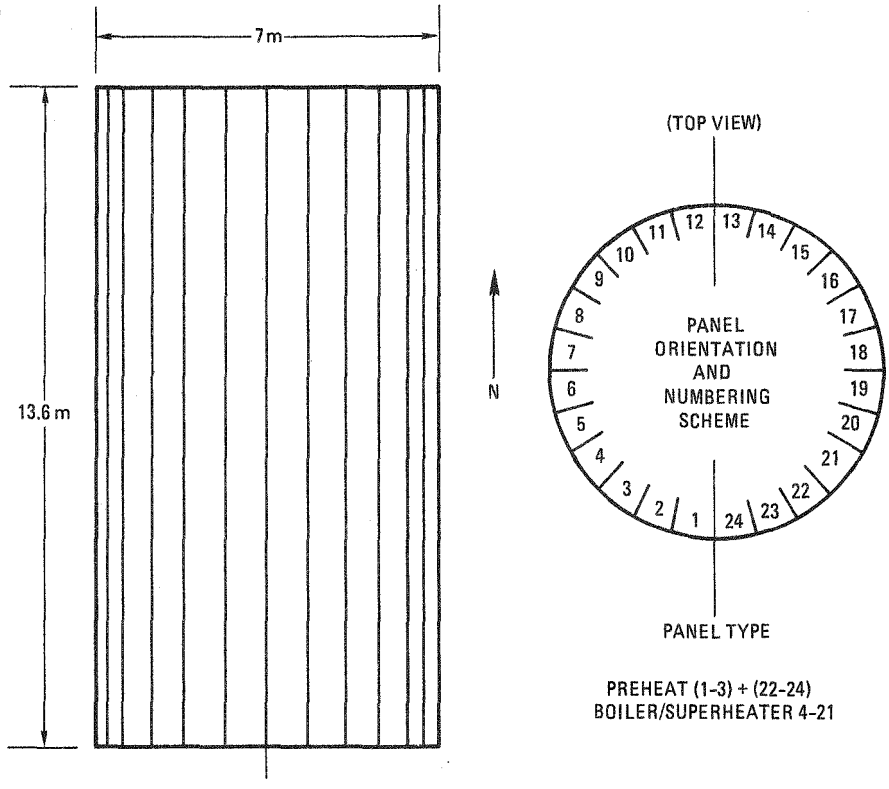

Figure 3. Receiver physical characteristics

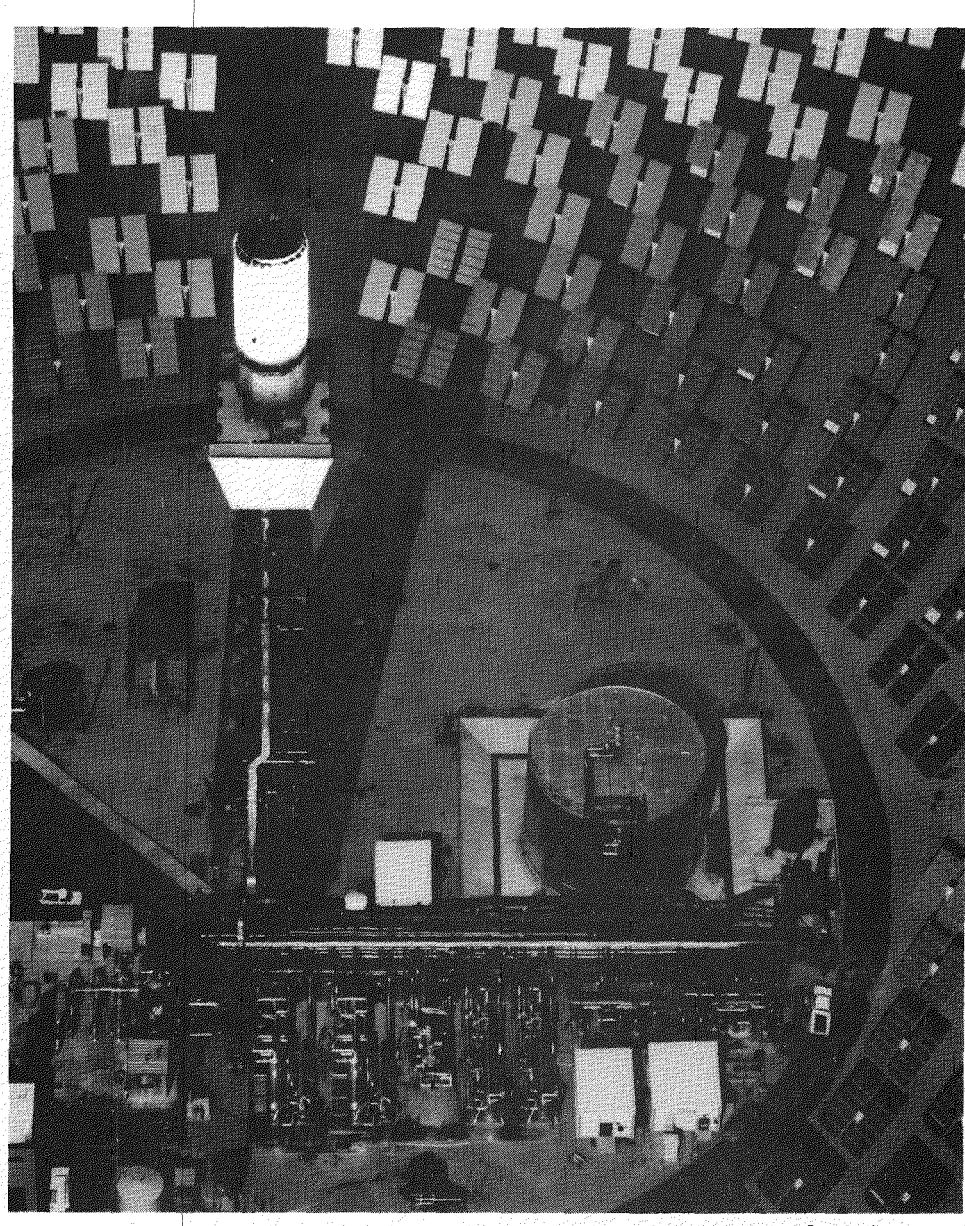

Figure 4. Solar One central receiver, with associated piping

An energy balance can be defined around the operating receiver as the power into the receiver equal to the power out of the receiver. Explicitly, the power incident on the receiver (P_{inc} = solar flux) equals the power gained by the receiver working fluid (P_{abs}) plus the power lost through reflection (P_{refl}), thermal radiation (P_{rad}), convection (P_{conv}), and conduction (P_{cond}).

$$P_{inc} = P_{abs} + P_{refl} + P_{rad} + P_{conv} + P_{cond}$$

Thus, convective losses (P_{conv}) can be inferred from data gathered during receiver operations provided that a reasonable measurement or calculation can be made of the other terms of the energy balance. However, a solar flux measurement system does not currently exist at Solar One; solar flux must be predicted from a computer code, which results in large uncertainties. The effect of wind speed on receiver efficiency has been sought in data from normal plant operations [22]. The results from

these analyses have proven inconclusive, with considerable scatter in the data. Apparently, the large uncertainties associated with estimating P_{inc} obscure any careful attempts to measure convective losses during receiver operation at Solar One.

In order to obtain meaningful results from the convective loss experiments, an experiment was designed in which solar flux was not a variable. To accomplish this, the convective loss experiments were performed mostly at night with no concentrated solar flux on the receiver.

Description of Experiment

Heated receiver feedwater is circulated through the receiver, exactly as it is during normal receiver operations; however there is no solar flux on the receiver. The total energy loss to the environment is measured as the energy loss in the feedwater as it passes through the receiver. The energy lost by conduction and thermal radiation is calculated, and the balance of the loss is attributed to convection. A root-sum-square error analysis was performed on the data analysis equations to quantify the uncertainty in the resultant convective coefficient.

The flow diagram of this experiment (Figure 5) is straightforward. The major requirement for the experiment was to find a way to heat the receiver feedwater. The thermal storage subsystem answered this requirement. Prior to running the test, the thermal storage tank was fully "charged"; that is, the thermal storage medium (oil) was heated during solar operations. Steam was then generated by operating an extraction heat exchanger, which transfers heat stored in the oil to generate steam. A small pipe added to the system transported the steam to one of the receiver feedwater heaters. Within one hour, the receiver feedwater was brought up to 180 °C (355 °F) and 3.45×10^6 N/m^2 (500 psi), the limit of the system, at which time the testing commenced.

Instrumentation and Data Acquisition

The Solar One Pilot Plant Data Acquisition System was used to record the test data. Only one addition was made to the plant instrumentation for these tests. A differential thermocouple was added to accurately determine the temperature difference between the receiver inlet and outlet. Plant instrumentation which provided the remaining data included thermocouples, flowmeters, and meteorological instruments.

Data Acquisition System–The data system scan rate for the receiver instrumentation is once every ten seconds. For the meteorological instrumentation it is once every sixty seconds. Data are recorded in engineering units. All data points used in this analysis are five minute averages of either the 10 or 60 second data. The data processing software package used in this analysis was written and is maintained by McDonnell Douglas Astronautics Company. The data processing program reads raw plant data tapes and provides either tabular output averaged over a requested time interval or plotted instrument output as a function of time. Both types of

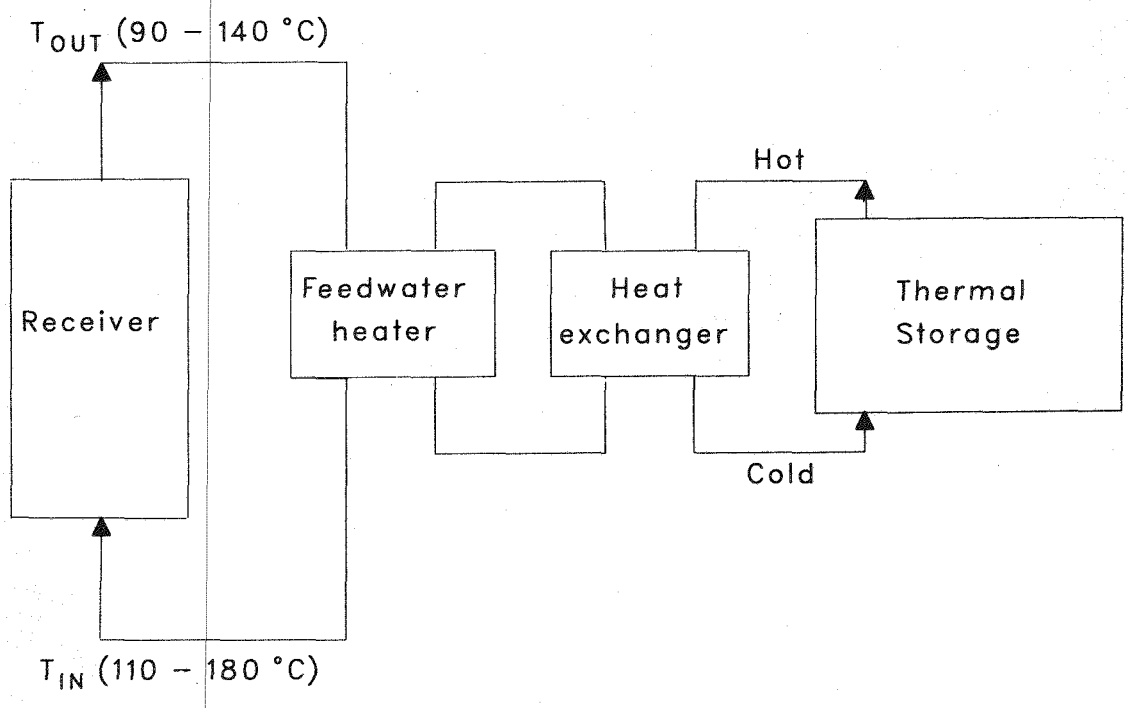

Figure 5. Convective loss experiment flow diagram

data processing were used, the tabular results providing data values and the plotted results providing time traces of various instruments for monitoring stability of flows or wind speeds, for example. Also, data analysis software was written to manipulate data and calculate results.

Thermocouples–Chromel-Alumel (Type K) thermocouples provided the preheat panel inlet (receiver inlet), ring manifold, mixed receiver outlet, and individual boiler panel outlet temperatures. These thermocouples are nominally ranged at –18 to 815 °C (0 to 1500 °F), except for the inlet thermocouples ranged at –18 to 260 °C (0 to 500 °F).

Flowmeters–Flowmeters, installed at the inlet to each of the eighteen boiler panels, provided the total receiver and individual panel flows. Three flowmeters are also located on the first pass of the preheat panels. The sum of these flows can be compared with the total flow from the eighteen flowmeters as a check for consistency. The flowmeters, manufactured by Ramapo, are generically called target-type, because the flow moves over a circular target on a cantilever beam. A strain gage mounted on the beam measures the deflection of the target, which is related to the flow rate. These flowmeters, like most flowmeters, lose accuracy at low flows. From flowmeter calibration test results, Abrams [23] recommended not using them to provide quantitative data at low flows. These calibration tests showed a steep decline in accuracy with decreasing flow rate, starting near 0.13 kg/s (1000 lb/hr), with a 25% flow deviation.

Meteorological Instrumentation–To measure and characterize the convective losses, four measurements are needed: dewpoint temperature, ambient temperature, wind speed, and wind direction. The meteorological instruments at Solar One

include two dewpoint temperature sensors and two ambient temperature sensors. These sensors are located at two stations: one in the heliostat field and the other at Level 7 (37.8m) on the receiver tower. The Level 7 data are used here.

For characterizing the wind, Solar One has wind direction vanes and anemometers. The anemometers are cup-type anemometers which measure the component of wind speed parallel to the ground. Twenty-four measurements of wind speed along with twelve measurements of wind direction are available at twelve locations throughout the plant. There are four stations at the edges of the heliostat field (north, east, south, and west), each with one anemometer, and six stations in the west field, each with an anemometer at 3.0, 6.1, and 10.0 meters.

Although standard correlations may be used [20] to estimate wind speed as a function of height above the ground, using ground level measurements, estimating the tower wind velocity with the correlations proved unsatisfactory. Solar One has two anemometer stations at Level 7 on the tower. These stations are located in the northeast and southwest corners of the tower. In the experiments, the tower anemometers were used to measure wind velocity since they provided actual data as opposed to extrapolated values. Since the two tower anemometers are 180 degrees apart on the receiver tower, one of them is obstructed by the tower depending on wind direction. It reads low due to this obstruction; thus, the higher velocity anemometer was used to supply the data.

Instrument Calibration– Preliminary analysis and a proof test (9/83) at the Pilot Plant [24] indicated that uncertainties in receiver fluid temperature measurements were so high that the experimental results would be rendered meaningless. Conflicting results were especially evident in redundant instrumentation, most notably at each boiler panel outlet, which has two thermocouples and one resistance temperature sensor. A campaign was undertaken to calibrate all receiver fluid thermocouples. Instruments which could not be checked in a calibration oven and/or adjusted to read correctly were removed from the data analysis instrumentation; these included resistance temperature sensors and preheat panel outlet thermocouples. During this campaign, a differential thermocouple circuit was installed between the receiver inlet and outlet for more accurate measurement of this temperature difference [25].

Accuracy in the thermocouples was also improved by calibrating the instruments in their expected range of use instead of at their limits. For example, the receiver outlet thermocouples were calibrated at 150 and 480 °C (300 and 900 °F) instead of at –18 and 815 °C (0 and 1500 °F). Also, since the data acquisition software uses a linear fit between the calibration points for temperature readings off the calibration points, software which interpolates the thermocouple table (2 °F increments) and makes corrections for this linear assumption was developed [25] for use in the convective loss data analysis program.

Receiver flow rate was another major source of error in the data analysis and the flow meters could not be calibrated prior to testing. Since flowmeters lose accuracy rapidly as flow rate decreases, the boiler panel flow rates were kept above 0.13

kg/s (1000 lb/hr) and then only in panels with low range flowmeters. This limit minimized the effect of the low flow range errors, yet still allowed flow rate to be a test variable.

The total receiver flow rate can be obtained in one of two ways: (*i*) by summing the three preheat flow rates or (*ii*) by summing the eighteen boiler panel flow rates. Error analysis shows that, in general, computing the total flow from the sum of eighteen boiler flows was more accurate than summing the three preheat flows. If each preheat flowmeter has a $\pm 5\%$ error, a $\pm 3\%$ error in the total mass flow rate results. However if each boiler panel flowmeter has a $\pm 5\%$ error, the error in the total mass flow rate is $\pm 1\%$. Each boiler flow rate must have a random error of $\pm 12\%$ before the error in the total mass flow rate equals that calculated from the three flowmeter sum.

Summary–The primary sources of error were identified prior to the experiments as solar flux calculation, receiver mass flow rate measurement, and receiver fluid temperature measurement. These potential problem areas were addressed in the experimental design in the following ways:

1. All tests were conducted with no solar flux on the receiver to eliminate the uncertainty associated with flux calculations (there are no solar flux measurements at Solar One). Except for one test set which was conducted on an overcast day, all tests were conducted at night, which eliminated the need to account for any solar input.

2. Individual boiler panel flow rates were at least 0.13 kg/s (1000 lb/hr). Flow rates less than this have unacceptably large measurement uncertainties.

3. All receiver fluid thermocouples used in the data analysis were calibrated.

Data Analysis Approach

The data analysis was divided into two categories: total receiver and panel data analyses. Both analyses refer to the measurement of energy loss: $\dot{m}C_p(T_{in} - T_{out})$.

In the receiver analysis, the receiver is considered a cylinder, with only one inlet, one outlet, and one mass flow rate. One convective coefficient is calculated for the entire cylinder. This convective coefficient is then compared with that predicted using the correlations from Siebers and Kraabel [20]. A goal of this experiment was to validate these correlations.

Local mixed convective heat transfer data has been obtained from individual panel measurements. An energy balance is formed for each panel in the same manner as for the entire receiver. Thus, a convective coefficient is calculated for each panel. No comparison with correlation is possible since there are no available correlations to predict convective coefficients on roughened flat plates as a function of wind speed and direction. However, the data are presented and the trends in heat transfer versus wind direction are compared with published data on flow over a roughened cylinder. An area-averaged convective coefficient is then calculated for the cylinder from the panel data and compared with the total cylinder calculation of the same quantity.

Measured Convective Coefficient

After the total heat loss from the receiver or the panel was measured, the convective heat loss was obtained by subtracting the calculated radiative and conductive losses. The equations used to calculate the radiation and conduction losses are described in this section.

Total Heat Loss–The total heat transfer, Q_{total}, was the primary measurement in the experiments. It is calculated as:

$$Q_{total} = \dot{m}\, C_p\, \Delta T \tag{1}$$

The mass flow rate, $\dot{m}$, for the entire receiver is a calculated quantity. It is the sum of the eighteen measured boiler panel flows after corrections have been applied for the density difference in water at operating versus calibration temperature. The mass flow rate for a boiler panel is the density corrected reading from its individual flowmeter. The specific heat is calculated at the average water temperature. The temperature difference, ΔT, for the entire receiver is measured directly using a differential thermocouple installed between the inlet and outlet of the receiver. The differential thermocouple is used for improving the accuracy of the measurement.

The temperature difference between the inlet and outlet of a boiler panel is the difference between the mixed fluid temperature in the ring manifold and the average of the two outlet thermocouples located at the outlet of each panel.

Thermal Radiation Loss–The receiver loses thermal energy by radiating to its surroundings—the sky and the ground.

$$Q_{rad} = \epsilon\, A\, \sigma (0.5\,(T_{wall}^4 - T_{sky}^4) + 0.5\,(T_{wall}^4 - T_{\infty}^4)) \tag{2}$$

The radiation, Q_{rad}, is split between the ground and the sky. The ground is assumed to be at the ambient air temperature, T_{∞} and the sky temperature, T_{sky}, is estimated using a method described by Berdahl and Fromberg [26]. The sky radiance can be described in alternate ways: $\sigma\, T_{sky}^4$ or $\epsilon_{sky}\, \sigma\, T_{\infty}^4$. A relationship between sky temperature and ambient temperature in terms of sky emissivity may be derived as:

$$T_{sky} = (\epsilon_{sky})^{0.25}\, T_{\infty} \tag{3}$$

Berdahl and Fromberg have correlated sky emissivity with dewpoint temperature for clear sky conditions according to the formula:

$$\epsilon_{sky} = 0.741 + 0.0062\, T_{dewpt}. \tag{4}$$

The difference between the receiver radiating only to the sky and radiating to both the sky and ground is small. However, for this experiment in which the wall temperature is low, even this small difference is appreciable. The assumption that the receiver radiates to both the sky and the ground reduces the radiative loss and increases the convective coefficient from 1.5 to 11% of its original value. The magnitude of this increase depends on the magnitude of the driving potential for radiation, that is, $({T_{wall}}^4 - {T_{sky}}^4)$ or $({T_{wall}}^4 - {T_{\infty}}^4)$, where the temperatures are absolute temperatures (Kelvin). For the lower bound, there is about 100K (180 °R) difference between T_{∞} and T_{wall}, whereas for the upper bound this temperature difference is 140K (250 °R).

The measured value of Solar One infrared emissivity is 0.80 ±0.1 [27]. An effective emissivity value, which uses the measured emissivity and incorporates the effect of the tube shape, is used for the receiver. Calculations have been performed [28] which use detailed shapefactor calculations and account for the scalloped tube surfaces causing some tubes to radiate to other tubes rather than to the environment. However, the radiating area is the total surface area of the scalloped receiver tubes and not its projected area (normally used for receiver area). So, while there is a decrease in overall radiation due to reabsorption of some radiative losses, the true surface area is increased and the net result is to increase the emissivity of the surface. The equation which describes this interaction for Solar One receiver tubes is given by:

$$\epsilon = \frac{1}{1 + \frac{2}{\pi}\left(\frac{1}{\epsilon_{flat}} - 1\right)}. \tag{5}$$

This equation results in an increase in apparent emissivity from 0.80 to 0.86. Incorporation of this change into the radiation loss calculation typically causes a decrease in the measured convective coefficients of from 2.5 to 10 percent. The effect is greater when radiation is a large portion of the total loss or when wall temperatures are higher.

The computer code SAPPHIR [29] was used to develop a simple expression for the wall temperature calculation. SAPPHIR models the thermal and hydraulic behavior of a Solar One boiler panel, representing the panel as a single tube. The code was used to calculate the average front wall temperature of representative panels under the test conditions. This average T_{wall} was then compared to an estimation of the same quantity using the average of the fluid inlet and outlet temperatures. There was a seven percent difference between the average wall temperature from the SAPPHIR calculation and the average wall temperature calculated as the arithmetic average of the inlet and outlet fluid temperatures. The difference between the SAPPHIR calculation and the average fluid temperature was therefore accounted for by using a weighted average, biased seven percent toward the outlet temperature. For a single panel, the average temperature is calculated using the ring manifold temperature as the inlet and the average of two thermocouples as the outlet temperature. For the entire receiver average temperature, an area-weighted average is calculated, with the six preheat panels comprising 25% of the receiver area, and the eighteen boiler panels the remaining 75%. A single average wall temperature is then calculated from these two areas by using three temperature measurements: the preheat inlet, the ring manifold (outlet temperature for the preheat panels and inlet temperature for the boiler panels), and the mixed receiver outlet temperature.

Conduction Loss–The conduction heat loss is a small percentage of the total heat loss from the cylinder, usually ranging from 3 to 6 percent. The conduction heat transfer, Q_{cond}, is calculated by:

$$Q_{cond} = kA(T_{wall} - T_{core}). \tag{6}$$

The back of the receiver is insulated with Kaowool insulation, 5.1 cm. thick. The conduction coefficient, k, is 1.136 W/m^2 °C [30]. The front wall temperature is used as T_{wall} for this calculation and the ambient air temperature serves as T_{core}, the receiver core temperature. Receiver backwall thermocouples do exist, so a better representation of backwall temperature could be made; however, there is no measurement of the core temperature, which is certainly higher than ambient temperature. Therefore, both front wall and ambient temperatures are low estimates, so the net effect of their difference is retained and a reasonable estimate of Q_{cond} is obtained.

Convective Heat Loss–The convective heat loss, Q_{conv}, is computed as the total heat loss minus the radiative and conduction losses.

$$Q_{conv} = \dot{m}\, C_p\, \Delta T - \epsilon\, A\, \sigma(0.5(T_{wall}^4 - T_{sky}^4) + 0.5(T_{wall}^4 - T_{\infty}^4)) - k\, A(T_{wall} - T_{\infty}) \tag{7}$$

$$Q_{conv} = h_{meas}\, A\, (T_{wall} - T_{\infty}). \tag{8}$$

By setting the right sides of equations (7) and (8) equal, the measured convective coefficient, h_{meas}, can be computed.

Predicted Mixed Convective Coefficient

The mixed convective coefficient, h_{pred}, is calculated using correlations proposed by Siebers and Kraabel [20] for an external, cylindrical central receiver. The natural and forced convective coefficients are calculated separately and then combined using the relation:

$$h_{pred} = (h_{nat}^{a} + h_{forc}^{a})^{1/a}, \text{ where } a = 3.2. \tag{9}$$

Natural Convective Coefficient–The natural convective correlation was developed by Siebers et al.[15] for heat transfer from a heated flat plate. The Solar One receiver is large enough that, in natural convective, it can be treated as a flat plate. Properties are calculated at the ambient temperature.

$$Nu_L = \frac{h_{nat}\, L}{k_{air}} = 0.098 Gr_L^{1/3} \left(\frac{T_{wall}}{T_{\infty}}\right)^{-0.14} \tag{10}$$

$$h_{nat}(rough) = \left(\frac{\pi}{2}\right) h_{nat}(smooth) \tag{11}$$

The inclusion of the factor $\pi/2$ was recommended by Siebers and Kraabel [20] to account for the effects of surface roughness of the tubes which could enhance the heat transfer.

Forced Convective Coefficient–The forced convective correlation has been interpolated for Solar One tube-sized roughness elements from the correlations presented by Siebers and Kraabel. A roughness parameter, k_s/d, of 90×10^{-5} is computed by defining k_s as the tube radius and d as the receiver diameter. Siebers notes that using the tube radius for k_s is probably a conservative estimate. This overestimation of the roughness elements may result in a slight overprediction of the convective coefficient. Thus, the forced convection correlation becomes:

$$Nu_d = \frac{h_{forc}\, d}{k_{air}} = 0.93(2.57 \times 10^{-3}) Re_d^{0.98} + 0.07(0.0135 Re_d^{0.89}). \tag{12}$$

This correlation is valid for $3.7 \times 10^5 \leq Re_d < 1.0 \times 10^7$. Properties are calculated at the film temperature. Measurements required for the calculation of h_{pred} include receiver wall temperature (T_{wall}), ambient temperature (T_{∞}), and wind velocity (u_{∞}). The wall and ambient temperatures are identical to those used in calculating h_{meas}.

Cylinder Data Analysis

Results

Convective loss tests were conducted on nine test days from February through July 1984. During these test days, a total of twenty-three data points were gathered. The data were analyzed to provide measured convective coefficients for each data point. Corresponding predicted convective coefficients were computed based on measured values of ambient wind speed and temperature, and receiver wall temperature. These results as well as the conditions during individual tests are presented in this section. Various plots are presented, accompanied by brief interpretive discussions. The discussion of individual test day conditions, which follows the plot presentation, gives interpretation to the plotted data. Results of the root-sum-square uncertainty analyses for both h_{meas} and h_{pred} are then presented.

Convective Coefficient versus Wind Speed–The measured convective coefficient, calculated from Equations (1–8), is plotted versus the ambient wind speed in Figure 6. The plot shows a clear increase in the convective coefficient as wind speed increases. Although the *calculation* of h_{meas} is independent of wind speed, u_∞, Figure 6 shows that h_{meas} increases with u_∞.

The predicted convective coefficient, h_{pred}, is plotted versus wind speed in Figure 7. Forced convection influences all calculations of h_{pred}. For lower wind speeds, the magnitude of the natural convective coefficient, h_{nat}, is roughly twice that of the forced convective coefficient, h_{forc}. At higher wind speeds, h_{pred} is completely dominated by h_{forc}. Both wind speed and wall temperature are used in the calculation of h_{pred}. The wall temperature dependence is present through the air property calculation in h_{forc} at the film temperature ($T_f = (T_{wall} + T_\infty)/2$). The wind speed dependence in the forced convective coefficient is strong (Eq. (12)), with a Reynolds number power of about 0.95. By comparison, the forced convection correlation for the smooth cylinder has a weaker dependence with a Reynolds number power of about 0.60.

Measured versus Predicted Convective Coefficient–The measured convective coefficient is plotted against the predicted convective coefficient in Figure 8. The solid line indicates where perfect agreement between the measured and predicted quantities would lie. The agreement between h_{meas} and h_{pred} is quite good, considering the uncertainties associated with both the data and the prediction. The correlation overpredicts the measured convective coefficient by roughly ten percent.

Two additional plots can be examined to understand in more detail the comparison between h_{meas} and h_{pred}. The first plot (Figure 9) shows the ratio of the

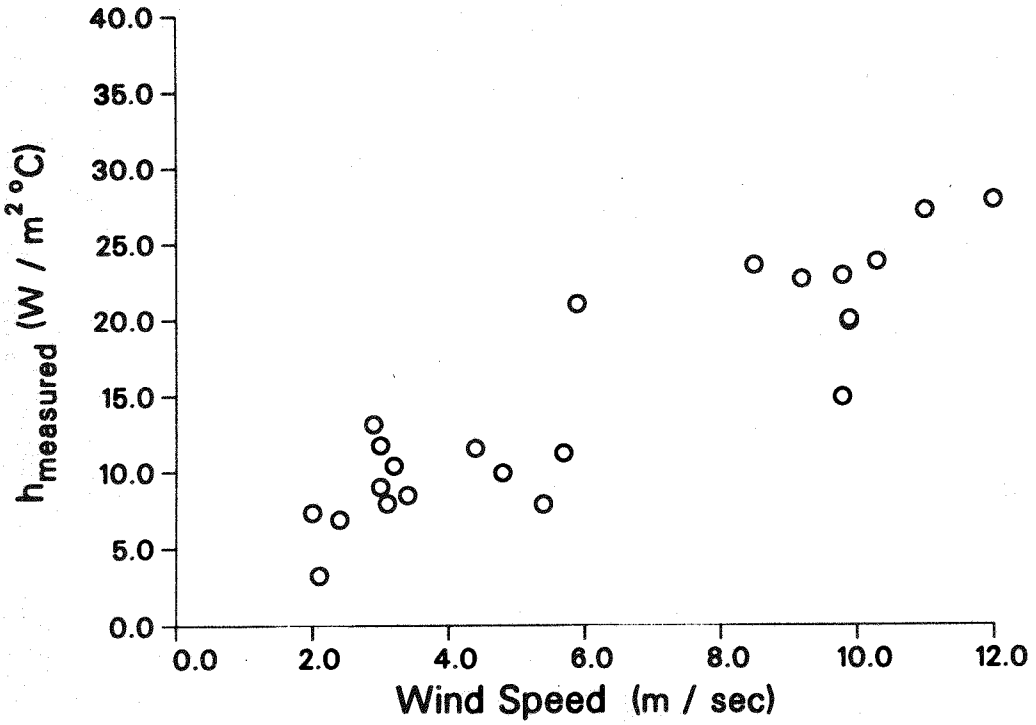

Figure 6. Measured convective coefficient as a function of wind speed

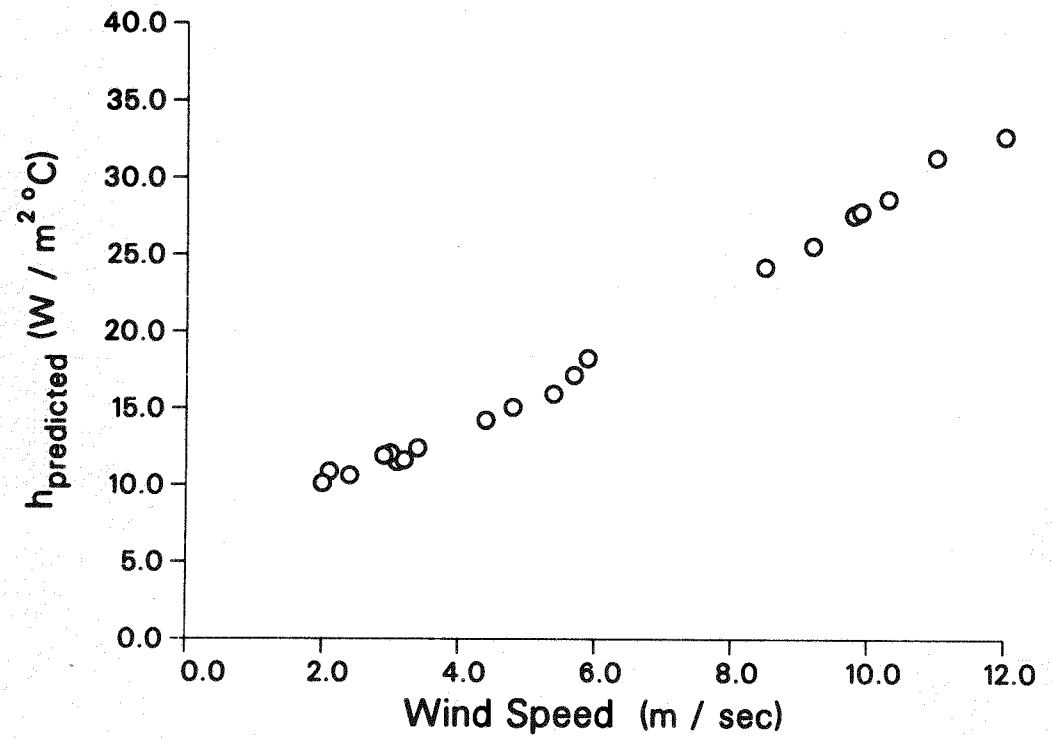

Figure 7. Predicted convective coefficient as a function of wind speed

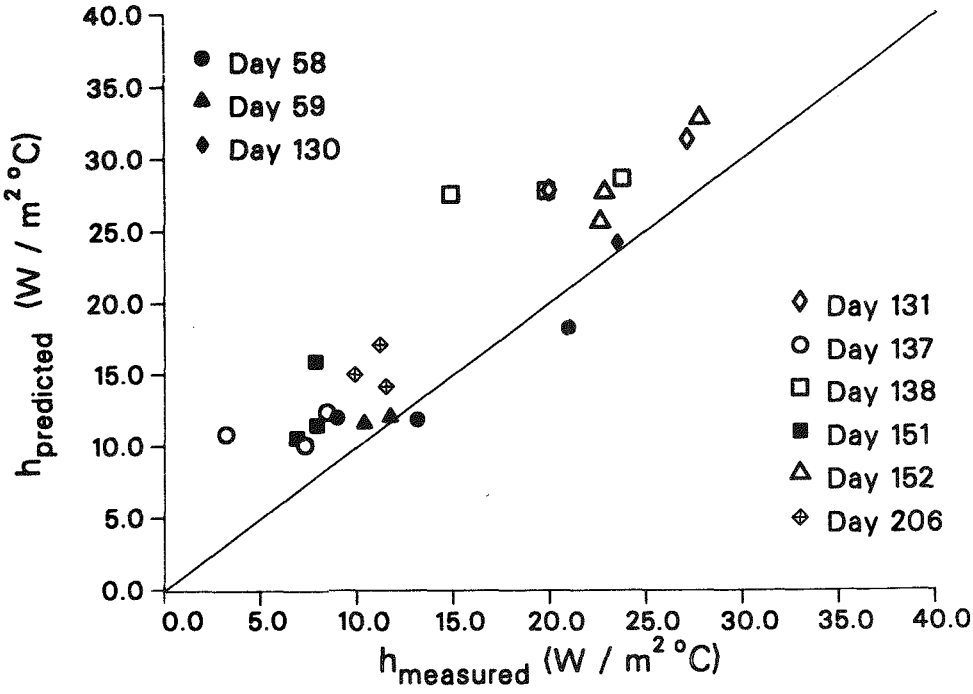

Figure 8. Measured versus predicted convective coefficient

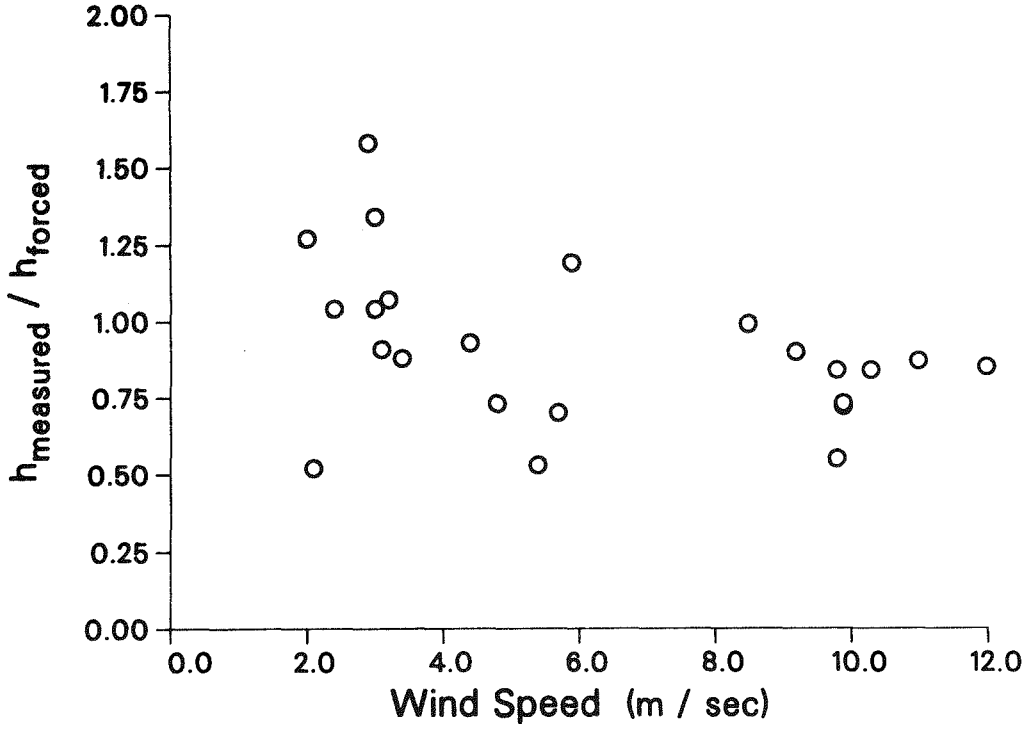

Figure 9. $h_{measured}/h_{forced}$ as a function of wind speed

measured and the forced convective coefficients plotted versus wind speed. At low wind speeds, the measured convective coefficient ranges from half of the predicted forced convective coefficient to 1.6 times h_{forc}. At low wind speeds, h_{forc} is relatively small. The variation in h_{meas}/h_{forc} for a single wind speed shows (*i*) a variation in the contribution of natural convection to the measured convective coefficient and (*ii*) scatter in the data. As wind speed increases, the range of values for h_{meas}/h_{forc} decreases, and above a wind speed of 10 m/s, the ratio becomes constant at about 0.90. At these wind speeds, h_{forc} completely dominates the mixed convective coefficient calculation, so if the correlation was to accurately predict the measurements, the ratio of h_{meas}/h_{forc} would equal 1.0 at high wind speeds. The difference between 1.0 and 0.90 is the magnitude of disagreement between h_{pred} and h_{meas} when forced convection dominates.

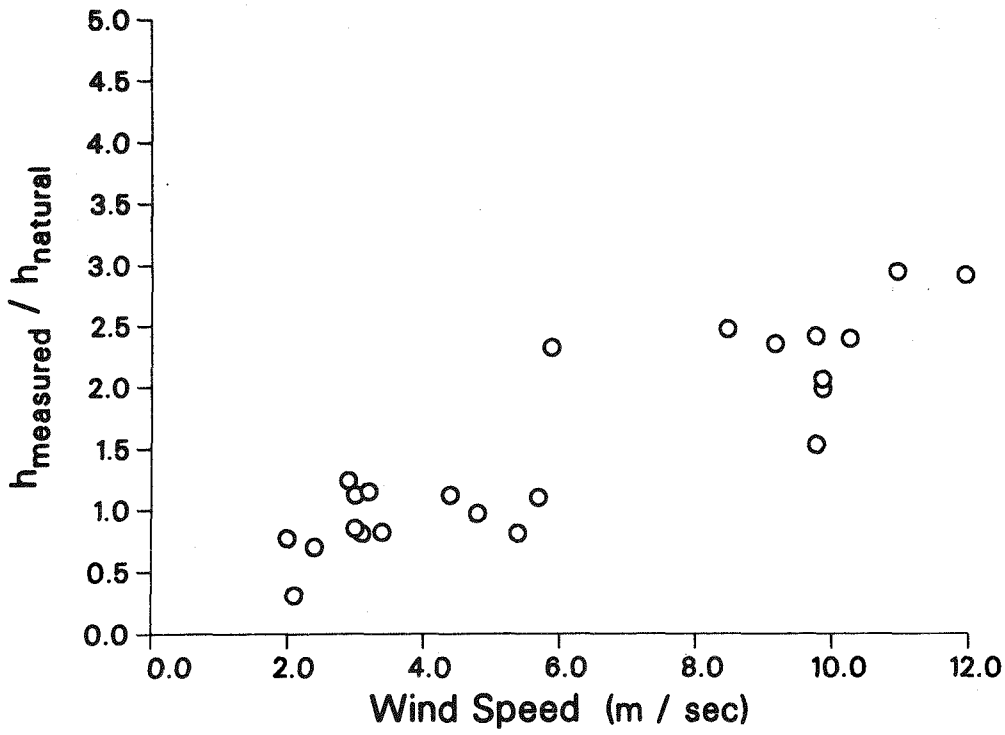

Figure 10. $h_{measured}/h_{natural}$ versus wind speed

Likewise, plotting h_{meas}/h_{nat} versus wind speed (Figure 10) highlights how well the natural convection correlation predicts the measured convective coefficient at low wind speeds. The natural convective coefficient, h_{nat}, is not dependent upon wind speed, but upon receiver wall temperature. So, for relatively constant wall temperatures, h_{nat} remains virtually constant. However, as shown in Figure 6, h_{meas} increases with wind speed. Thus, the ratio h_{meas}/h_{nat} also increases with wind speed. Under ideal conditions (perfect agreement between measurement and prediction) the ratio h_{meas}/h_{nat} would never be less than unity, since that means the measured convective coefficient is less than the contribution from natural convection alone. Ideally, the curve of h_{meas}/h_{nat} would remain unity from wind speeds of zero up to the point where forced convection becomes a significant contributor. The curve would then begin to increase with wind speed as the total

heat transfer was more and more influenced by the forced convection contributions. Figure 10 depicts less than ideal agreement between measurement and prediction, with eight data points having the ratio h_{meas}/h_{nat} less than unity. This plot indicates that h_{nat} overpredicts the total convective loss.

One simple adjustment can be made to the natural convection correlation which will reduce its magnitude on the low end. In the recommended correlations [20] for external receivers, a factor of $\pi/2$ is added to account for the unknown effect of surface roughness introduced by the receiver tubes (Eq. (11)). It was felt that roughness could serve to enhance the natural convective heat transfer, but to what extent was unknown. The experimental data indicate that inclusion of the recommended roughness factor is not warranted.

The same plot of h_{meas}/h_{nat} versus wind speed, is shown in Figure 11 where the natural convective coefficient was calculated without the roughness factor. Now only one point has the ratio h_{meas}/h_{nat} less than unity. For completeness, h_{meas} versus h_{pred} is replotted in Figure 12 with the $\pi/2$ factor removed from the natural convection correlation. The effect of this change is evidenced by better agreement between measurement and prediction for convective coefficients less than about 10 $W/m^2\,°C$.

Interpretation of Results

The results of the data analysis show good agreement between the measured convective coefficient and that predicted using the correlations proposed by Siebers and Kraabel. The scatter in the data is primarily the result of the large experimental uncertainties inherent in field testing. However, a more detailed examination of the particular conditions during each test does provide further insight into the results.

Test Conditions–Table 1 summarizes the receiver and ambient conditions during the convective loss testing. The test numbers (1–23) have been assigned for convenience. The day number refers to the Julian date in 1984 on which that particular test was run. In general, two or three tests were run per test date. Table 2 gives the results of Siebers and Kraabel's correlations for the test conditions.

Early in the testing, there are some tests with lower than normal inlet temperatures. The lower inlet temperatures resulted from physical difficulties which arose during some tests that kept us from achieving a higher inlet temperature. The goal was to always achieve the highest possible inlet temperature. However, if steady conditions were reached at a low inlet temperature, the data point was taken. Note that tests 1, 4–7, and 9 have low inlet temperatures.

During successive tests on the same test date, the variable that was intentionally changed was the receiver mass flow rate. Each of the eighteen boiler panel flow valves was adjusted. The goal, which was realized more often in the latter half of the test program, was to run one high flow case, one medium flow case, and one low flow case. Different groups of panels have different sizes of flow control valves;

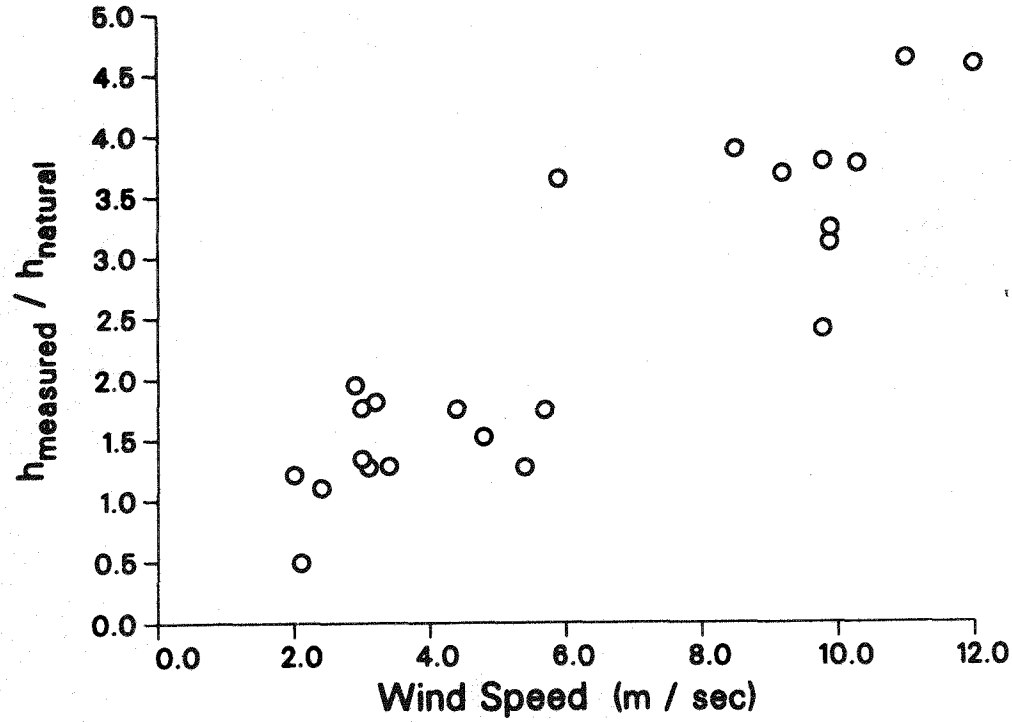

Figure 11. $h_{measured}/h_{natural}$ versus wind speed, no roughness factor

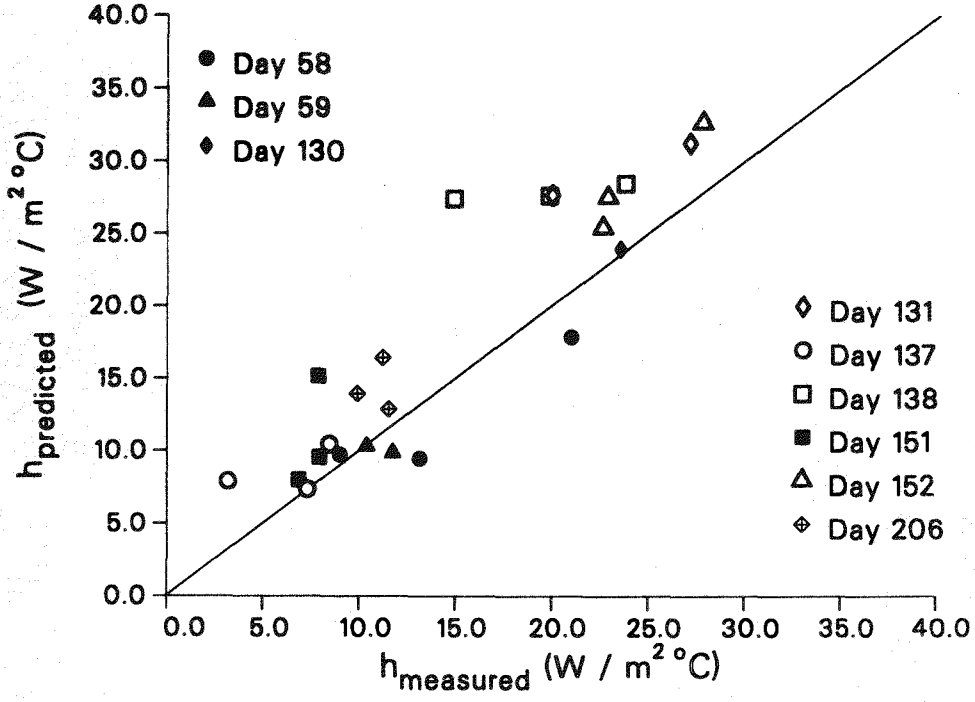

Figure 12. Measured versus predicted convective coefficient, no roughness factor

Table 1. Summary of Test Data

Test	Day	T_∞ °C	u_∞ m/s	T_{wall} °C	$\dot{m}$ kg/s	T_{in} °C	T_{out} °C	h_{meas} W/m^2°C
1	58-1	18.4	5.9	105.0	6.16	121.2	92.4	21.0
2	58-2	15.6	2.9	158.6	6.03	180.8	141.3	13.1
3	58-3	16.6	3.0	159.7	5.06	181.6	142.2	9.0
4	59-1	19.2	3.2	104.7	7.35	112.3	97.7	10.4
5	59-2	13.7	3.0	147.8	7.18	163.0	134.6	11.7
6	130-1	27.5	8.5	140.6	6.30	164.4	122.0	23.5
7	131-1	26.2	11.0	126.3	6.34	149.1	109.0	27.1
8	131-2	24.6	9.9	141.5	3.96	178.5	115.9	20.0
9	137-1	25.1	2.0	136.7	6.34	147.4	126.2	7.3
10	137-2	22.9	3.4	166.1	6.22	182.7	151.7	8.5
11	137-3	21.3	2.1	160.5	3.31	184.4	141.7	3.2
12	138-1	25.4	10.3	153.4	6.25	181.6	132.4	23.8
13	138-2	24.4	9.8	141.9	3.10	182.8	116.0	14.9
14	138-3	22.3	9.9	149.3	4.83	182.4	126.3	19.8
15	151-1	34.2	2.4	168.0	6.22	182.2	155.1	6.9
16	151-2	33.8	3.1	163.6	4.91	182.5	147.5	7.9
17	151-3	31.1	5.4	155.0	3.49	181.6	135.1	7.9
18	152-1	32.9	12.0	151.4	6.24	180.4	129.7	27.8
19	152-2	29.1	9.2	148.8	4.84	182.4	125.2	22.6
20	152-3	27.9	9.8	140.0	3.78	182.7	113.7	22.8
21	206-1	21.4	4.4	162.0	6.21	181.6	145.7	11.5
22	206-2	21.1	4.8	156.7	4.51	182.0	138.1	9.9
23	206-3	19.9	5.7	149.3	3.52	182.6	126.2	11.2

the high flow panels are located on the northern side of the receiver because the concentration of solar flux on these panels is greater. Higher flow rates, therefore larger control valves are required for the high flux panels. The high and low flow cases used boiler panel flow distributions which were in proportion to the control valve size, whereas in the medium flow case, the flows in each panel were nearly identical. The different distributions had no discernible effect on the results.

Tests 4 and 5 have exceptionally high flows because the flow valve on boiler panel 5 was stuck open, allowing about 1 kg/s (8000 lb/hr) of flow through that panel alone. During Test 1, five of the boiler panel flowmeters recorded severe oscillations (0 to 100 % of the flow setting). These oscillations most likely indicate that the flow control valves were oscillating between open and closed. The averaging technique used to obtain data points produced reasonable values for the flow in these panels, however, the resulting temperature drops in these panels are not consistent with those in neighboring panels. The details of these panel results will be discussed in the Panel Data Analysis section. The point is that, since the flow rates

Table 2. Predictions from Convective Correlations[20]

Test	Day	T_∞ °C	u_∞ m/s	T_{wall} °C	h_{nat} W/m^2°C	h_{forc} W/m^2°C	h_{pred} W/m^2°C
1	58-1	18.4	5.9	105.0	5.8	17.7	17.8
2	58-2	15.6	2.9	158.6	6.8	8.3	9.5
3	58-3	16.6	3.0	159.7	6.7	8.7	9.7
4	59-1	19.2	3.2	104.7	5.7	9.7	10.3
5	59-2	13.7	3.0	147.8	6.7	8.8	9.8
6	130-1	27.5	8.5	140.6	6.1	23.8	23.9
7	131-1	26.2	11.0	126.3	5.9	31.1	31.2
8	131-2	24.6	9.9	141.5	6.2	27.5	27.6
9	137-1	25.1	2.0	136.7	6.1	5.8	7.4
10	137-2	22.9	3.4	166.1	6.6	9.6	10.4
11	137-3	21.3	2.1	160.5	6.6	6.1	7.9
12	138-1	25.4	10.3	153.4	6.3	28.3	28.4
13	138-2	24.4	9.8	141.9	6.2	27.2	27.3
14	138-3	22.3	9.9	149.3	6.4	27.4	27.5
15	151-1	34.2	2.4	168.0	6.3	6.6	8.0
16	151-2	33.8	3.1	163.6	6.2	8.7	9.5
17	151-3	31.1	5.4	155.0	6.2	14.9	15.1
18	152-1	32.9	12.0	151.4	6.1	32.5	32.5
19	152-2	29.1	9.2	148.8	6.1	25.2	25.3
20	152-3	27.9	9.8	140.0	6.0	27.3	27.4
21	206-1	21.4	4.4	162.0	6.6	12.4	12.9
22	206-2	21.1	4.8	156.7	6.5	13.5	13.9
23	206-3	19.9	5.7	149.3	6.5	16.1	16.4

are suspect on a panel basis and the total flow is computed as the sum of the panel flows, Test 1 may not provide a good data point.

Other special circumstances during testing include the one test date (Day 151) on which all tests were run during the day. The day was completely overcast, with the threat of rain (which did not occur during the tests). All other tests were run on clear nights. The fact that the tests were run during the day does not seem to have noticeably influenced the test results. In addition, on Day 206, one of the electronic remote stations for processing the output of a group of instrumentation, was not working. This station processed much of the meteorological instrumentation, notably the receiver tower anemometers, and ambient and dewpoint temperature sensors. Therefore, it was necessary to use other field sensors to supply this data for Day 206.

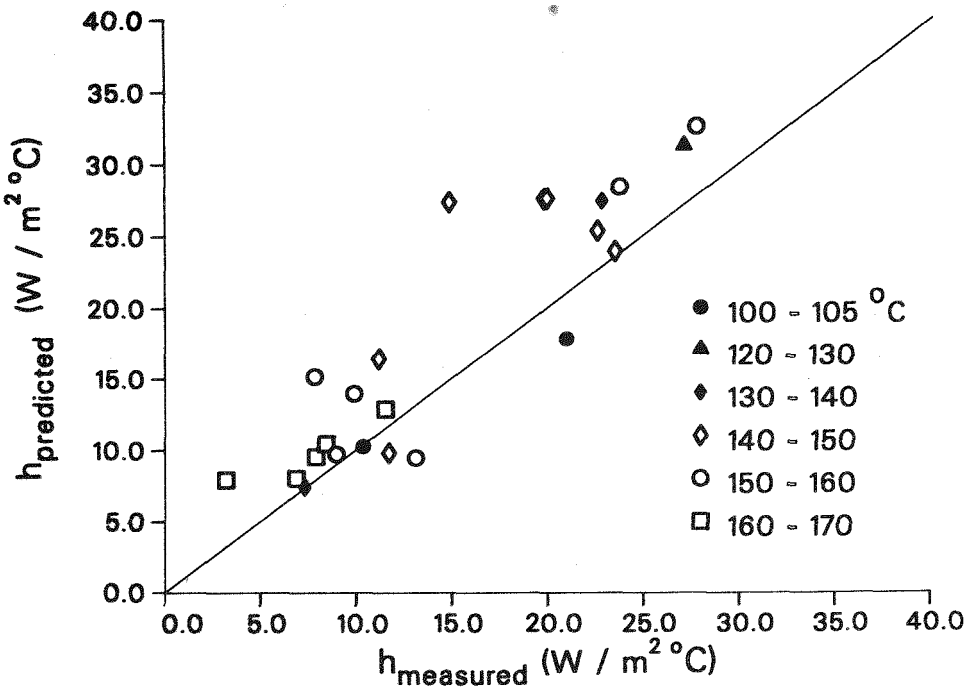

Figure 13. Effect of wall temperature

Influence on Test Results–Possible biases in the data resulting from these anomalous test conditions were examined. Test characteristics that were considered include wall temperature, mass flow rate, wind direction, wind direction fluctuations, and percent wind speed fluctuations. The results of these examinations are presented in a series of plots (Figures 13–17). The measured versus predicted convective coefficient was plotted and each data point was associated with a specified range of the test characteristic under consideration. The purpose of these plots is to determine if there are ranges of the test characteristic for which agreement between h_{meas} and h_{pred} tends to be better or worse.

Wall temperature was not a test variable; however a range of values resulted due to varying wind speeds and other physical test conditions which prohibited the inlet temperature from reaching its targeted value. Wind direction measurements are expressed in degrees from due north (between panels 12 and 13), as shown in Figure 3. Wind direction fluctuations were estimated from time plots of the wind vane output. Time plots of the wind direction were not recorded for Tests 1–5. The percent wind speed fluctuations were calculated in the same manner as the wind direction fluctuations. The magnitude of the fluctuation was estimated from the time plot and then expressed as a percentage of the total wind speed reading. No biases appear to exist for T_{wall} (Figure 13), wind direction (Figure 15), wind direction fluctuations (Figure 16), or percent wind speed fluctuations (Figure 17).

The only factor which was found to influence the agreement between the measured and predicted convective coefficient was the receiver mass flow rate (Figure 14). For higher values of $\dot{m}$, the agreement is better than for lower values. This agreement is not unexpected, since it is known that the flowmeter errors increase

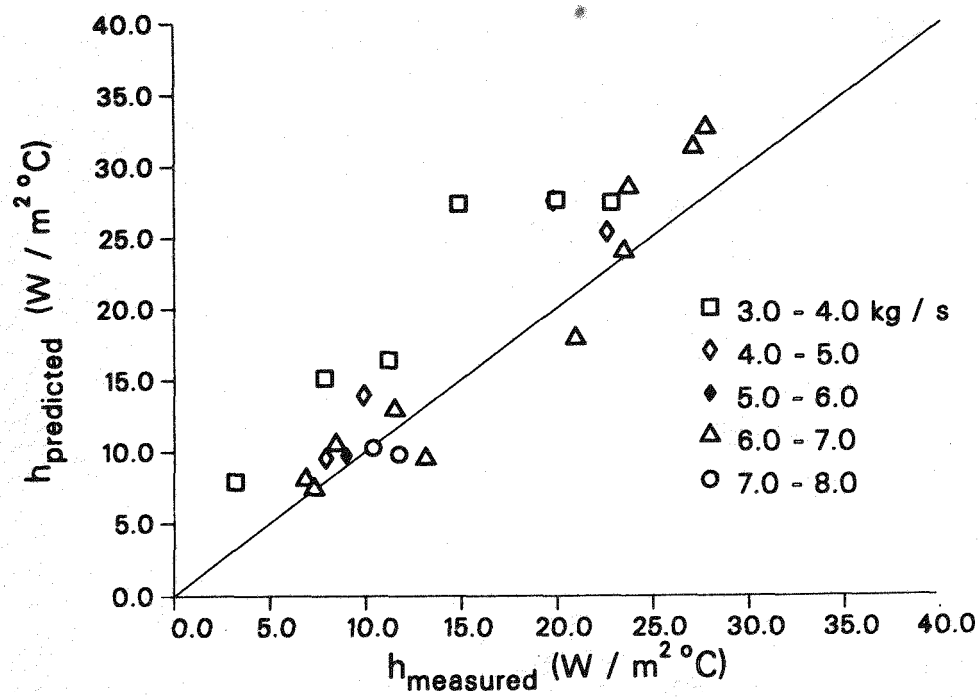

Figure 14. Effect of receiver mass flow rate

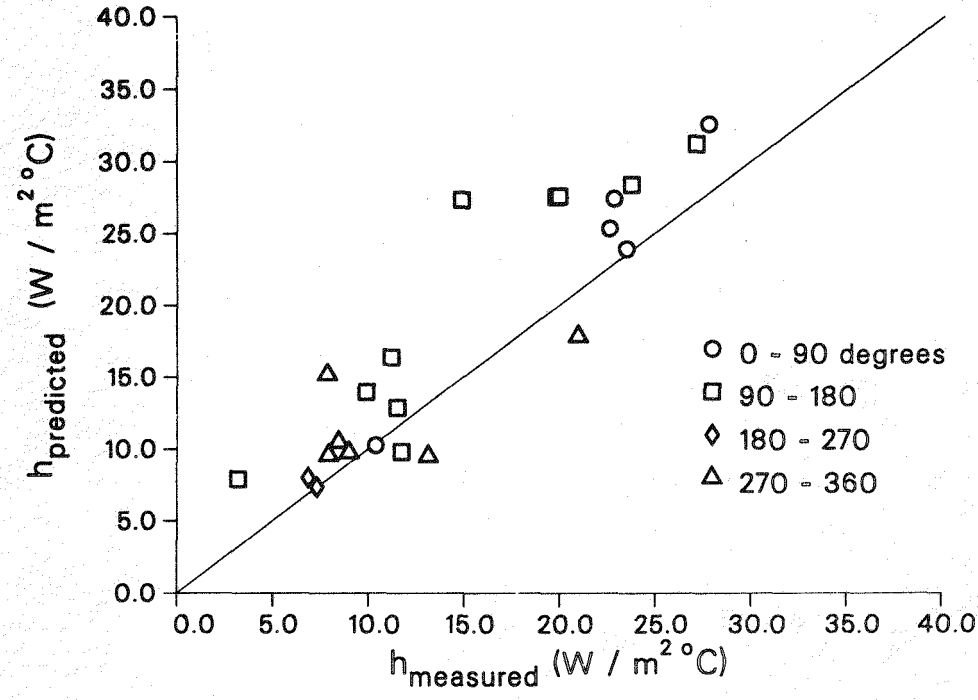

Figure 15. Effect of wind direction

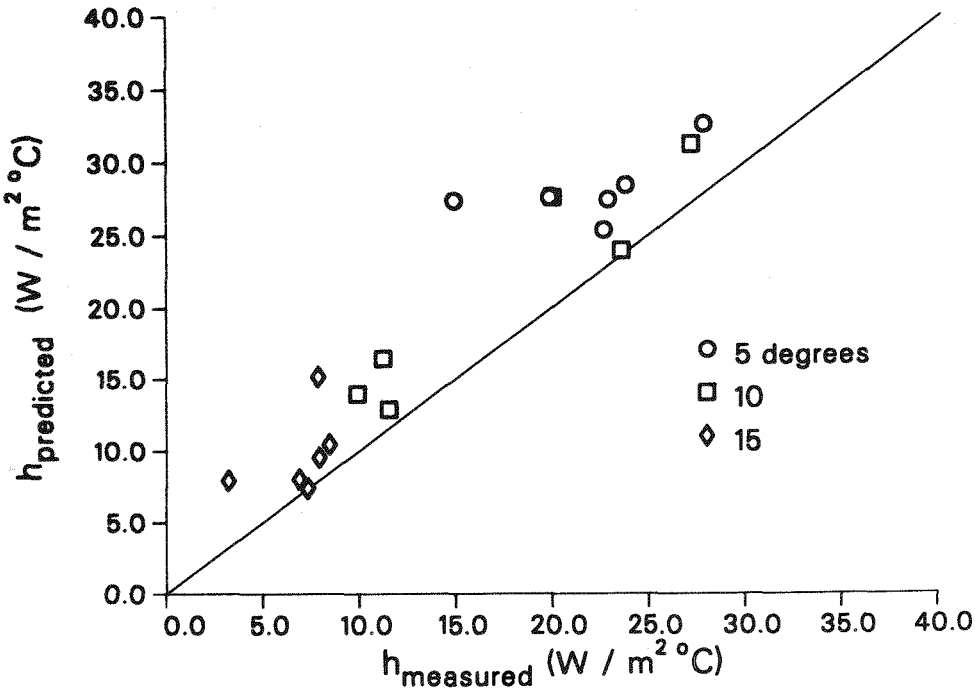

Figure 16. Effect of wind direction fluctuations

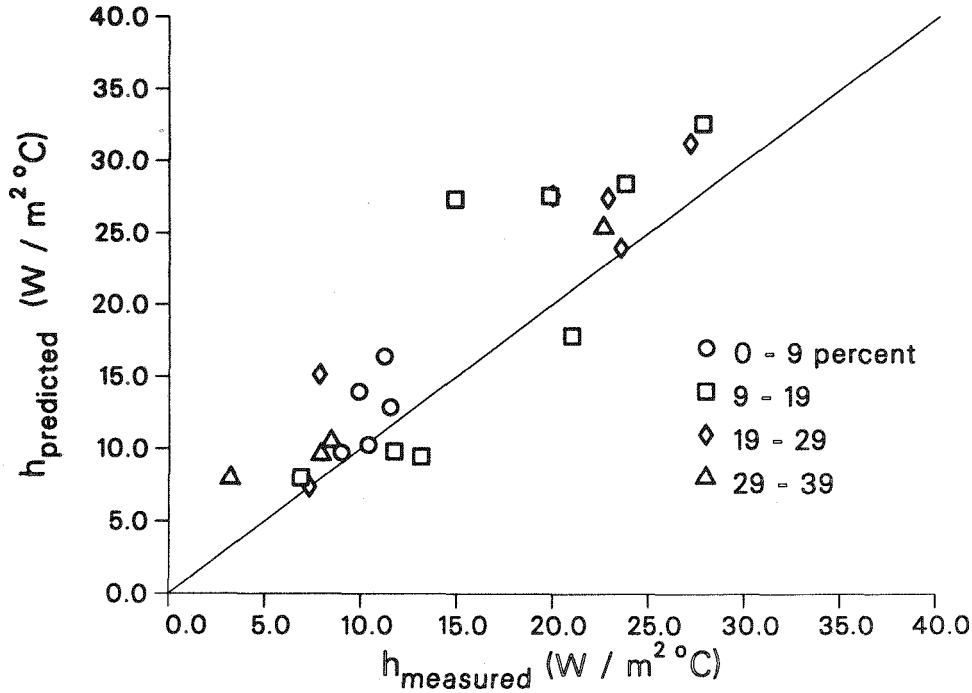

Figure 17. Effect of percent variation in wind velocity

with decreasing flow. Figure 18 shows a more dramatic representation of the influence of mass flow rate with a plot of only data which have a flow over 5 kg/s (40,000 lb/hr).

Experimental results of heat transfer over rectangular bodies [31] and spheres [32] have shown increases in heat transfer in the field of up to 200% from similar experiments performed in the wind tunnel. This may be due to atmospheric turbulence in the field that was not duplicated in the wind tunnel. Since the heat transfer correlations used to predict h_{pred} were developed from wind tunnel testing, Siebers [20] suggested that convective losses at Solar One may also exhibit such an enhancement in heat transfer. The data collected in these experiments do not seem to show increased heat transfer due to increased turbulence intensity. However, the meteorological instrumentation used in this study to assess the turbulence intensity was not complete enough to properly characterize it. A topic for further study would be to assemble more detailed measurements of atmospheric turbulence using three-dimensional anemometers and a faster data scan rate. From the results of this work, it does appear that the effect of atmospheric turbulence may be negligable.

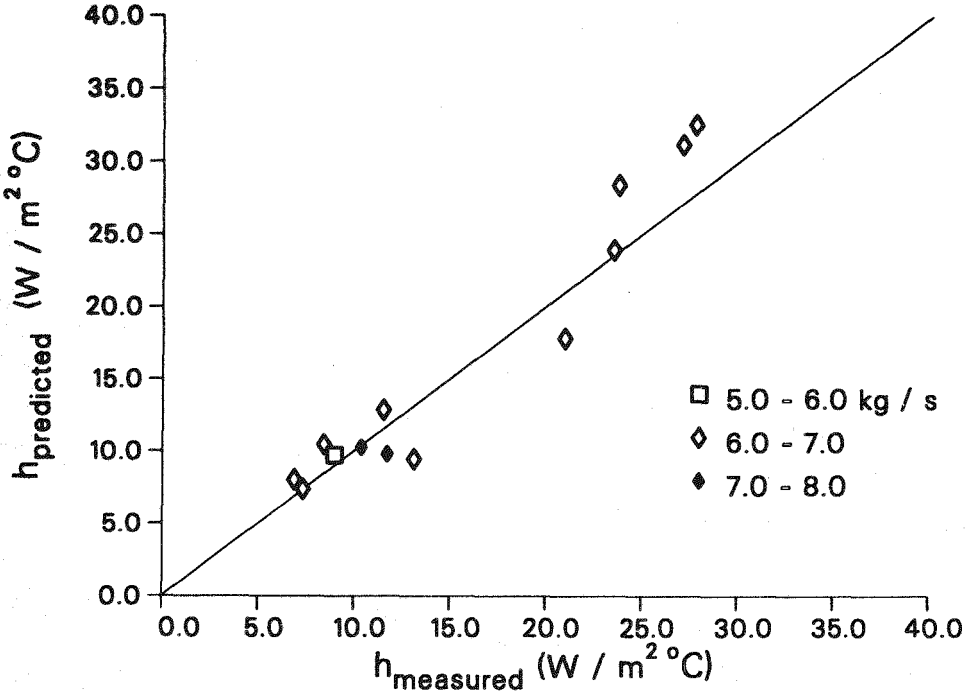

Figure 18. Measured versus predicted convective coefficient, high mass flow rate

Uncertainty Analysis–A root-sum-square uncertainty analysis for determining the uncertainty in single-sample experiments was performed on the data analysis and correlation equations. The uncertainty in the predicted convective coefficient, h_{pred}, is from 40 to 60% and in the measured convective coefficient, h_{meas}, 30 to 50%.

The procedure for using the root-sum-square analysis was established by Kline and McClintock [33] and is recommended by Siebers and Kraabel for convective loss experiments. An enhancement was made to the basic uncertainty analysis following the recommendations by Abernethy et al. [34] , which separately accounts for the precision and bias errors in the equation variables. Briefly, the precision errors reflect the repeatability of the instrumentation, which can be reduced by multiple sampling of the output, and bias errors reflect an offset in the instrument's reading. The two results are then added together for the final uncertainty. Table 3 summarizes the results of the uncertainty analysis, listing the values of the measured and predicted convective coefficients and their associated uncertainties. The main contributors to the uncertainty in h_{meas} are receiver mass flow rate ($\dot{m}$), wall temperature (T_{wall}), and the receiver emissivity (ϵ). For h_{pred}, the main contributors to the uncertainty are the uncertainties in the constants used in the correlations. More detail on the uncertainty analysis is provided in Appendix A.

Table 3. Results of Uncertainty Analysis for h_{pred} and h_{meas}

Test	Correlation h_{pred}	Uncertainty δh_{pred}	Measurement h_{meas}	Uncertainty δh_{meas}
1	17.8	±11.4	21.0	±6.5
2	9.5	±4.9	13.1	±5.6
3	9.7	±5.2	9.0	±5.0
4	10.3	±6.0	10.4	±4.7
5	9.8	±5.3	11.7	±5.1
6	23.9	±15.5	23.5	±7.5
7	31.2	±20.3	27.1	±8.1
8	27.6	±18.0	20.0	±6.8
9	7.4	±3.3	7.3	±3.7
10	10.4	±5.9	8.5	±5.1
11	7.9	±3.4	3.2	±4.2
12	28.4	±18.3	23.8	±7.6
13	27.3	±17.7	14.9	±5.9
14	27.5	±18.0	19.8	±6.7
15	8.0	±3.6	6.9	±5.2
16	9.5	±4.9	7.9	±5.2
17	15.1	±9.4	7.9	±5.1
18	32.5	±20.3	27.8	±8.6
19	25.3	±16.3	22.6	±7.5
20	27.4	±17.7	22.8	±7.5
21	12.9	±7.9	11.5	±5.4
22	13.9	±8.6	9.9	±5.1
23	16.4	±10.3	11.2	±5.2

Panel Data Analysis

The panel data analysis shows the variation of the convective coefficient around the receiver as a function of wind direction. The panel data analysis allows a more detailed examination of the data. The trends in the convective coefficient around the receiver are qualitatively compared to results in the literature for flow over roughened cylinders. Finally, an area-averaged convective coefficient is calculated for the cylinder from the panel data and compared with the total cylinder calculation and the correlation prediction of the same quantity.

Convective Coefficient versus Wind Direction

Panel Heat Transfer–An individual convective coefficient, h, was calculated for each boiler panel, using equations (1–8). The six preheat panels were treated as one large panel. Since the flow through a preheat panel is roughly five times as high as through a boiler panel, the temperature drop is smaller and its accurate measurement is more difficult. In addition, the thermocouples used for fluid temperature measurement on the preheat panels were found to be inaccurate and not adjustable during the instrument calibration campaign. Aggregating the preheat panels into a single panel minimized these effects.

The convective coefficient determined for each panel in the experiments is plotted as the Nusselt number ($Nu = hd/k$) normalized by the square root of the Reynolds number for data presentation. This parameter, $Nu/Re^{0.5}$, is used by Achenbach [35] in the presentation of local heat transfer around a roughened cylinder; $Nu/Re^{0.5}$ equals unity for laminar boundary layers at stagnation (zero angle of wind incidence) over a variety of Reynolds numbers. Panel number, rather than angle of incidence, is plotted as the abscissa since the latter is less precise. The angle of incidence can, however, be inferred from the plots which list the panel number at which the angle between the panel normal and the ambient wind direction is approximately zero. It should be noted that the wind direction is obtained from a single wind vane halfway down the tower. This vane is the one closest to the receiver and is considered an approximation of wind direction. Adjacent panels are 15 degrees apart. Figure 19 shows a qualitative representation of the different regions occurring in flow around a central receiver. Stagnation always occurs at a zero wind angle, although the other regions, such as transition, shift with respect to wind angle due to surface roughness and Reynolds number.

As indicated in Figure 20 (a–f), all of the plots show similar trends in the heat transfer as a function of wind angle. A few characteristic plots are presented and discussed in this chapter, with a complete presentation of all twenty-three plots in Appendix C. Figure 20a shows the results from Test 14, a high wind case, with

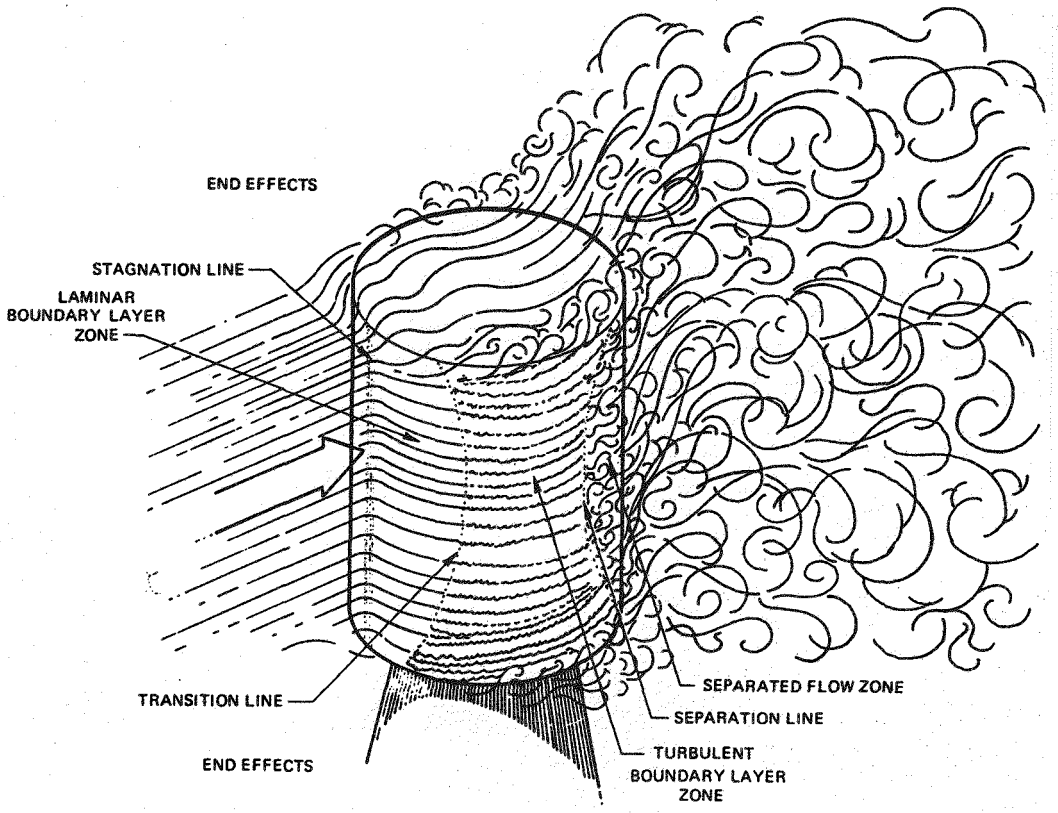

Figure 19. Convective heat transfer zones on a cylindrical, external receiver

the wind incident at panel 18. The data point at panel number 0 is that for the six preheat panels, combined as one. The heat transfer is fairly uniform up to 90 degrees from stagnation, where it increases to a maximum at about 115 degrees and then falls to a minimum at about 180 degrees. The results shown in Figure 20a are typical for a high wind test run, although some of the profiles are not as uniform. Test 8 (Figure 20b) is such an example, having the same wind speed and virtually the same direction as Test 14, yet exhibiting a much rougher profile. The point of increase for this plot is about 105 degrees; the minimum is reached at about 195 degrees where, as in Test 14, the heat transfer again begins to increase. The major difference between Tests 8 and 14 is the receiver mass flow rate; Test 14 has a higher flow rate than Test 8.

The low wind tests also show similar trends. In Test 2 (Figure 20c), the wind is incident on panel 7. The heat transfer remains uniform until about 105 degrees, where it increases to a maximum and then declines at about 180 degrees. It appears that the panel 5 heat transfer is too high in Tests 1–5. An examination of the raw data confirms an apparent problem with the panel flow reading during these tests. In all cases, the reading is from 75 to 100 % higher than that of panel 6, yet the outlet temperatures are identical. Other panels with flow rates about equal to panel 6 show outlet temperatures similar to that of panel 6. Therefore, the high value of $Nu/Re^{0.5}$ at panel 5 is believed to be anomalous.

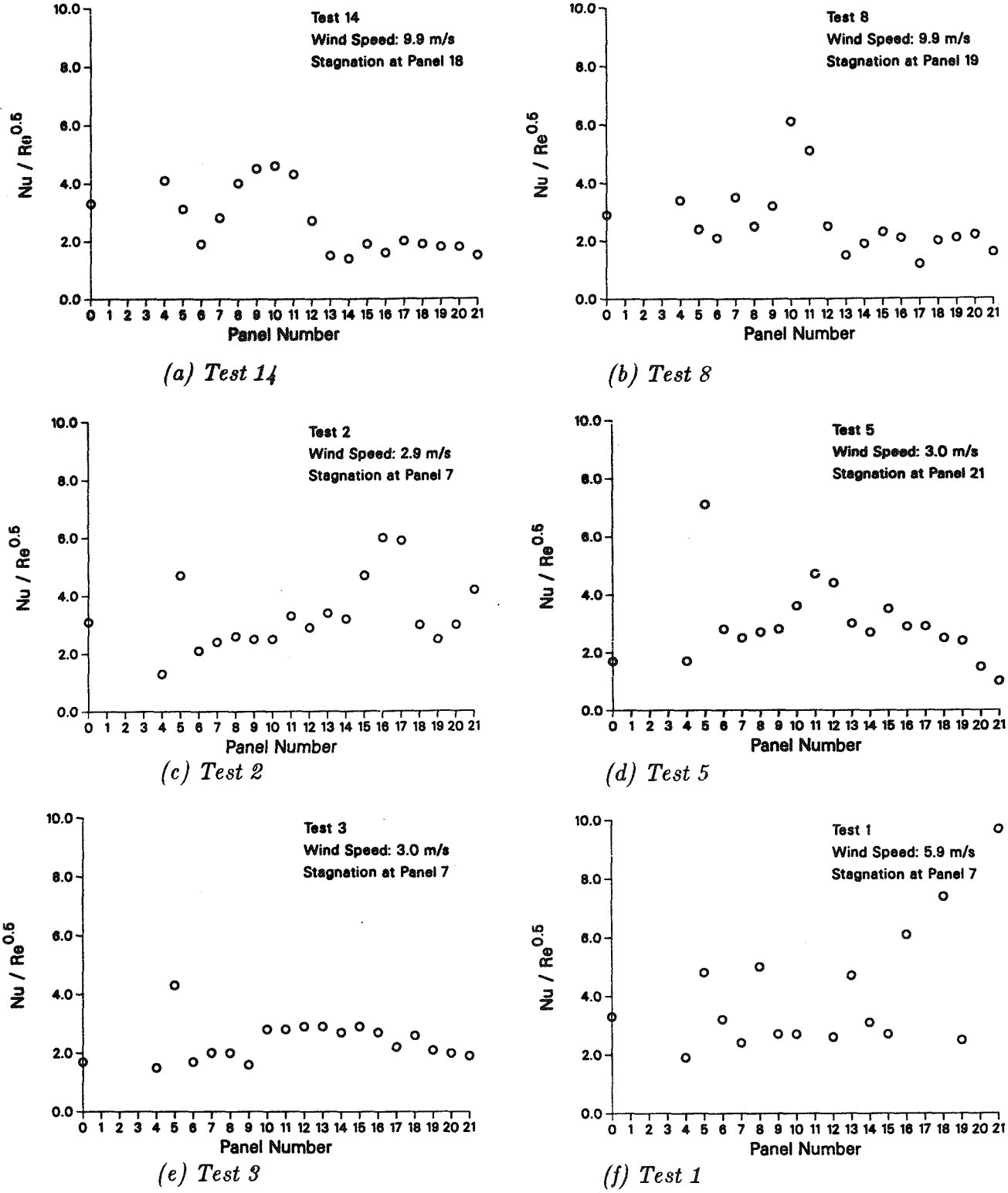

Figure 20. Convective heat transfer versus wind direction

Test 5 (Figure 20d) is similar to Test 2, except that the wind is incident upon panel 21. The heat transfer initially increases gently, then shows a more abrupt increase at about 105 degrees and falls to a minimum near 195 degrees. Test 3, shown in Figure 20e is a second type of result seen in some of the low wind tests. These profiles are considerably less pronounced. There is not a definitive explanation for this change in profile, especially for these two tests (2 and 3) which were run on the same night. The major change between the two runs was in the panel mass flow rates; Test 3 was conducted with lower flows than Test 2. The complete set of test profiles in Appendix C shows that, in general, the more clearly defined profiles are associated with high mass flow rate tests, whereas the rougher or less well-defined profiles tend to be associated with low and in some cases, medium, flow rate tests.

Test 1 (Figure 20f) is the only plot in which the data appears to be totally scattered. Three points are out of range on the $Nu/Re^{0.5}$ axis. Examination of the raw data shows several inconsistencies between reported panel mass flow rates and outlet temperatures - some of the reported outlet temperatures are exceedingly low. These results are believed to be due to errors in the flowmeter readings, although it is unclear why these errors are not present in Tests 2 and 3, which were conducted on the same date as Test 1.

Heat Transfer from a Roughened Cylinder–Qualitative comparisons are made between trends in the data and in heat transfer around a roughened cylinder under controlled laboratory conditions, such as described by Achenbach [35]. The local heat transfer was measured as a function of angle around a roughened cylinder; Achenbach reports results for three roughness values (k_s/d of 75×10^{-5}, 300×10^{-5}, and 900×10^{-5}), and for Reynolds numbers ranging from 4.8×10^4 through 4.0×10^6. Results at the smallest roughness are of interest since they are closest to the calculated roughness at Solar One (90×10^{-5}).

The local heat transfer ($Nu/Re^{0.5}$) is, in all cases, very nearly unity at stagnation ($\phi = 0°$) where the boundary layer is laminar. At the lower Reynolds numbers, the boundary layer remains laminar until it separates from the cylinder (from $\phi = 80°$ to $\phi = 105°$ with increasing Reynolds number). Separation is indicated by a minimum in the local heat transfer. At a Reynolds number of 5.9×10^5, the laminar boundary layer transitions to turbulence near $\phi = 60°$, which causes an increase in heat transfer, and then separates near $\phi = 115°$, indicated by another, more gradual increase in heat transfer. With increasing Reynolds number, the boundary layer transition to turbulence moves closer to the stagnation point; separation remains in the vicinity of 120 degrees.

Although no quantitative comparison was made between the Achenbach and Solar One data, the Solar One data is self-consistent. A distinct increase in heat transfer, beginning somewhere between 75 and 105 degrees, was observed which indicates that separation occurs just before this increase in heat transfer.

Unlike the results presented by Achenbach, $Nu/Re^{0.5}$ is seldom unity at the stagnation point for the Solar One data. This is likely due to the presence of freestream turbulence in the environment at Barstow and possibly also to natural

convection. The meteorological instrumentation was inadequate for fully characterizing wind speed and direction fluctuations. Additionally, the effect of buoyancy (natural convection) on $Nu/Re^{0.5}$ versus wind direction in Solar One data is unknown.

Total Receiver Convective Coefficient

The total convective coefficient can be calculated from the individual boiler panel and preheat panel convective coefficients, according to the equation:

$$(h_{meas})_{panel\ data} = \frac{\sum_{i=4}^{21}(h_i\ A_{panel})\ +\ 6\,h_{preheat}\ A_{panel}}{24\ A_{panel}} \tag{13}$$

Comparisons can then be made to the measured convective coefficient, $(h_{meas})_{bulk}$, as calculated in Chapter 2, and to that predicted using the correlations proposed by Siebers and Kraabel [20], $h_{predicted}$.

Comparison to $(h_{meas})_{bulk}$–Figure 21 shows a plot of $(h_{meas})_{panel\ data}$, calculated from equation (13), versus $(h_{meas})_{bulk}$, calculated from equations (1–8). The agreement is quite good. The calculation of $(h_{meas})_{panel\ data}$ is related to the calculation of $(h_{meas})_{bulk}$ in the mass flow rate measurement. Nineteen calculations of $\dot{m}\,C_p\,(T_{in} - T_{out})$ are made for $(h_{meas})_{panel\ data}$. One thermocouple in the ring manifold supplies the eighteen boiler panel inlet temperatures as well as the preheat panel outlet temperature. Each boiler panel outlet temperature is the average of two thermocouples located at its outlet. In the calculation of $(h_{meas})_{bulk}$, one calculation of $\dot{m}\,C_p\,\Delta T$ is performed. The mass flow rate, $\dot{m}$, is the sum of the eighteen boiler panel flows and ΔT is the temperature measured by the differential thermocouple between the receiver inlet (preheat panel inlet) and outlet (boiler panel outlet). So, although the calculations of $(h_{meas})_{panel\ data}$ and $(h_{meas})_{bulk}$ are not completely independent, they are arrived at using different temperature data. The agreement between $(h_{meas})_{panel\ data}$ and $(h_{meas})_{bulk}$ adds confidence to both sets of data.

The one data point in Figure 21 which is seriously out of agreement is Day 58 (Test 1). The problems with the individual panel data in Test 1 were described in the previous section. The large discrepancies between panel flows and temperature drops have not affected $(h_{meas})_{bulk}$ to the extent that they have $(h_{meas})_{panel\ data}$. The method used to calculate $(h_{meas})_{bulk}$ is less subject to inaccuracy in flowmeter readings. For example, one of the erroneous sets of panel data in Test 1 produced a convective coefficient over 500% greater than the average of the other panels. The total convective coefficient which is calculated by summing the panel mass flow rates and using them in a single calculation of $\dot{m}\ C_p\ \Delta T$, and thus h, is more accurate than the total convective coefficient which is calculated as the average of the individual panel convective coefficients. This is because the latter method is more susceptible to influence by the highest uncertainty measurement of these tests — mass flow rate.

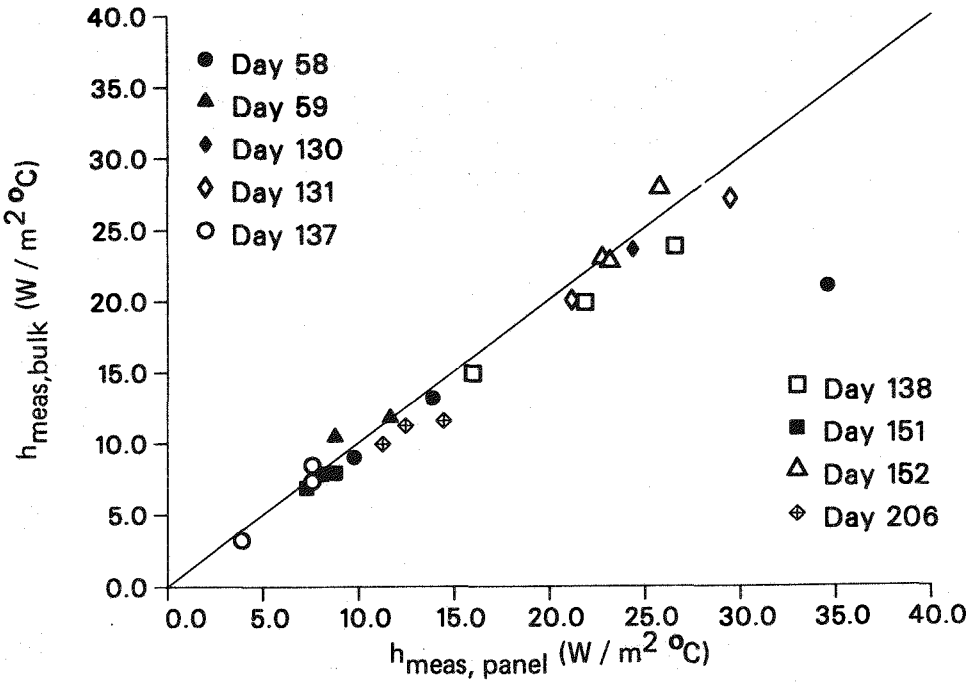

Figure 21. Measured convective coefficient—panel versus total measurement

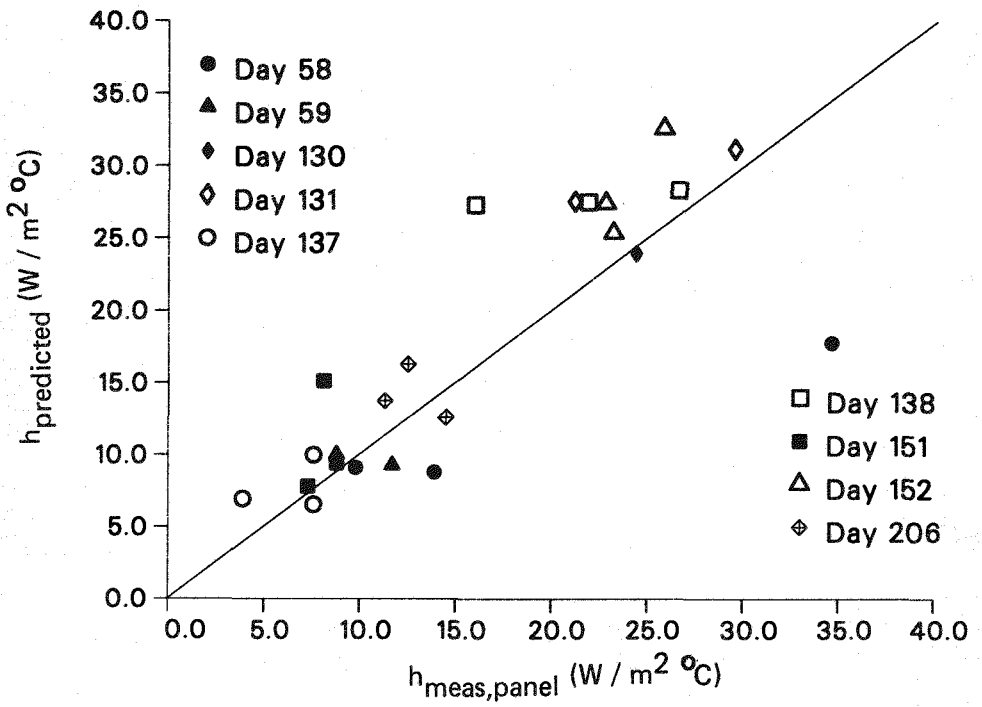

Figure 22. Measured convective coefficient from panel data versus predicted convective coefficient

Comparison to $h_{predicted}$–For completeness, a plot showing $(h_{meas})_{panel\ data}$ versus $h_{predicted}$, calculated from equations (9–12), is shown in Figure 22. Agreement between the measured and predicted values is roughly the same as in Figure 12, which is expected due to the high degree of agreement between $(h_{meas})_{panel\ data}$ and $(h_{meas})_{bulk}$ in Figure 21.

A summary of the measured ($(h_{meas})_{bulk}$), predicted ($h_{predicted}$), and panel-averaged ($(h_{meas})_{panel\ data}$) convective coefficients is presented in Table 4.

Table 4. Comparison Among $(h_{meas})_{bulk}$, $h_{predicted}$, and $(h_{meas})_{panel\ data}$

Test	Day	u_∞ m/s	$(h_{meas})_{bulk}$ W/m^2°C	$h_{predicted}$ W/m^2°C	$(h_{meas})_{panel\ data}$ W/m^2°C
1	58-1	5.9	21.0	17.8	34.6
2	58-2	2.9	13.1	9.5	13.9
3	58-3	3.0	9.0	9.7	9.6
4	59-1	3.2	10.4	10.3	8.8
5	59-2	3.0	1.7	9.8	11.7
6	130-1	8.5	23.5	23.9	24.4
7	131-1	11.0	27.1	31.2	29.5
8	131-2	9.9	20.0	27.6	21.2
9	137-1	2.0	7.3	7.4	7.6
10	137-2	3.4	8.5	10.4	7.6
11	137-3	2.1	3.2	7.9	3.9
12	138-1	10.3	23.8	28.4	26.6
13	138-2	9.8	14.9	27.3	16.0
14	138-3	9.9	19.8	27.5	21.9
15	151-1	2.4	6.9	8.0	7.3
16	151-2	3.1	7.9	9.5	8.8
17	151-3	5.4	7.9	15.1	8.1
18	152-1	12.0	27.8	32.5	25.6
19	152-2	9.2	22.6	25.3	23.2
20	152-3	9.8	22.8	27.4	22.8
21	206-1	4.4	11.5	12.9	14.5
22	206-2	4.8	9.9	13.9	11.3
23	206-3	5.7	11.2	16.4	12.5

Conclusions

Convective Loss Measurements

Convective losses were calculated from energy loss measurements made at the Solar One external, cylindrical receiver. The measured convective coefficient increases with increasing wind speed. A root-sum-square uncertainty analysis established confidence bounds for the experimental results. Despite the restrictions placed on the range of flowmeter operation, receiver flow rate appeared to influence the test results. Tests which had low receiver flow rates showed less consistent trends than high flow rate tests.

Comparison with Predictions

The data analysis yielded convective coefficients over a range of ambient wind speeds and wall temperatures. Testing at lower wall temperatures did not obscure the trends which would be present at higher wall temperatures (operating conditions). Mixed convective coefficients for the test conditions were predicted using measured ambient temperature, wind velocity, and receiver wall temperature from correlations developed by Siebers and Kraabel [20]. The comparison between the measured and predicted convective coefficients is good, although the correlations tend to overpredict the measured data by about 10% .

The predicted mixed convective coefficient, h_{pred}, is calculated from the natural and forced convective coefficients (h_{nat} and h_{forc}). The correlations for both h_{nat} and h_{forc} include a term to account for the surface roughness introduced by the receiver tubes. However the predicted mixed convective coefficient would fit the experimental results better if the roughness factor is removed from the natural convection correlation.

Validation of the mixed convection correlation by these experiments increases the confidence with which it is used. The mixed convection correlations verified by these experiments are currently being used to:

a. provide a value for the convective coefficient in the Solar One thermal hydraulic panel model in the SAPPHIR and PARFLO [29] computer codes,

b. estimate the annual energy loss at Solar One due to convection [36], and

c. calculate the convective loss from an external receiver in the central receiver design code, DELSOL2 [37] [38] .

Local Measurements

The convective coefficient was also calculated for individual receiver panels. The relative wind direction for a panel was estimated as the angle between the panel normal and the ambient wind direction. The variation of the normalized convective energy loss ($Nu/Re^{0.5}$) as a function of wind direction was examined. These results were qualitatively compared with data presented in the literature [35] for forced convection heat transfer over a roughened cylinder. The comparison could not be rigorous since (*i*) the Solar One measurement of wind direction is approximate, (*ii*) the wind speed and turbulence intensity are not well characterized, (*iii*) the local heat transfer measurement is averaged for each panel, and (*iv*) it is not known how bouyancy (natural convection) influences the results. However, a consistent trend is observed in the heat transfer around the receiver. The smoothness of the plot is related to the receiver mass flow rate; low flow rate tests have more irregularly shaped curves.

The panel data were averaged to give an overall convective coefficient for the receiver. These results compared well with the convective coefficient as calculated from the single measurement of $\dot{m}\, C_p\, \Delta T$. The total convective coefficient which is calculated by summing the panel mass flow rates and using them in a single calculation of $\dot{m}\, C_p\, \Delta T$, and thus h, is more accurate than the total convective coefficient which is calculated as the average of the individual panel convective coefficients. This is because the latter method is more susceptible to influence by the highest uncertainty measurement of these tests – mass flow rate.

APPENDIX A

Uncertainty Analysis

An uncertainty analysis investigates the propagation of errors through the data analysis equations. It also the establishes the confidence with which predictive correlations can be used.

The uncertainty analysis uses the root-sum-square technique. Measured parameters which affect the accuracy of the result are identified. A partial derivative of the data analysis equation is taken with respect to each of these parameters. If F represents the data analysis equation and x_i are the parameters, where F is a function of the parameters, then the root-sum-square equation which expresses the error E in the result is:

$$E = \sqrt{\left(\frac{\partial F}{\partial x_1}\delta x_1\right)^2 + \left(\frac{\partial F}{\partial x_2}\delta x_2\right)^2 + \cdots + \left(\frac{\partial F}{\partial x_n}x_n\right)^2}. \qquad (A-1)$$

The δx_i values are the errors associated with the data values, x_i.

The method for performing the uncertainty analysis, described by Abernethy et al., [34] accounts for both the random and biased errors. Equation (A-1) is applied twice: the first time using the random or precision errors as the x_i; and the second time using the biased or offset errors as the x_i. The two results are then combined according to:

$$U = \pm(B + t_{95}S) \qquad (A-2)$$

The term S is the uncertainty from equation (A-1) for the random errors, B is the uncertainty for the biased errors, and U is the final uncertainty in the result. The term t_{95} is the 95^{th} percentile from the Student's t distribution. This term increases the random error for small samples. Since a data point is recorded every ten seconds during the convective loss experiment, then averaged over five minutes, the sample size is thirty. For sample sizes from thirty to infinity, t_{95} is 2.

The random errors account for the repeatability of the instrument and signal processing system. The biased errors account for offsets due to instrument calibration, estimates of physical constants (ie. receiver emissivity), and the unknown influences of conditions present during testing. An example of the last type is the estimation by Siebers and Kraabel [20] that turbulence in the ambient environment could enhance the convective losses by up to 70% . This is an asymmetric offset. Biased errors can be either symmetric (i.e. $\pm$ 5 °C) or asymmetric (ie. + 70%).

Table A.1. Errors used in the Root-Sum-Square Uncertainty Analysis

Parameter	Units	Random Error	Biased Error
$\dot{m}$	kg/s	2%	5%
T [1]	°C	2	2
ΔT [2]	°C	2	—
T_{wall}	°C	—	10
D	m	—	2
L	m	—	2
T_∞	°C	1	2
ϵ	—	—	0.1 [3]
C_{nat} [4]	—	—	40
C_{1-forc} [5]	—	—	50
C_{2-forc} [5]	—	—	50
u_∞	m/s	10	5
a [6]	—	—	50

[1] Any fluid thermocouple (inlet, outlet, ring manifold)
[2] Differential thermocouple
[3] This error in measurement units, not percent
[4] Constant in natural convection correlation, Eqn. (10)
[5] Constants in forced convection correlation, Eqn. (12)
[6] Exponent in mixed convection correlation, Eqn. (9)

The biased errors in this analysis are considered symmetric. Table A.1 lists both the random and biased errors which were included in this uncertainty analysis.

Using these errors, the random and biased uncertainties can be calculated for both the measured and predicted convective coefficients. These quantities are presented in Table A.2. The total uncertainty in h_{meas} and h_{pred} was presented in Table 3 in the Cylinder Data Analysis section.

Table A.2. Random and Biased Errors in Data and Correlations

Test	δh_{pred} Prec	δh_{meas} Prec	δh_{pred} Bias	δh_{meas} Bias	δh_{pred} Total	δh_{meas} Total
1	1.7	1.0	8.0	4.5	11.4	6.5
2	0.7	0.9	3.5	3.8	4.9	5.6
3	0.8	0.8	3.6	3.4	5.2	5.0
4	0.9	0.8	4.2	3.1	6.0	4.7
5	0.8	0.8	3.7	3.5	5.3	5.1
6	2.3	1.1	10.8	5.3	15.5	7.5
7	3.0	1.2	14.3	5.7	20.3	8.1
8	2.7	1.0	12.6	4.8	18.0	6.8
9	0.4	0.7	2.3	3.1	3.3	3.7
10	0.9	0.8	4.1	3.5	5.9	5.1
11	0.5	0.7	2.4	2.8	3.4	4.2
12	2.7	1.1	12.9	5.4	18.3	7.6
13	2.6	0.9	12.5	4.1	17.7	5.9
14	2.7	1.0	12.6	4.7	18.0	6.7
15	0.5	0.8	2.6	3.6	3.6	5.2
16	0.7	0.8	3.5	3.6	4.9	5.2
17	1.4	0.8	6.6	3.5	9.4	5.1
18	3.2	1.2	14.9	6.2	20.3	8.6
19	2.4	1.1	11.5	5.3	16.3	7.5
20	2.6	1.1	12.5	5.3	17.7	7.5
21	1.2	0.8	5.5	3.8	7.9	5.4
22	1.3	0.8	6.0	3.5	8.6	5.1
23	1.5	0.8	7.3	3.6	10.3	5.2

APPENDIX B

Effect of Lower Wall Temperatures in Testing

Since the tests were performed with no solar flux on the receiver, the wall temperature was considerably lower than it is during normal operations (150 °C versus 400 °C). To assess the effect of the lower wall temperatures, h_{nat}, h_{forc}, and h_{pred} were calculated from the Siebers and Kraabel correlations at the test conditions for wall temperatures of 300 and 400 °C. The results are shown in Table B.1; the convective coefficient units are W/m^2 °C. Increasing the wall temperature increases the natural convective coefficient, particularly through the ratio (T_{wall}/T_∞) in equation (10). However, the forced convective coefficient decreases due to changes in the air properties, which are calculated at the film temperature, $(T_{film} = (T_{wall} + T_\infty)/2)$. These effects do not quite cancel each other. The net result is that the mixed convective coefficient, h_{pred}, increases if h_{forc} and h_{nat} are about equal, and that h_{pred} decreases if h_{forc} is greater than h_{nat}. The magnitudes and trends of h_{pred} in the low wall temperature case are present in the high wall temperature cases. It is therefore concluded that testing at lower wall temperatures has not obscured the trends which would be present at higher wall temperatures.

Table B.1 Predicted Convective Coefficients for Higher Wall Temperatures

	T_{wall}	*test*		T_{wall}	300°C		T_{wall}	400°C
h_{nat}	h_{forc}	h_{pred}	h_{nat}	h_{forc}	h_{pred}	h_{nat}	h_{forc}	h_{pred}
5.8	17.7	17.8	8.1	15.3	15.9	8.7	13.5	14.5
6.8	8.3	9.5	8.2	7.6	9.8	8.8	6.8	9.9
6.7	8.7	9.7	8.1	8.0	10.0	8.8	7.1	10.0
5.7	9.7	10.3	8.0	8.4	10.2	8.7	7.4	10.1
6.7	8.8	9.8	8.2	8.0	10.1	8.9	7.1	10.1
6.1	23.8	23.9	7.8	21.7	22.0	8.4	18.9	19.3
5.9	31.1	31.2	7.8	27.9	28.1	8.5	24.3	24.6
6.2	27.5	27.6	7.9	25.0	25.2	8.5	21.9	22.2
6.1	5.8	7.4	7.8	5.2	8.5	8.5	4.6	8.8
6.6	9.6	10.4	7.9	9.0	10.5	8.6	7.9	10.2
6.6	6.1	7.9	8.0	5.7	8.7	8.6	5.0	9.1
6.3	28.3	28.4	7.8	26.1	26.3	8.5	22.8	23.1
6.2	27.2	27.3	7.9	24.8	25.0	8.5	21.7	22.0
6.4	27.4	27.5	7.9	25.2	25.4	8.6	22.1	22.4
6.3	6.6	8.0	7.6	6.3	8.7	8.3	5.4	8.9
6.2	8.7	9.5	7.6	8.2	9.8	8.3	7.1	9.6
6.2	14.9	15.1	7.7	13.8	14.5	8.3	12.0	13.0
6.1	32.5	32.5	7.6	30.2	30.3	8.3	26.0	26.2
6.1	25.2	25.3	7.7	23.3	23.5	8.4	20.2	20.6
6.0	27.3	27.4	7.8	24.9	25.1	8.4	21.7	22.0
6.6	12.4	12.9	8.0	11.5	12.5	8.6	10.1	11.7
6.5	13.5	13.9	8.0	12.5	13.4	8.6	11.0	12.4
6.5	16.1	16.4	8.0	14.7	15.4	8.7	13.0	14.0

APPENDIX C

Panel Data

Included in this appendix are the complete set of plots ($Nu/Re^{0.5}$ versus wind direction) which are discussed in the Panel Data Analysis section.

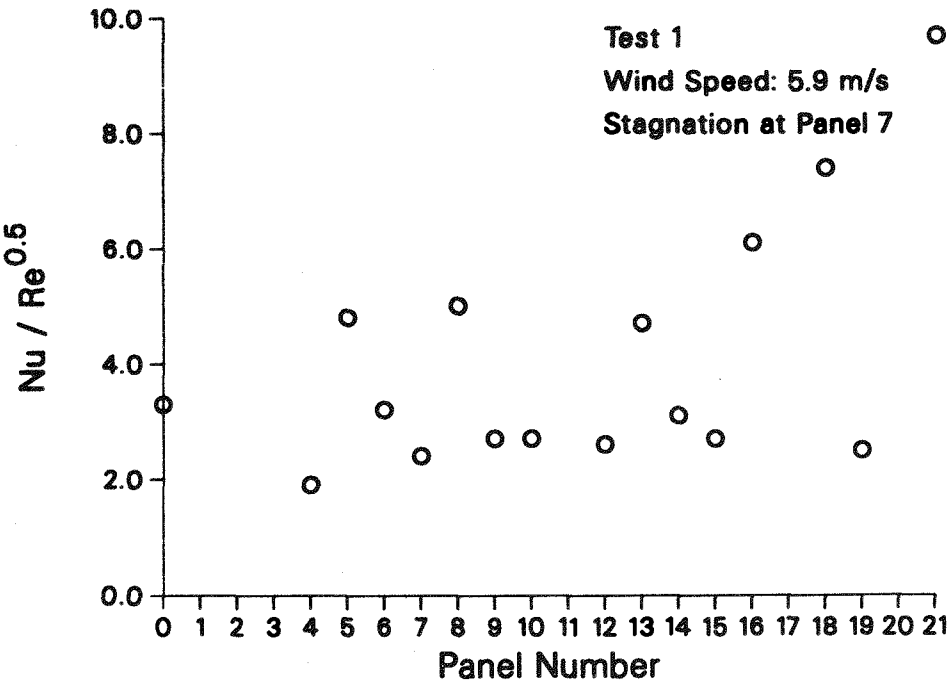

Figure C-1. Test 1, Day 58-1

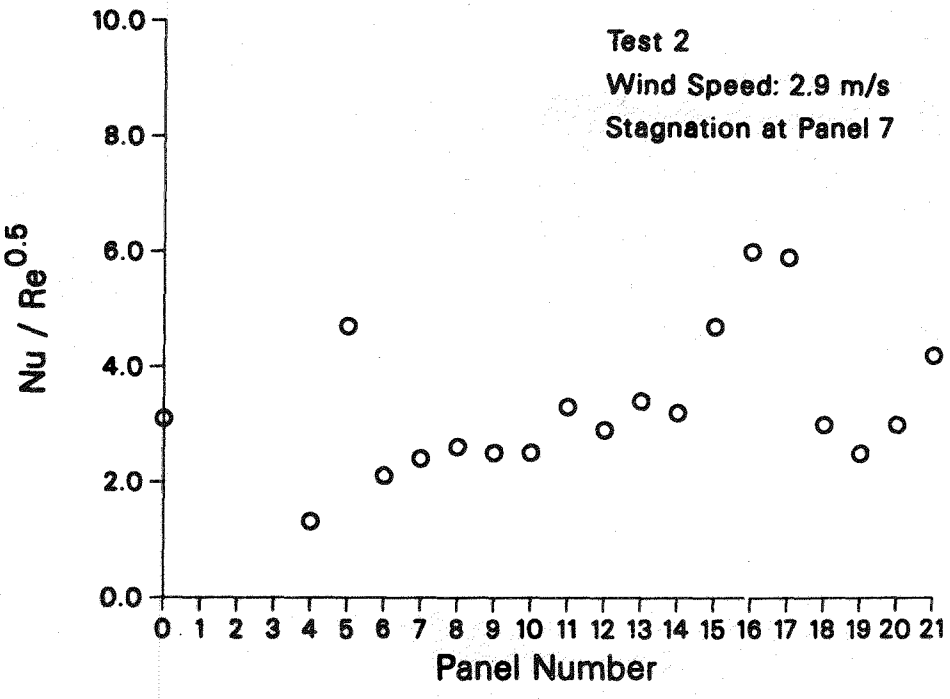

Figure C-2. Test 2, Day 58-2

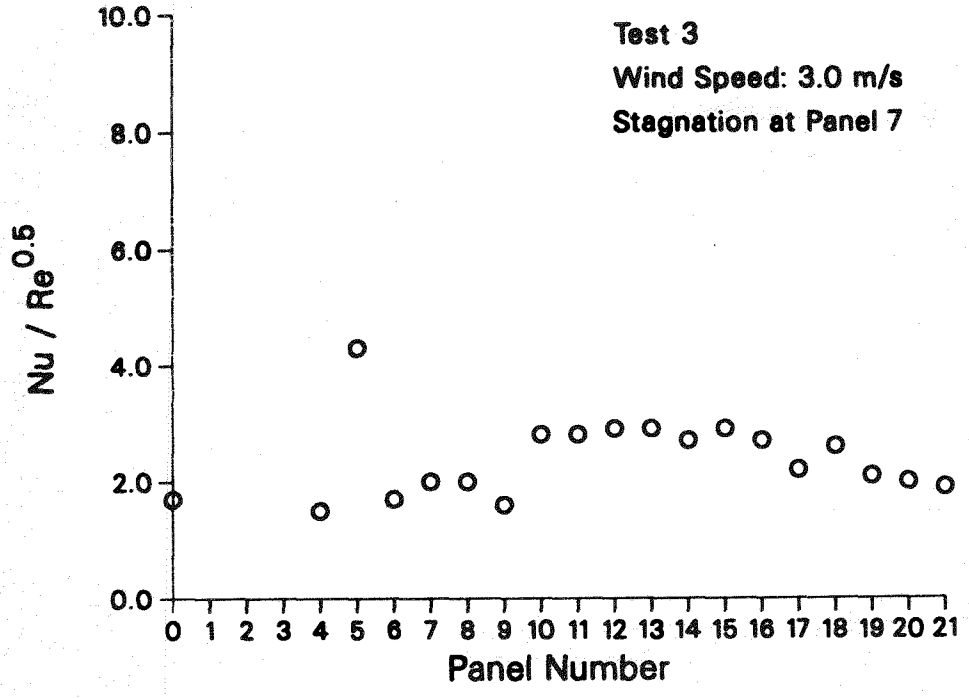

Figure C-3. Test 3, Day 58-3

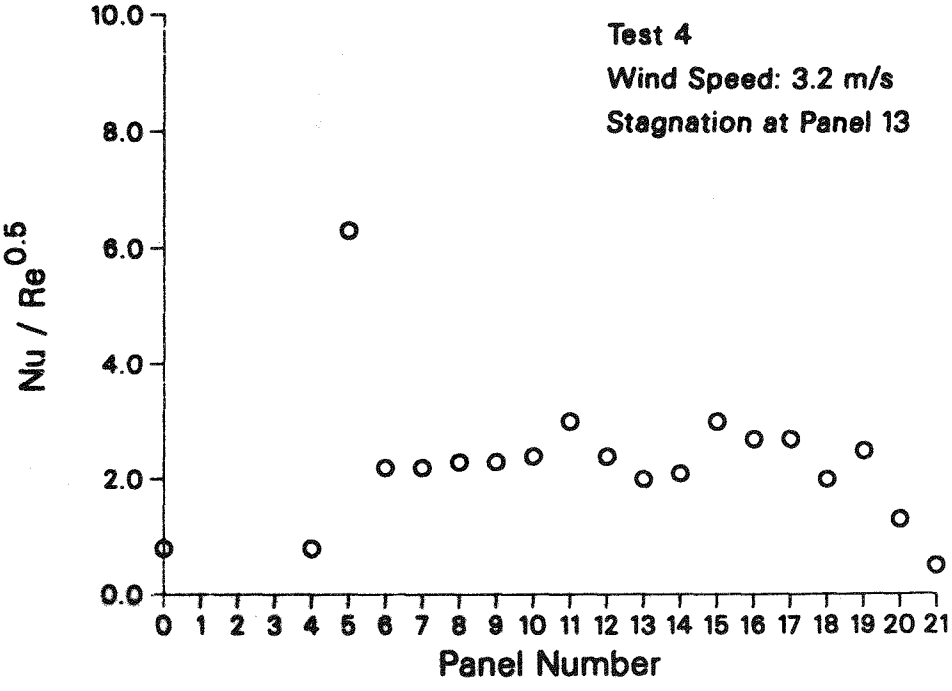

Figure C-4. Test 4, Day 59-1

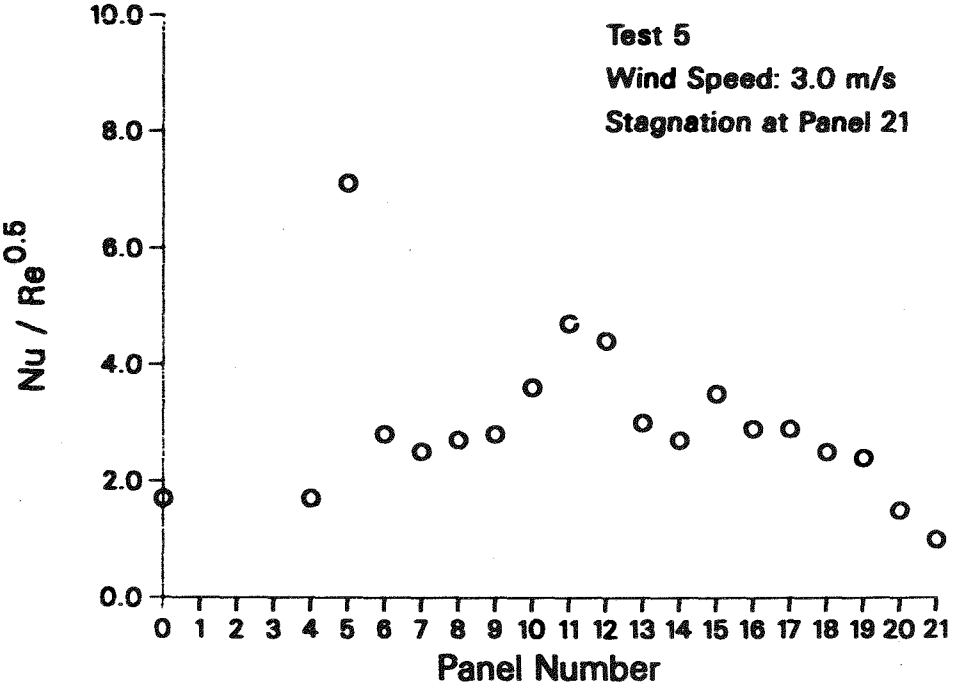

Figure C-5. Test 5, Day 59-2

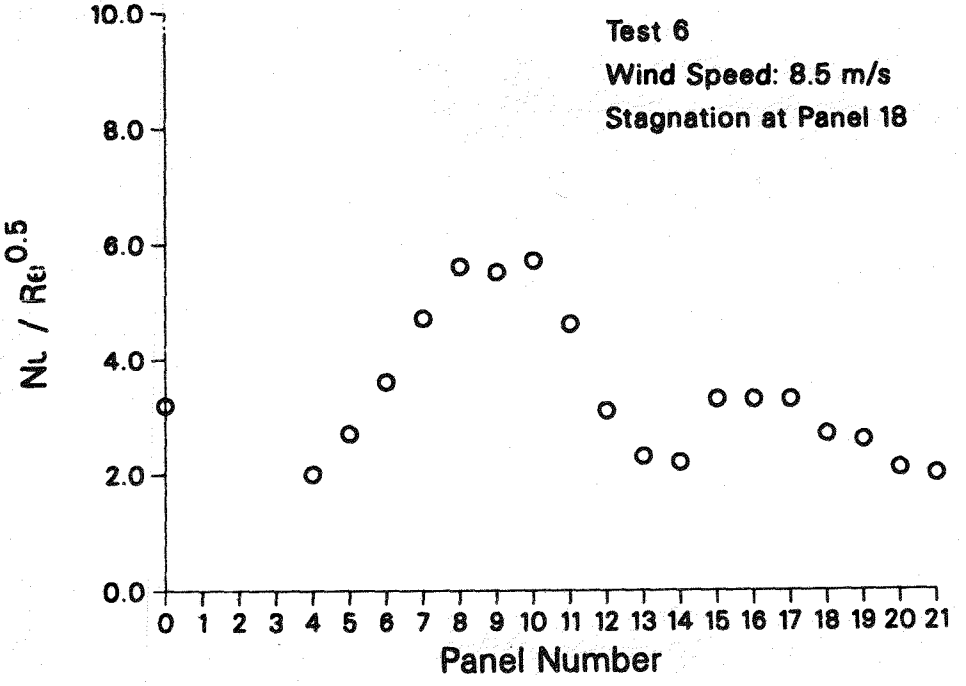

Figure C-6. Test 6, Day 130-1

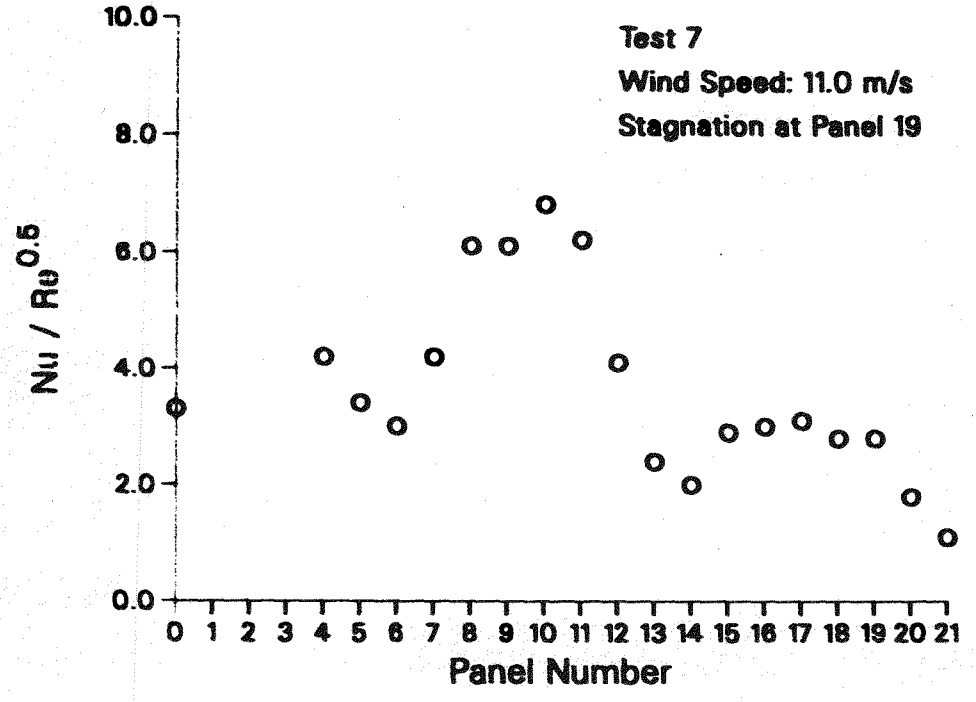

Figure C-7. Test 7, Day 131-1

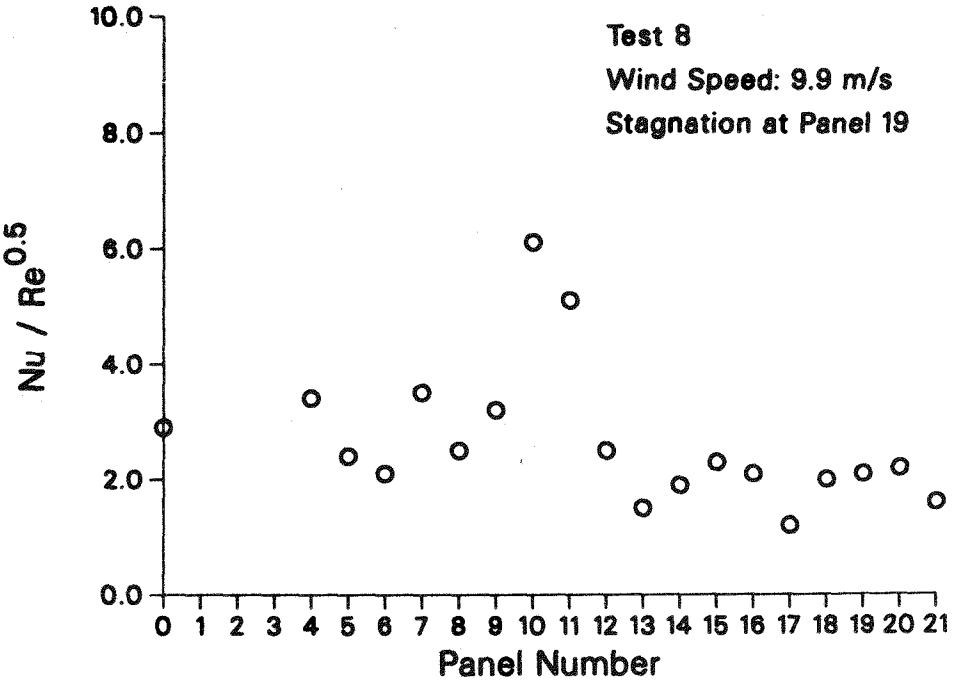

Figure C-8. Test 8, Day 131-2

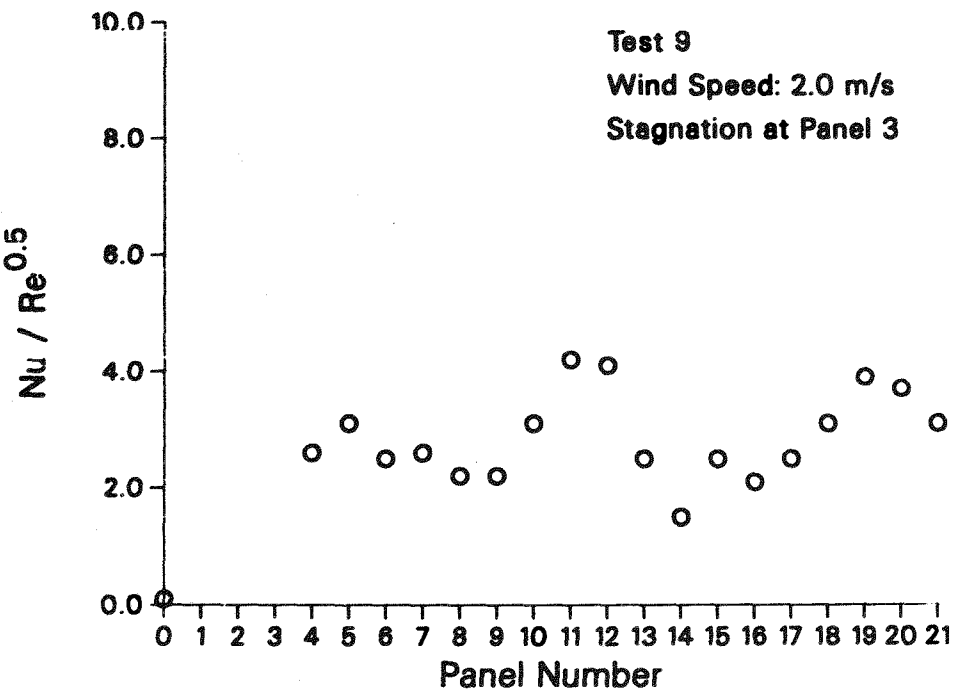

Figure C-9. Test 9, Day 137-1

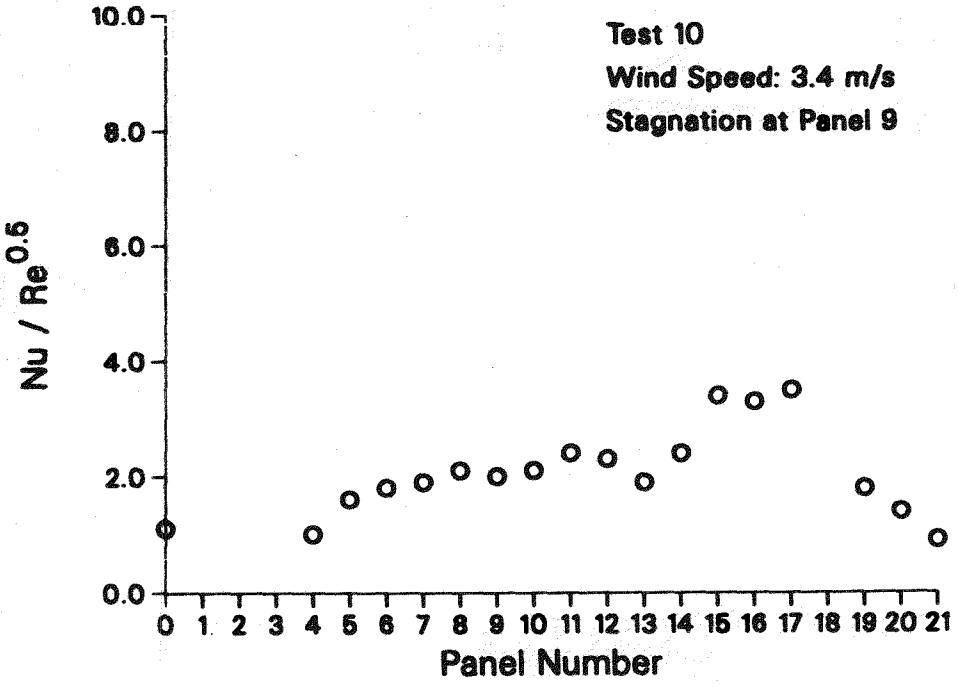

Figure C-10. Test 10, Day 137-2

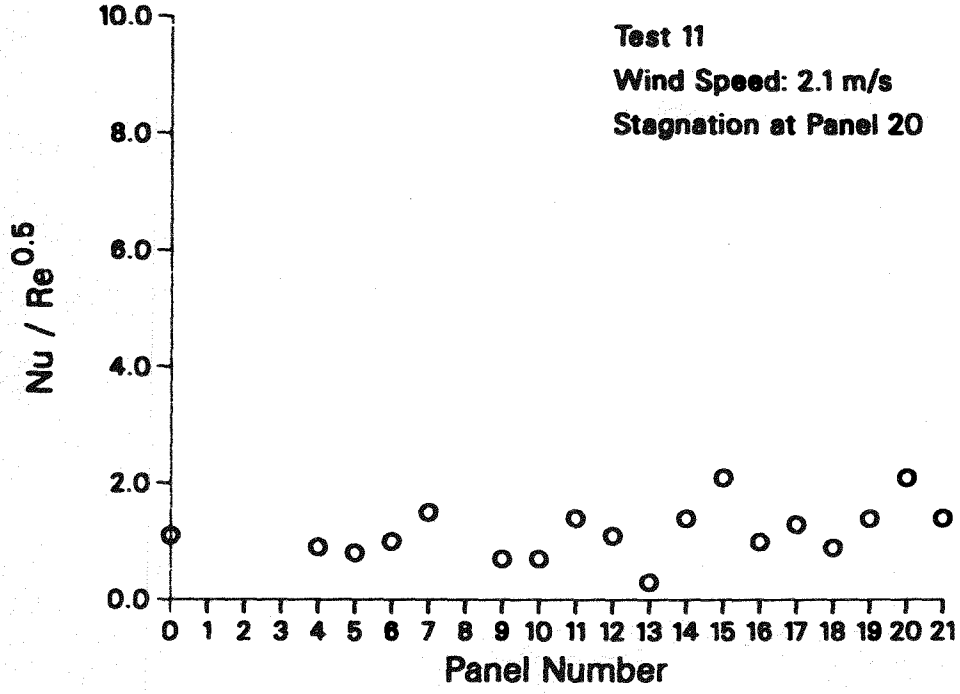

Figure C-11. Test 11, Day 137-3

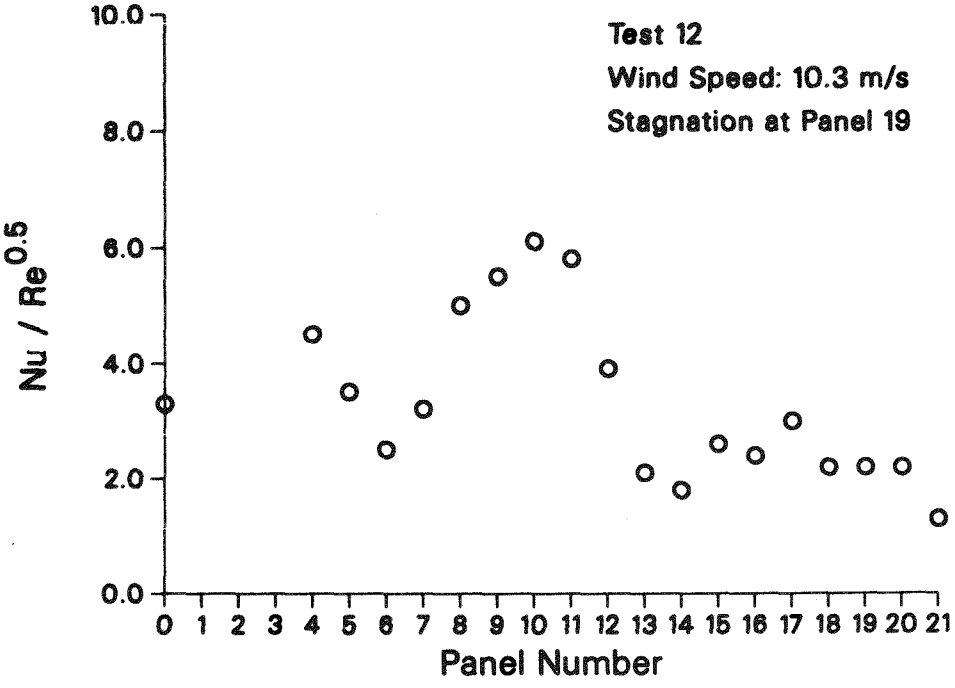

Figure C-12. Test 12, Day 138-1

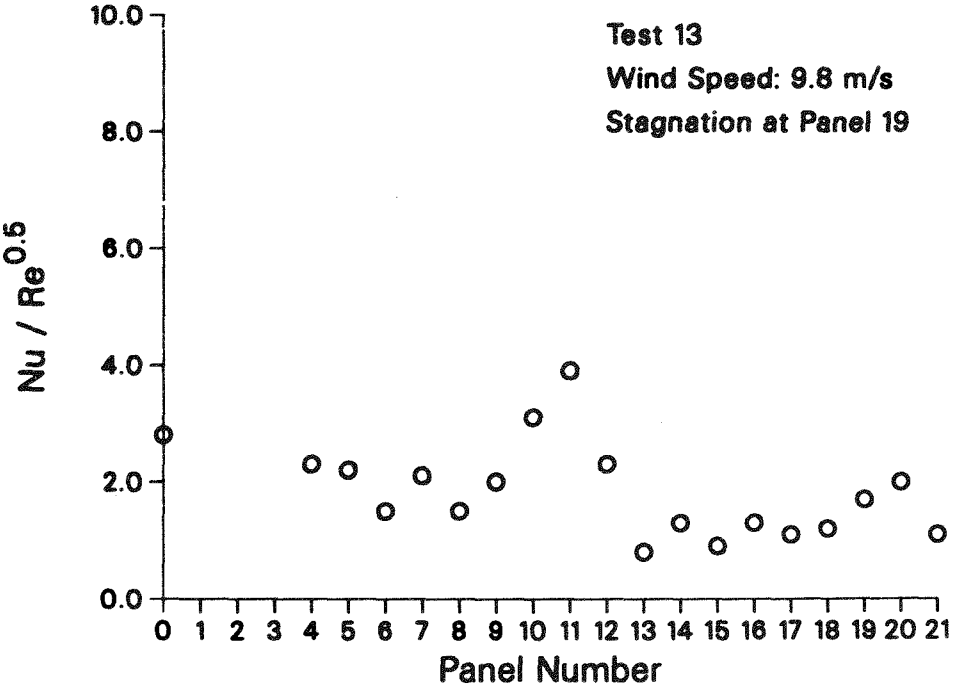

Figure C-13. Test 13, Day 138-2

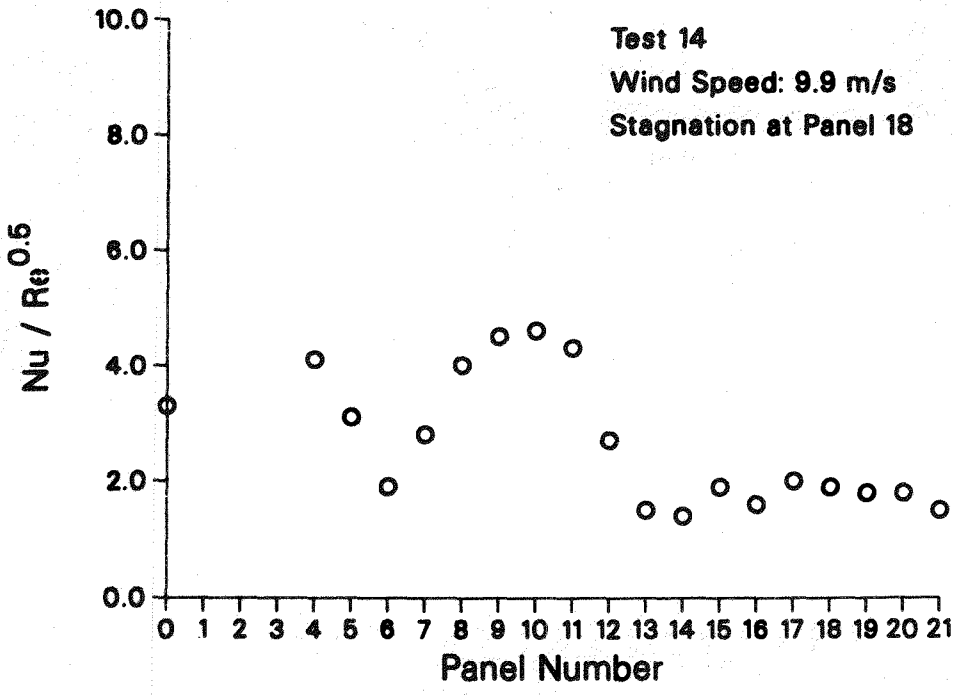

Figure C-14. Test 14, Day 138-3

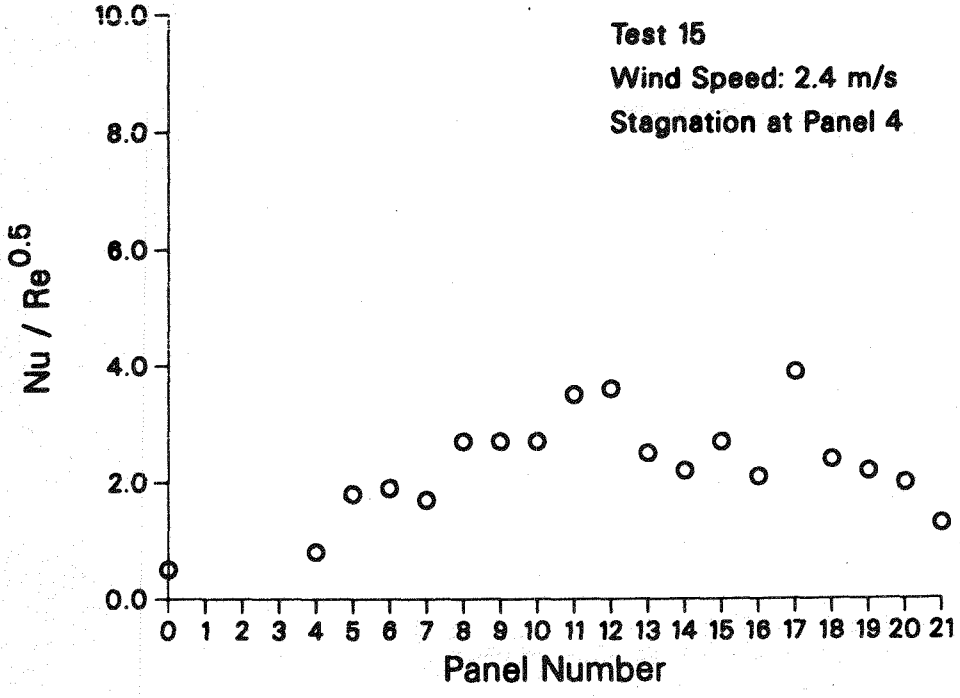

Figure C-15. Test 15, Day 151-1

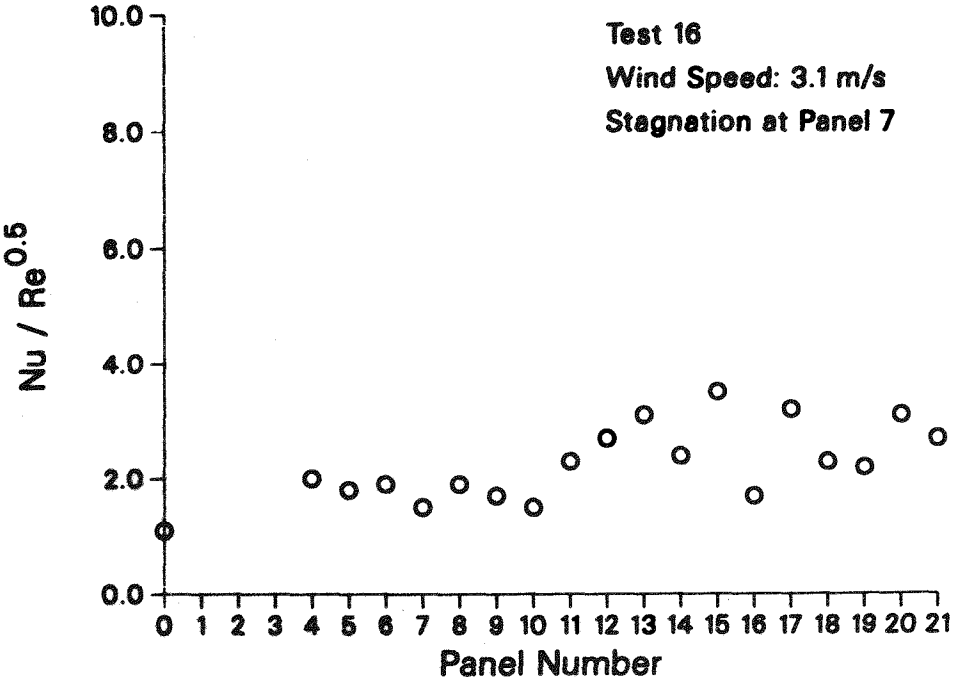

Figure C-16. Test 16, Day 151-2

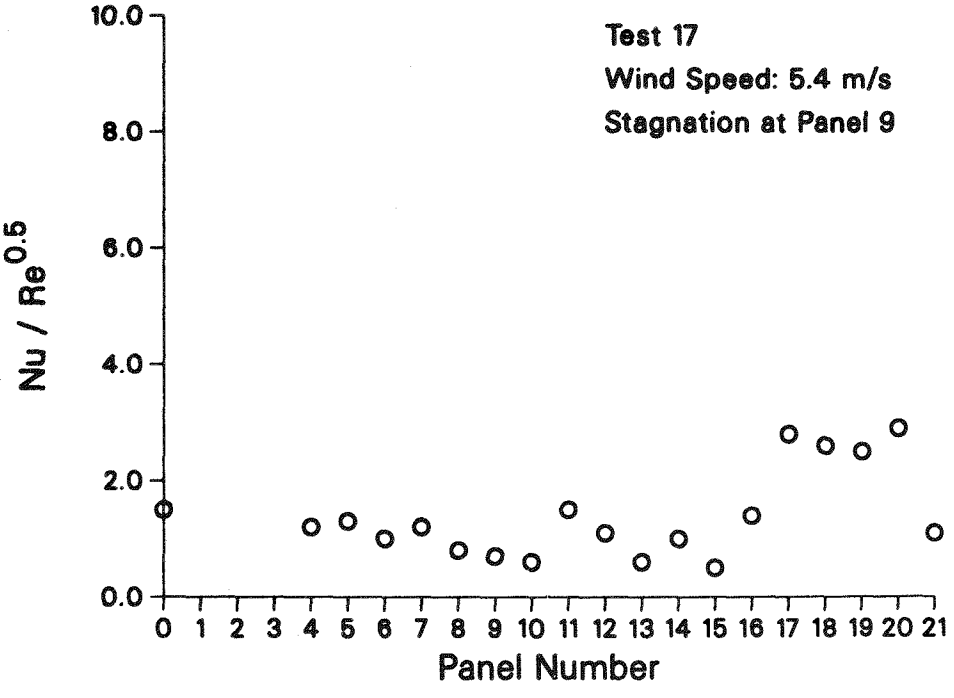

Figure C-17. Test 17, Day 151-3

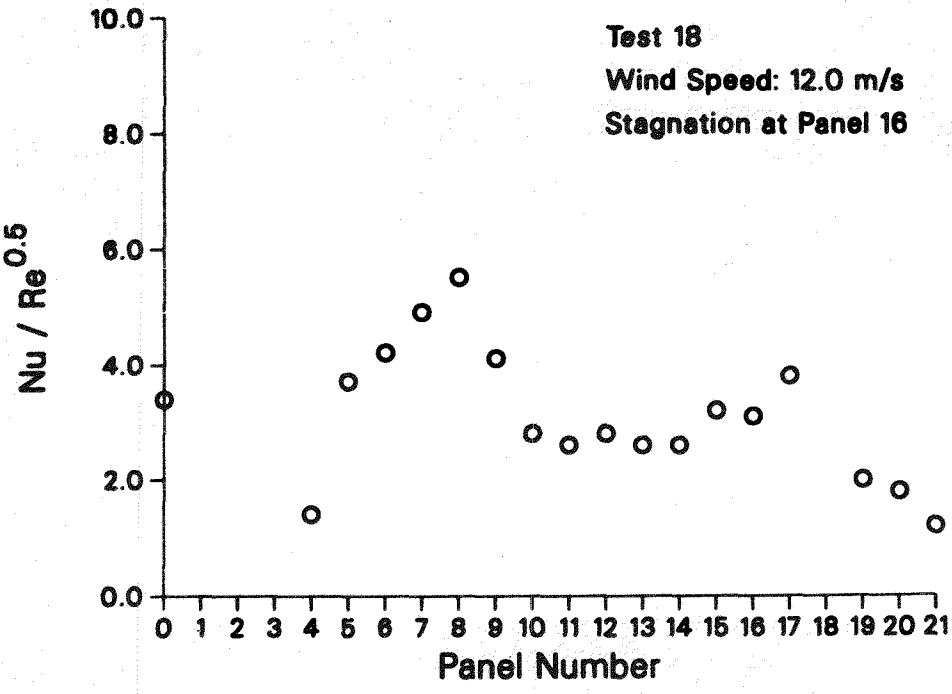

Figure C-18. Test 18, Day 152-1

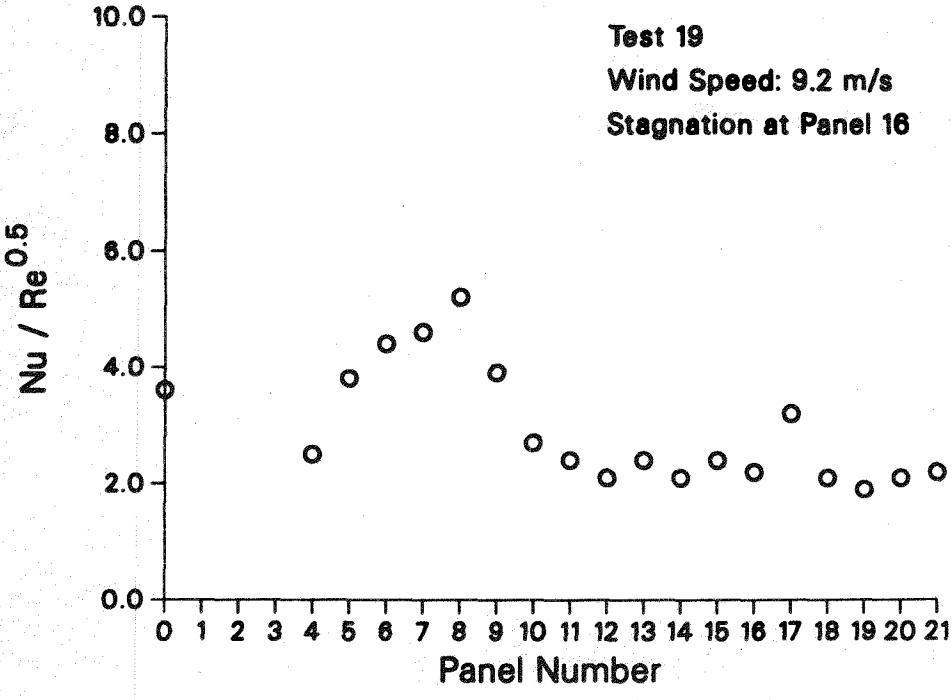

Figure C-19. Test 19, Day 152-2

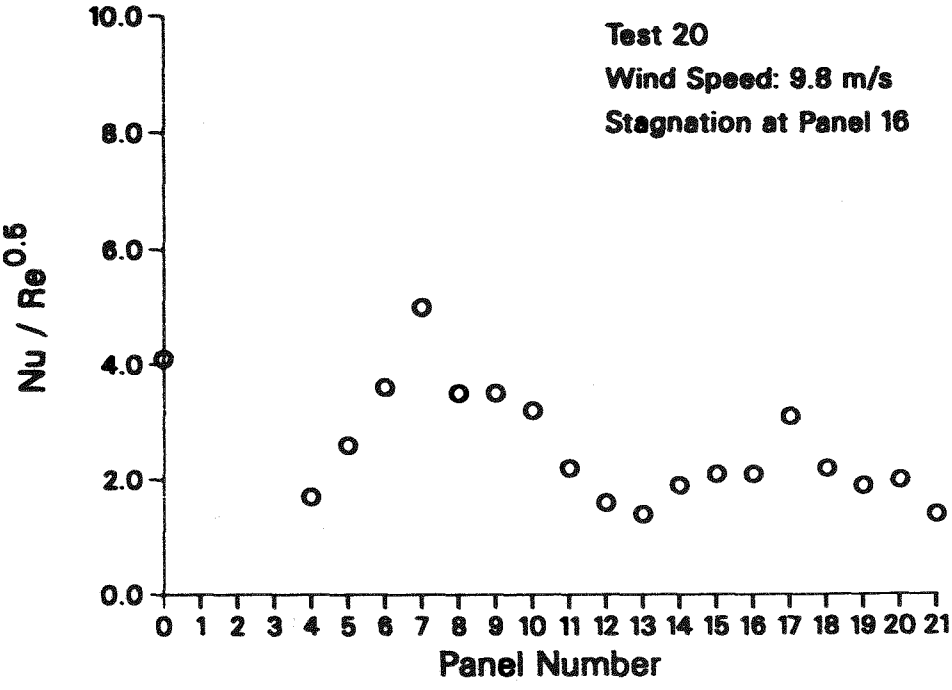

Figure C-20. Test 20, Day 152-3

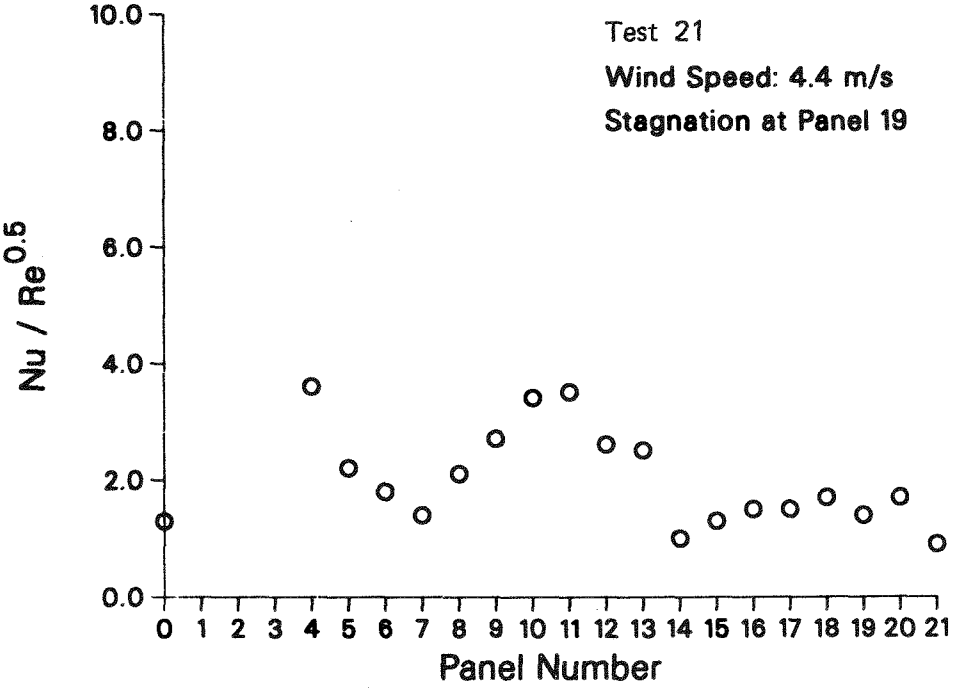

Figure C-21. Test 21, Day 206-1

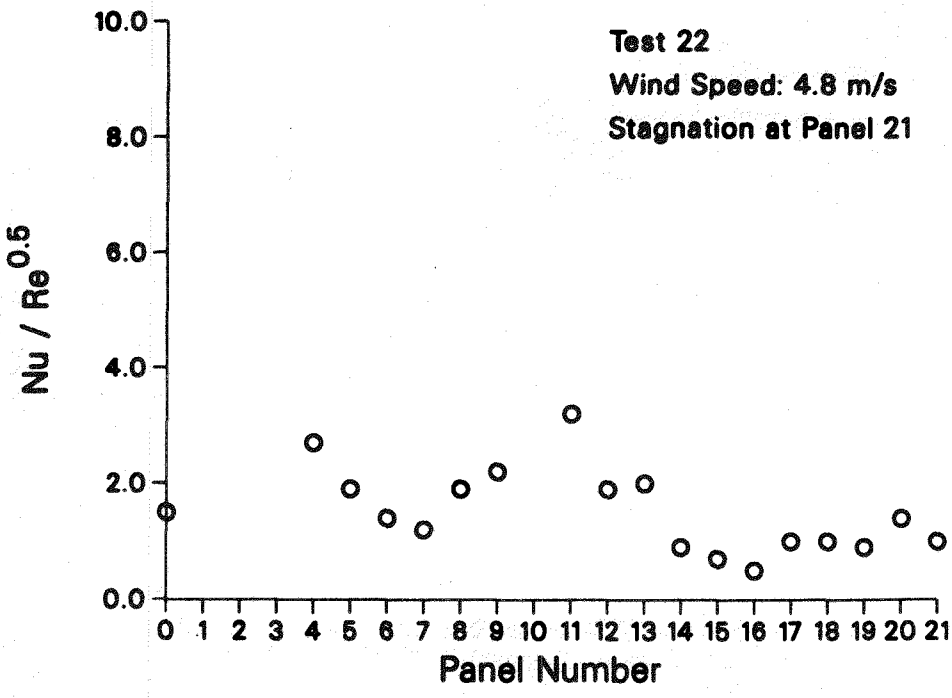

Figure C-22. Test 22, Day 206-2

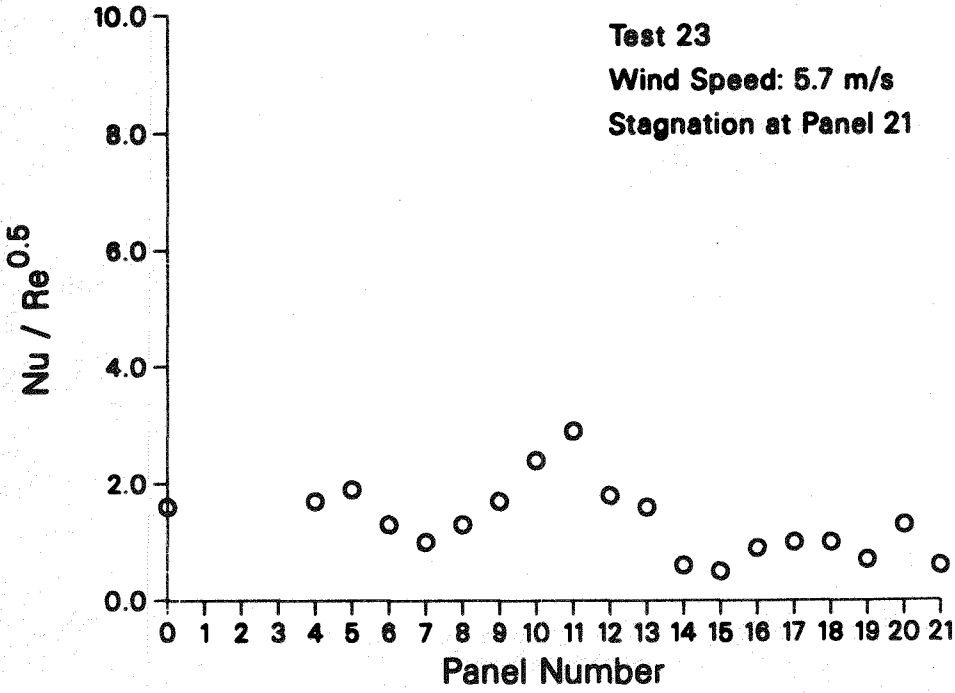

Figure C-23. Test 23, Day 206-3

APPENDIX D

The Effect of Convective Loss on Receiver Efficiency During Operations

Calculations were made to determine the effect of convective losses on the overall receiver efficiency during normal operations. The wind speeds and ambient temperatures from the convective loss experiments were used. A receiver wall temperature of 300 °C (572 °F) was used and a receiver absorptivity of 0.88 was assumed [27]. The efficiency was calculated by:

$$\eta = \frac{P_{inc} - P_{loss}}{P_{inc}} \qquad (D.1)$$

The incident power, P_{inc}, was 45 MW_t. The losses due to reflection, convection and thermal radiation were calculated. The convective loss was calculated using Siebers and Kraabel's correlations [20] . Conductive loss was neglected since it is small. Table D.1 gives the results of these calculations. The reflective loss was roughly equal to the sum of the convective and thermal radiative losses and the total loss was about 20% of the incident power. Figure D-1 shows a plot of wind speed versus receiver efficiency.

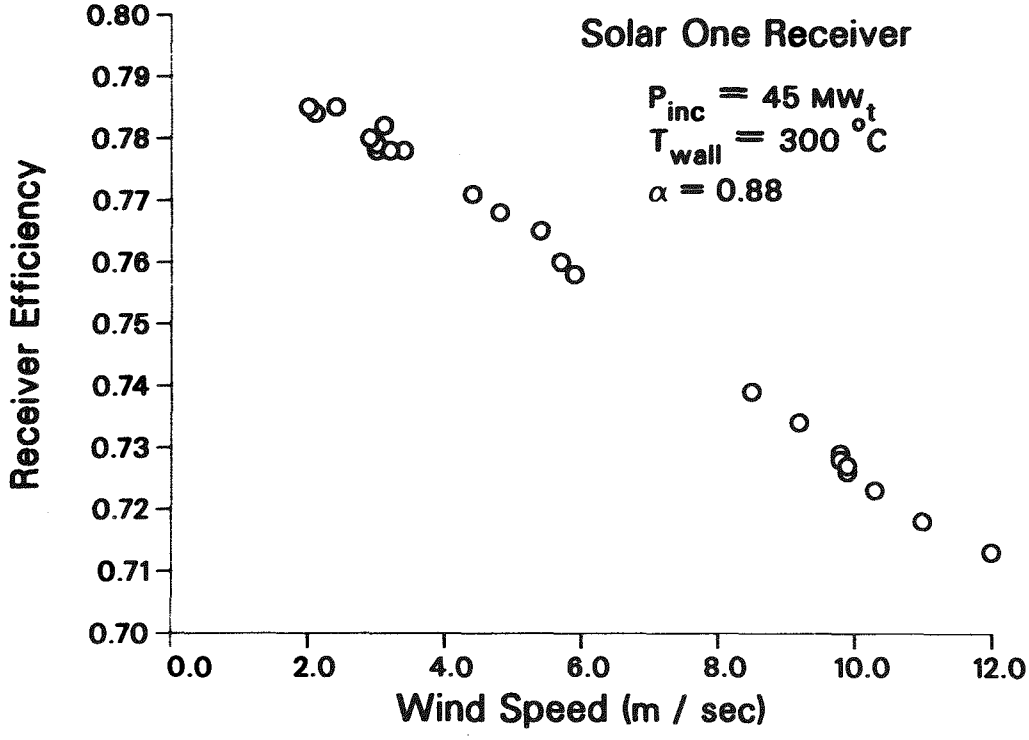

Figure D-1 Wind speed versus calculated receiver efficiency during normal operations

Table D.1. Predicted Receiver Efficiency versus Wind Speed

Test	T_∞ °C	u_∞ m/s	h_{pred} W/m^2°C	P_{conv} MW	P_{rad} MW	P_{refl} MW	η
1	18.4	5.9	15.9	2.369	2.749	5.04	0.758
2	15.6	2.9	9.8	1.473	2.749	5.04	0.780
3	16.6	3.0	10.0	1.497	2.749	5.04	0.779
4	19.2	3.2	10.2	1.517	2.749	5.04	0.778
5	13.7	3.0	10.1	1.528	2.749	5.04	0.778
6	27.5	8.5	22.0	3.166	2.749	5.04	0.739
7	26.2	11.0	28.1	4.074	2.749	5.04	0.718
8	24.6	9.9	25.2	3.667	2.749	5.04	0.727
9	25.1	2.0	8.5	1.237	2.749	5.04	0.785
10	22.9	3.4	10.5	1.539	2.749	5.04	0.778
11	21.3	2.1	8.7	1.284	2.749	5.04	0.784
12	25.4	10.3	26.3	3.827	2.749	5.04	0.723
13	24.4	9.8	25.0	3.651	2.749	5.04	0.728
14	22.3	9.9	25.4	3.736	2.749	5.04	0.726
15	34.2	2.4	8.7	1.225	2.749	5.04	0.785
16	33.8	3.1	9.8	1.379	2.749	5.04	0.782
17	31.1	5.4	14.5	2.064	2.749	5.04	0.765
18	32.9	12.0	30.3	4.281	2.749	5.04	0.713
19	29.1	9.2	23.5	3.370	2.749	5.04	0.734
20	27.9	9.8	25.1	3.612	2.749	5.04	0.729
21	21.4	4.4	12.5	1.845	2.749	5.04	0.771
22	21.1	4.8	13.4	1.978	2.749	5.04	0.768
23	19.9	5.7	15.4	2.282	2.749	5.04	0.760

As the wind speed varies from 2.0 to 12.0 m/s (4.5 to 27.0 mph), the receiver efficiency varies from 78.5 to 71.3% . This conclusion assumes that the incident power and the average receiver wall temperature are constant, which implies that the reflection and thermal radiation losses remain constant.

Solar One receiver efficiency has been plotted versus wind speed by Baker [22] for data collected during normal operations. The absorbed power was computed as $\dot{m}C_p(T_{out} - T_{in})$ from measured plant data. The incident power was calculated using "look-up tables"constructed from MIRVAL computer code predictions. The calculated efficiencies ranged from 70 to 80%, with considerable scatter in the data. A statistical fit to the data indicates virtually no decline in efficiency over the wind speed range of 1.0 to 8.7 m/sec (2.2 to 19.4 mph). No error analysis or uncertainty was associated with this data, however the predicted effect of wind speed on efficiency from Table D.1 falls well within the scatter of the data presented in Baker's report. It is not clear that the experimental method used to determine these reported efficiencies has sufficient resolution to discern the effect of wind speed.

References

[1] Stoddard, M. C. and G. H. Evans, "Solar One Convective Loss Experiments: A Status Report," SAND84-8731, presented at the International Energy Agency Workshop on the Design and Performance of Large Solar Thermal Collector Arrays, June 10–14, 1984, San Diego, CA.

[2] Abrams, M., Sandia memorandum to A. C. Skinrood, "Plan for Determining the Thermal Performance of the Receiver at the Solar 10 MW_e Power Plant," February 10, 1982.

[3] Kraabel, J. S., "Receiver Efficiency, Fall Measurement Campaign, 1982," Sandia National Laboratories report in preparation.

[4] Falcone, P. K. (ed.), "Convective Losses From Solar Central Receivers Proceedings of a DOE/SERI/SNLL Workshop," Sandia National Laboratories report, SAND81-8014, October 1981.

[5] Afshari, B. and J. H. Ferziger, "Development of a Predictive Computer Code for Heat Losses from External Recievers," in Reference 4.

[6] Afshari, B. and J. H. Ferziger, "Computation of Orthogonal Mixed-Convection Heat Transfer," *ASME-JSME Thermal Engineering Joint Conference Proceedings* **3** 169 (1983).

[7] Evans, G. H. and O. A. Plumb, "Laminar Mixed Convection from a Vertical Heated Surface in a Crossflow," *ASME Journal of Heat Transfer* **104** 554 (1982).

[8] Plumb, O. A. and G. H. Evans, "Turbulent Mixed Convection from a Vertical Heated Surface in a Crossflow," *ASME-JSME Thermal Engineering Joint Conference Proceedings* **3** 47 (1983).

[9] LeQuere, P., J. A. C. Humphrey, and F. S. Sherman, "Numerical Calculations of Thermally Driven Two-Dimensional Unsteady Laminar Flow in Cavities of Rectangular Cross-Section," *Num. Heat Transfer* **4** 249 (1981).

[10] Kraabel, J. S., "An Experimental Investigation of the Natural Convection from a Side-Facing Cubical Cavity," *ASME-JSME Thermal Engineering Joint Conference Proceedings* **1** 299 (1983).

[11] Humphrey, J. A. C., et al., "Investigation of Free-Forced Convection Flows in Cavity-Type Receivers," Sandia National Laboratories Contractor Report, SAND79-8196, January 1982.

[12] Clausing, A. M., K. C. Wagner, and R. J. Skarda, "An Experimental Investigation of Combined Convection from a Vertical Cylinder in a Crossflow," *ASME-JSME Thermal Engineering Joint Conference Proceedings* **3** 155 (1983).

[13] Siebers, D. L., R. G. Schwind, and R. J. Moffat, "Experimental Mixed Convection from a Large, Vertical Plate in a Horizontal Flow," *Proceedings of the 7th International Heat Transfer Conference* Paper MC 13 **3** (1982).

[14] Siebers, D. L., R. J. Moffat, and R. G. Schwind, "Experimental, Variable Properties Natural Convection from Large, Vertical, Flat Surface," *ASME-JSME Thermal Engineering Joint Conference Proceedings* **3** 269 (1983).

[15] Siebers, D. L., R. G. Schwind, and R. J. Moffat, "Experimental Mixed Convection Heat Transfer from a Large, Vertical Surface in a Horizontal Flow," Sandia National Laboratories report, SAND83-8225, July 1983.

[16] Kraabel, J. S., "Convection Testing of the Central Receiver System, Fall 1982," Sandia National Laboratories report in preparation.

[17] Jacobs, H., M. Sanchez, and R. Carmona, "Receiver Losses: Results of Tests," *I.E.A. Small Solar Systems Project Final Evaluation Report, Vol. 1, Central Receiver Systems* (1984).

[18] McMordie, P. K., "Convection Losses from a Cavity Receiver," *AIChE 20th National Heat Transfer Conference* August 2–5, 1981.

[19] Beninga, K. J. and T. Buna, "In Situ Evaluation of Convective Losses in Molten Salt Central Receivers," *American Solar Energy Society Conference Proceedings* (1984).

[20] Siebers, D. L. and J. S. Kraabel, "Estimating Convective Energy Losses From Solar Central Receivers," Sandia National Laboratories report, SAND84-8717, April 1984.

[21] Abrams, M., "The Status of Research on Convective Losses from Solar Central Receivers," Sandia National Laboratories report, SAND83-8224, June 1983.

[22] Baker, A. F. and D. L. Atwood, "Monograph Series, No. 2: 10 MW_e Solar Thermal Central Receiver Pilot Plant, Receiver Performance Evaluation," Sandia National Laboratories report in preparation.

[23] Abrams, M., Sandia memorandum to A. F. Baker, "Results of the Ramapo Flow Meter Calibration Tests at General Electric and Recommendations for Boiler Panel Flow Meter Modifications," February 21, 1983.

[24] Stoddard, M. C. and G. H. Evans, Sandia memorandum to A. C. Skinrood, "Convection Loss Measurements at the Barstow Central Receiver," November 7, 1983.

[25] Klevgard, P., Sandia memorandum, "Test Report: Solar One Thermocouple Calibration," February 7, 1984.

[26] Berdahl, P. and R. Fromberg, "The Thermal Radiance of Clear Skies," *Solar Energy* **29**, 299 (1982).

[27] Baker, A. F., "Monograph Series No. 3: 10 MW_e Solar Thermal Central Receiver Pilot Plant Receiver Absorptivity Measurements and Results," Sandia National Laboratories report in preparation.

[28] Abrams, M., Member of the Technical Staff, Sandia National Laboratories, private communication.

[29] Abrams, M., W. G. Houf, and G. H. Evans, "PARFLO and SAPPHIR: Computer Codes which Predict the Thermal Hydraulic Performance of the Central Receiver at Solar One," Sandia National Laboratories report in preparation.

[30] Kaowool data sheet, Babcock and Wilcox.

[31] Test, F. L., R. C. Lessmann, and A. Johary, "Heat Transfer During Wind Flow over Rectangular Bodies in the Natural Environment," *ASME Journal of Heat Transfer* **103** 262 (May 1981).

[32] Kowalski, G. J. and J. W. Mitchell, "Heat Transfer From Spheres in the Naturally Turbulent, Outdoor Environment," *ASME Journal of Heat Transfer* **98** 649 (November 1976).

[33] Kline, S. J. and F. A. McClintock, "Describing Uncertainties in Single-Sample Experiments," *Mechanical Engineering* **75** 3 (January 1953).

[34] Abernethy, R. B. et al., Measurement Uncertainty Handbook, Revised 1980, sponsored by The Aerospace Industries Division of the Instrument Society of America, a reprint of NTIS AEDC-TR-73-5 Handbook: Uncertainty in Gas Turbine Measurements.

[35] Achenbach, E. "The Effect of Surface Roughness on the Heat Transfer from a Circular Cylinder to the Cross Flow of Air," *Int. J. Heat Mass Transfer* **20** 359 (1977).

[36] Sayers, D. D., "Estimation of Convective Losses from Solar Central Receivers," Sandia memorandum, RS 8245/17, March 1985.

[37] Dellin, T. A., M. J. Fish, and C. L. Yang, "A User's Manual for DELSOL2: A Computer Code for Calculating the Optical Performance and Optimal System Design for Solar Thermal Central Receiver Plants," Sandia National Laboratories report, SAND81-8237, August 1981.

[38] Stoddard, M. C., Sandia memorandum to B. L. Kistler, "Revised Thermal Loss Calculations for DELSOL2 - External Receivers," August 13, 1985.

UNLIMITED RELEASE
INITIAL DISTRIBUTION

U.S. Department of Energy (6)
Forrestal Building, Room 5H021
Code CE-314
1000 Independence Avenue, S.W.
Washington, D.C. 20585
Attn: C. Carwile
H. Coleman
S. Gronich
F. Morse
M. Scheve
R. Shivers

U. S. Department of Energy (2)
P.O. Box 5400
Albuquerque, NM 87115
Attn: D. Graves
J. Weisiger

U.S. Department of Energy (2)
1333 Broadway
Oakland, CA 94612
Attn: R. Hughey
M. Lopez

University of California
Department of Mechanical Engineering
Berkeley, CA 94720
Attn: R. Greif

University of California
Department of Mechanical Engineering
Irvine, CA 92717
Attn: M. Young

University of California (2)
Department of Mechanical Engineering
Davis, CA 95616
Attn: A. A. McKillop
J. W. Baughn

University of California
Environmental Science and Engineering
Los Angeles, CA 90024
Attn: R. G. Lindberg

University of Houston (2)
Solar Energy Laboratory
4800 Calhoun
Houston, TX 77704
Attn: A. F. Hildebrandt
L. Vant-Hull

University of Illinois
Dept. of Mechanical and Industrial Engineering
Urbana, IL 61801
Attn: A. M. Clausing

Purdue University (2)
School of Mechanical Engineering
West Lafayette, IN 47907
Attn: F. P. Incropera
R. Viskanta

Stanford University
Department of Mechanical Engineering
Stanford, CA 94305
Attn: R. J. Moffat

University of Utah
Mechanical and Industrial Engineering Department
Salt Lake City, UT 84112
Attn: R. F. Boehm

Washington State University
Department of Mechanical Engineering
Pullman, WA 99164
Attn: O. A. Plumb

AMFAC
P.O. Box 3230
Honolulu, HI 96801
Attn: G. E. St. John

ARCO Power Systems
302 Nichols Drive
Hutchins, TX 75141
Attn: R. L. Henry

Argonne National Laboratory
9700 South Cass Avenue
Argonne, IL 60439
Attn: W. W. Schertz

Arizona Public Service Company
P.O. Box 21666
Phoenix, AZ 85036
Attn: E. Weber

Babcock and Wilcox (3)
91 Stirling Avenue
Barberton, OH 44203
Attn: G. Grant
M. Seale
D. C. Smith

Bechtel Group, Inc.
P. O. Box 3965
San Francisco, CA 94119
Attn: S. Fleming

Black & Veatch Consulting Engineers (2)
P.O. Box 8405
Kansas City, MO 64114
Attn: J. C. Grosskreutz
S. L. Levy

Boeing Aerospace Co., Energy Systems
P. O. Box 3999, MS87-63
Seattle, WA 98124
Attn: W. D. Beverly

California Energy Commission
1516 Ninth St., M/S 40
Sacramento, CA 95814
Attn: A. Jenkins

California Public Utilities Com.
Resource Branch, Room 5198
455 Golden Gate Ave.
San Francisco, CA 94102
Attn: T. Thompson

Combustion Engineering, Inc.
1000 Prospect Hill Road
Winsor, CT 06095
Attn: C. R. Buzzuto

DFVLR SSPS
Linder Hohe
D 5000 Cologne 90
West Germany
Attn: W. Grasse

El Paso Electric Company
P.O. Box 982
El Paso, TX 79946
Attn: J. E. Brown

Electric Power Research Institute (2)
P.O. Box 10412
Palo Alto, CA 94303
Attn: J. Bigger
E. DeMeo

Électricité de France
Ream
140 Av. Viton
13009 Marseille
France
Attn: F. Pharabod

Elliott, S. D.
1801 Highway 128
Star Route 7550
Philo, CA 95466

Exxon Enterprises, Inc.
P.O. Box 592
Florham Park, NJ 07932
Attn: T. L. Guckes

Foster Wheeler Development Corp.
12 Peach Tree Hill Road
Livingston, NJ 07039
Attn: R. J. Zoschak

Georgia Institute of Technology (2)
Engineering Experiment Street
Atlanta, GA 30332
Attn: C. T. Brown
S. H. Bomar

HMJ Corporation
P. O. Box 15128
Chevy Chase, MD 20815
Attn: W. D. Johnson

IEA/SSPS Project
Apartado 649
Almeria, Spain
Attn: C. Arano

Jet Propulsion Laboratory (3)
4800 Oak Grove Drive
Pasadena, CA 91103
Attn: M. Alper
W. A. Owen
J. W. Stearns

Los Angeles Department of Water and Power
Alternate Energy Systems
P.O. Box 111
111 North Hope St.
Los Angeles, CA 90051
Attn: D. Chu

Martin Marietta Aerospace (2)
P.O. Box 179, MS L0450
Denver, CO 80201
Attn: H. Wroton
T. Buna

McDonnell Douglas Astronautics Company (3)
5301 Bolsa Avenue
Huntington Beach, CA 92647
Attn: R. L. Gervais
R. Riedesel
J. Raetz

Meridian Corporation
5113 Leesburg Pike
Falls Church, VA 22041
Attn: R. King

Olin Chemicals Group (2)
120 Long Ridge Road
Stamford, CT 06904
Attn: F. N. Christopher
L. C. Fiorucci

Pacific Gas and Electric Company
77 Beale Street
San Francisco, CA 94105
Attn: R. E. Price

Pacific Gas and Electric Company (2)
3400 Crow Canyon Road
San Ramon, CA 94526
Attn: G. Braun
C. Weinberg

Pioneer Mill Company (AMFAC)
P.O. Box 727
Lahaina, HI 96761
Attn: R. K. MacMillan

Rockwell International
Energy Systems Group
8900 De Soto Avenue
Canoga Park, CA 91304
Attn: T. Springer

Rockwell International
Rocketdyne Division
6633 Canoga Avenue
Canoga Park, CA 91304
Attn: J. Friefeld

Solar Energy Industries Association
1140 19th St. N.W.
Suite 600
Washington, D.C. 20036
Attn: C. LaPorta

Solar Energy Research Institute (3)
1617 Cole Boulevard
Golden, CO 80401
Attn: B. Gupta
D. Hawkins
R. Hulstrom

Southern California Edison
P.O. Box 325
Daggett, CA 92327
Attn: C. Lopez

Southern California Edison (31)
P.O. Box 800
Rosemead, CA 92807
Attn: J. N. Reeves
P. Skvarna (30)

Stearns Catalytic Corp.
P.O. Box 5888
Denver, CO 80217
Attn: J. Hobson

Stone and Webster Engineering Corporation
P.O. Box 1214
Boston, MA 02107
Attn: R. W. Kuhr

Westinghouse Electric Corporation
Advanced Energy Systems Division
P.O. Box 10864
Pittsbugh, PA 15236
Attn: J. R. Maxwell

E. H. Beckner, 6000; Attn: V. Dugan, 6200
D. G. Schueler, 6220
J. V. Otts, 6222
J. T. Holmes, 6226
R. S. Claassen, 8000; Attn: E. E. Ives, 8100
A. N. Blackwell, 8200
D. L. Hartley, 8300
J. S. Kraabel, 8132
C. S. Selvage, 8234
C. E. Hackett, 8244
C. M. Hartwig, 8244
G. H. Evans, 8245
R. J. Kee, 8245
D. L. Siebers, 8362
R. C. Wayne, 8400; Attn: L. D. Bertholf, 8430
H. Hanser, 8440
M. Abrams, 8431
R. L. Rinne, 8470
A. F. Baker, 8471
P. K. Falcone, 8471
A. C. Skinrood, 8471 (25)
M. C. Stoddard, 8471 (10)
D. N. Tanner, 8471
Sandia Solar One Office, 8471
N. E. Bergan, 8473
J. C. Swearengen, 8473
R. J. Gallagher, 8474
M. E. John, 8478

Publications Division 8265, for TIC (30)
Publications Division 8265/Technical Library Processes Division, 3141
Technical Library Processes Division, 3141 (3)
M. A. Pound, 8024, for Central Technical Files (3)